BIOSENSOR DEVELOPMENT FOR FIELD-DEPLOYABLE DIAGNOSTICS

A Dissertation
Presented to
The Academic Faculty

By

Monica P. McNerney

In Partial Fulfillment
of the Requirements for the Degree
Doctor of Philosophy in
Bioengineering

Georgia Institute of Technology

August 2019

BIOSENSOR DEVELOPMENT FOR FIELD-DEPLOYABLE DIAGNOSTICS

Approved by:

Dr. Mark P. Styczynski, Advisor
School of Chemical & Biomolecular Engineering
Georgia Institute of Technology

Dr. Brian Hammer
School of Biological Sciences
Georgia Institute of Technology

Dr. Andreas Bommarius
School of Chemical & Biomolecular Engineering
Georgia Institute of Technology

Dr. Pamela Peralta-Yahya
School of Chemistry & Biochemistry
Georgia Institute of Technology

Dr. Hang Lu
School of Chemical & Biomolecular Engineering
Georgia Institute of Technology

Date Approved: April 19 2019

ACKNOWLEDGEMENTS

This thesis would not have been possible without the guidance and support of many people.

I would first like to thank my advisor, Mark Styczynski, who has had the biggest impact on this thesis and on my development into a researcher and a scientist. He has continually challenged me to think creatively and has given me the freedom to explore new ideas. Beyond scientific advising, he has given me the confidence to aim higher than I otherwise would have and has helped shape my future career goals. I am very grateful to have had the opportunity to learn from him over the past five years.

I would also like to thank my thesis committee members – Dr. Hammer, Dr. Lu, Dr. Peralta-Yahya, and Dr. Bommarius – who have given excellent advice and insights. Each of their unique perspectives has influenced different portions of this work, and their comments and questions have helped me think more critically and more creatively. I am also indebted to Dr. Michael Jewett and Adam Silverman for training me in preparation and use of cell-free systems and for all of the subsequent troubleshooting assistance.

I would also like to thank all members of the Styczynski group – past and present – for the collaborations, the conversations, and the camaraderie. Daniel Watstein deserves special thanks for training me in synthetic biology techniques and for being a great interview and travel partner throughout all of our I-Corps adventures. April Miguez, Yan Zhang, and Cirstyn Michel also deserve thanks for help with side projects that furthered the boundaries and impact of this thesis.

I need to thank many people outside of the lab who have helped me balance the trials and tribulations of graduate school with friendship and fun. I have been lucky to make great friends in Atlanta and to be able to spend so much time with friends from Notre Dame. While it is impossible to name everyone, a few people deserve special thanks: Corinne Lawler, Alex Tsoras, Krysten Minnici, Adam Caparco, Sabina Fischer, Amanda Frick, and Alex Brown.

Finally, I would like to thank my sister Natalie and my parents, Neal and Rose Ann. They have been role models for me in many different ways, and their endless support and encouragement throughout my entire academic journey has meant the world to me.

TABLE OF CONTENTS

ACKNOWLEDGEMENTS **iii**

LIST OF FIGURES **viii**

LIST OF SYMBOLS AND ABBREVIATIONS **xi**

SUMMARY **xii**

CHAPTER 1. Introduction **1**
1.1 Bacterial biosensors for point-of-care diagnostics **1**
1.2 Prevalence and assessment of micronutrient deficiencies **3**
1.3 Previous work towards a whole-cell zinc biosensor **6**
1.4 Metabolic pigments for visual test interpretation **7**
1.5 Cell-free expression systems for diagnostic applications **11**
1.6 Contribution of this thesis **13**

CHAPTER 2. Engineering pigments for use as reporter outputs **15**
2.1 Introduction **15**
2.2 Materials and Methods **18**
2.2.1 Materials 18
2.2.2 Strains and plasmids 18
2.2.3 Cloning and construct assembly 19
2.2.4 Promoter Assembly 19
2.2.5 Cell culture 20
2.2.6 Measurement of optical density and fluorescence 21
2.2.7 Lycopene extraction and HPLC analysis 21
2.3 Results **22**
2.3.1 Standard inducible promoter systems cannot repress lycopene production 22
2.3.2 Promoter engineering decreases leaky protein expression 25
2.3.3 Qualitative and quantitative evaluation of visible lycopene 28
2.3.4 Reduced RBS strength enables full lycopene repression and proper induction 30
2.3.5 The P_{Lac} system produces visible lycopene most quickly 33
2.3.6 Precursor supplementation reduces time to visible lycopene 35
2.4 Discussion **37**

CHAPTER 3. Design of a fast-responding, tunable zinc sensor **43**
3.1 Introduction **43**
3.2 Materials and Methods **45**
3.2.1 Materials 45
3.2.2 Strains and plasmids 45
3.2.3 Cloning and construct assembly 45
3.2.4 Cell culture 46
3.2.5 Serum processing and zinc measurement 48
3.2.6 Measurement of optical density and fluorescence 48

3.2.7 Pigment extraction and quantification 49
3.2.8 Protein mutagenesis experiments 49
3.3 Results 50
3.3.1 Synthetic promoters to separate chemical production from cell growth 51
3.3.2 A multi-colored, fast-responding zinc sensor 57
3.3.3 Rational tuning of color switch points 61
3.3.4 Assessment of physiologically relevant zinc concentrations in human serum 69
3.4 Discussion 73

CHAPTER 4. Point-of-care biomarker quantification in cell-free diagnostics 76
4.1 Introduction 76
4.2 Materials and Methods 78
4.2.1 Construction of zinc-responsive circuit 78
4.2.2 Construction of knockout strains 78
4.2.3 Preparation of cellular lysate 79
4.2.4 Cell-free reactions: constitutive expression and zinc-sensing 80
4.2.5 Cell-free reactions: toehold switches 82
4.2.6 Determination of best-fit reactions and predictive standard reactions 83
4.2.7 Quantitative Error Metric Calculations 83
4.2.8 Preparation of human serum 85
4.2.9 Zinc measurements 85
4.2.10 Spectra analysis 86
4.2.11 Color imaging and processing 87
4.2.12 Lyophilization 87
4.3 Results 88
4.3.1 Development of a cell-free zinc detection system 88
4.3.2 CFE systems sense and respond to zinc in human serum 94
4.3.3 Development of parallelized calibration method 97
4.3.4 Parallel calibration reliably quantifies zinc concentrations 101
4.3.5 Addition of small molecules enables equipment-free quantitation in serum 105
4.3.6 Tests reliably quantify zinc in the matrix of single-donor human serum 109
4.3.7 Approach to semi-quantitation is generalizable to toehold sensors 114
4.4 Discussion 117

CHAPTER 5. Conclusions and Future Directions 123
5.1 Novelty of thesis research 123
5.2 Development of a field-deployable biosensor for zinc deficiency 124
5.3 Expansion of cell-free quantification platform to new biomarkers 127
5.4 Microbial factories for targeted chemical production 129
5.5 Closing remarks 132

REFERENCES 134

LIST OF TABLES

Table 1	Description and sequences of inducible promoters tested.	25
Table 2	Sequences of all dual-input promoters	55
Table 3	Fold change of all characterized promoters in response to the inducer and to zinc.	56

LIST OF FIGURES

Figure 1	Estimated country-specific prevalence of inadequate zinc intake.	5
Figure 2	Pigment production pathways, with different pigmented metabolites indicated by colored boxes.	8
Figure 3	Standard inducible promoters cannot adequately control lycopene production.	24
Figure 4	Discrepancy between fluorescent protein production and lycopene production from engineered promoter systems	28
Figure 5	Evaluation of “colorlessness” and “redness” in cells producing different amounts of lycopene.	30
Figure 6	Effect of RBS strength on lycopene production across different promoter systems.	33
Figure 7	Time to response of three different promoter systems.	34
Figure 8	The effect of inoculation density on lycopene production.	35
Figure 9	Effects of precursor supplementation on lycopene production.	37
Figure 10	Schematic illustrating the overall design of a dual-input system that decouples cell growth from pigment production.	51
Figure 11	Circuit diagrams and schematics depicting the design of a dual-input promoters to regulate production of the violacein pathway genes.	53
Figure 12	Design and characterization of synthetic dual-input promoters.	54
Figure 13	Violacein production from the best-responding hybrid promoters.	57
Figure 14	Initial multi-color sensor cells.	58
Figure 15	Color classification of cells with different pigment concentrations.	60
Figure 16	Effect of Zur levels on zinc response.	62
Figure 17	Response of heterologous Zur to added zinc.	63

Figure 18	Zur mutagenesis to move Zur response point.	64
Figure 19	Tuning color thresholds with an inverter.	66
Figure 20	Multi-color sensor cells that respond to physiologically relevant zinc concentrations.	68
Figure 21	Effect of serum percentage and inoculation density on cell growth and pigment production.	69
Figure 22	Pigment quantification and visualization of sensor cells grow in 25% serum with IPTG and specified zinc concentrations.	70
Figure 23	Quantitative color assessment of cells grown in human serum	72
Figure 24	Cell-free expression systems respond to added zinc.	89
Figure 25	Colorimetric response to added zinc in CFE reactions.	91
Figure 26	Effect of reporter plasmid concentration on ability to distinguish between different zinc concentrations.	92
Figure 27	Direct addition of ZntR protein mediates a response to added zinc.	93
Figure 28	Quantitative colorimetric response to zinc of lyophilized reactions that were rehydrated in different zinc concentrations.	94
Figure 29	Protein production in high concentration of serum.	95
Figure 30	Zinc response in high concentrations of serum.	97
Figure 31	Matrix-specific quantification scheme for test standardization.	98
Figure 32	Development of matrix-specific quantification scheme for test standardization.	100
Figure 33	Quantification approach provides high prediction accuracy.	102
Figure 34	Quantification error for tests run in nonideal reaction conditions.	103
Figure 35	Validation of zinc quantification with direct protein addition.	104
Figure 36	Serum alters the color of reactions, making test interpretation more difficult.	106

Figure 37	Addition of small molecules that interact with serum albumin reverses the spectral shift and restores distinct colored intermediates	107
Figure 38	Effect of small molecules on output from CFE reactions.	109
Figure 39	Development of CFE assay to assess serum zinc concentrations.	111
Figure 40	Accurate quantification of zinc in human serum.	113
Figure 41	Equipment free test interpretation in 25% serum.	114
Figure 42	Quantification approach is generalizable to toehold switches.	116

LIST OF SYMBOLS AND ABBREVIATIONS

AAS	Atomic absorption spectrometry
ASSURED	Affordable, Sensitive, Specific, User friendly, Rapid and Robust, Delivered
BSA	Bovine serum albumin
CDC	Center for Disease Control
CFE	Cell-free expression
CPR	Chlorophenol red
CPRG	Chlorophenol red-β-D-galactopyranoside
DHS	Demographic Health Surveys
DTT	dithiothreitol
EP-PCR	Error-prone polymerase chain reaction
FPP	Farsenyl diphosphate
GFP	Green fluorescent protein
HSA	Human serum albumin
ICP-MS	Inductively coupled plasma mass spectrometry
IPTG	Isopentenyl ß-D-1-thiogalactopyranoside
PCR	Polymerase chain reaction
RBS	Ribosomal binding site
RFP	Red fluorescent protein
SSE	Sum of squared error
WHO	World Health Organization

SUMMARY

Almost all current tests for biomarkers require venous blood draws, extensive sample processing, and analysis with complex equipment. Inexpensive, easy-to-use tests are critical for expanding healthcare to under-developed regions, but the requirement for reliable quantification in complex sample types (like blood) has been a critical roadblock in developing such diagnostics. Microbial-based biosensors have the potential to serve as a robust and generalizable platform for such diagnostics, as microbes can sense a wide variety of clinically relevant analytes and can produce colored outputs that are visible to the naked eye. Further, cell-free systems, which use bacterial protein extract to implement genetic networks, can be freeze-dried and rehydrated in the sample to be analyzed, enabling long-term storage at ambient temperatures and point-of-care test implementation and interpretation. This work describes the development of bacteria-based diagnostic assays that use bacterial sensing methods to control production of different colored readouts that are visible to the naked eye, yet quantitative and robust to the interference effects seen in complex samples. Using this platform, I develop a nearly field-deployable test for zinc deficiency (which is estimated to cause over 100,000 childhood deaths annually) that accurately measures clinically relevant zinc concentrations. The test requires just a finger-prick of blood, is robust to temperature variation, and can be freeze-dried for long term storage. I also use this approach to measure other classes of biomarkers, demonstrating a generalizable platform for low-cost quantitative diagnostics.

CHAPTER 1. INTRODUCTION

Biosensors have been developed for a wide variety of compounds, but the vast majority of sensors use fluorescence as a readout (necessitating equipment to interpret), respond to a limited concentration range (often preventing testing of relevant concentrations) and do not work in complex matrices (preventing testing of biological samples). Bacterial biosensors that overcome these problems could be particularly useful in developing low-cost, point-of-care diagnostic tools that could expand healthcare to low-resource settings and better enable large-scale public health assessments. Bacteria can be engineered to produce colored pigments, potentiating the creation of sensor cells that produce easy-to-interpret, visible outputs. Related bacterial "cell-free" assays have been recently used in diagnostic development for infectious diseases, but their scope has been limited to detection (not quantification) of diseases with nucleic acid biomarkers.

1.1 Bacterial biosensors for point-of-care diagnostics

Low-cost, point-of-care diagnostic tools have the potential to transform healthcare by eliminating the cost and logistical challenges associated with sample transport, advanced analytical equipment, and trained personnel. Further, point-of-care tests enable diagnoses in low-resource settings, which can help expand healthcare to locations that do not have the infrastructure and resources to support analytical laboratories. The World Health Organization has set the ASSURED criteria to describe the ideal test for use in low-resource settings: a test should be Affordable, Sensitive, Specific, User-friendly, Rapid and Robust, Equipment-free, and Deliverable to the end user.

Bacteria-based biosensors have the potential to expand the scope of point-of-care tests to a wide variety of diseases and conditions. All bacterial biosensors have two main components: a sensing method that responds to the target compound, and a signal transduction method that leads to a detectable output. Bacteria have a wide variety of naturally evolved sensors that can be harnessed to control cell output. Allosterically-regulated transcription factors differentially control gene expression upon metabolite binding[1]; two-component systems transduce external signals into transcriptional changes[2]; and small-molecule responsive riboswitches can alter transcriptional termination and protein translation[3]. Engineering strategies such as directed evolution can be used to alter substrate specificity or to engineer entirely new sensing domains[4], further broadening the scope of compounds that can be detected with biosensors. In most existing biosensors, signal transduction leads to altered expression of a reporter gene, such as a fluorescent protein or an enzyme that can cleave a substrate into a colored product. Bacteria can be engineered to produce distinct colored proteins proteins or pigments that are visible to the naked eye, potentiating the possibility of equipment-free detection. The resulting equipment-free tests would be particularly useful in low-resource settings, as they would reduce the cost and logistical challenges associated with sample transport, storage, and test interpretation.

Whole cell-biosensors have already been developed to detect and respond to a variety of compounds. Engineered cells can detect and respond to levels of pollutants[5,6], pathogenic bacteria[7], and inflammation markers[8,9]. Bacterial “theranostics” take biosening a step further and can deliver a drug, therapeutic protein, or other payload upon sensing a

target biomarker. Responsive bacterial therapies show promise for treatment of cancer[10,11], metabolic disorders[12,13], and gut inflammation[14].

Cell-free sensor systems have recently emerged as an alternative bacteria-based biosensing approach, and these systems show great potential for use in point-of-care diagnostic tools. Cell-free systems (discussed in more depth below) use bacterial proteins to implement genetic programs. They have been successfully used to make a suite of infectious disease diagnostic tools that can specifically and sensitively detect essentially a user-defined nucleic acid sequence[15,16]. These systems can be lyophilized and stably stored on filter paper, function properly upon rehydration, and produce visible, enzyme-mediated output within 30 minutes of sample addition.

1.2 Prevalence and assessment of micronutrient deficiencies

In efforts to expand the scope of bacteria-based biosensors for diagnostic applications, this thesis focuses primarily on developing tools to diagnose micronutrient deficiencies, with the lack of available micronutrient diagnostic tools being significant motivation. Further, micronutrient deficiencies are the underlying cause for many diseases, which makes their treatment a high global health priority.

Micronutrients are vitamins and minerals essential for proper growth and development, and micronutrient deficiencies account for over 3 million annual childhood deaths and 35% of the childhood disease burden[17]. Micronutrient deficiencies are generally treated at a population level through supplementation or food fortification programs, but survey data on specific affected areas are required to inform intervention programs. Micronutrient deficiencies, often described as “hidden hunger”, have no immediately

apparent physical markers and require quantitative biomarker assessment for accurate diagnoses. This is in contrast to macronutrient deficiencies, which can be easily diagnosed through anthropometric measurements.

The Demographic Health Surveys (DHS) program performs regular assessments of public health, and the program can incorporate micronutrient tests into these surveys if "field-friendly" micronutrient analysis methods are available. To be considered field-friendly, tests must be done in the field, require minimal equipment and minimal training to perform, have an easy sample collection and transport protocol, and have a short turnaround time[18], requirements that are largely in agreement with the WHO's ASSURED guidelines. Through conversations with DHS leaders, I have learned that a useful test must produce results within four hours, which is the time it usually takes to complete a household survey that assesses multiple factors (ie: water quality, access to education, child height and weight). This would allow a surveyor to perform the test at the beginning of the survey and have results before leaving the home. Currently, DHS surveys are limited to assessing anemia (measured via hemoglobin quantification) largely because of the field-friendliness of the hand-held Hemocue device, which can quickly report hemoglobin levels from a fingerprick of blood. To date, there is no fully field-friendly test for any other nutritional biomarker.

Efforts to create new micronutrient diagnostic tools have largely focused on developing assays that can be performed in minimally equipped regional laboratories. These assays could be used in a small subset of public health surveys that have additional resources and the capacity for short-term sample storage and transport. A recently developed multiplexed ELISA platform[19] enables quantification of several micronutrient

biomarkers, including those for iron, vitamin A, and iodine, and it is being expanded to quantify markers for folate and vitamin B_{12}[20]. However, there is currently no assay for zinc, which is one of the six primary micronutrients of global health interest[21]. Zinc deficiency alone is estimated to affect 17% of the world's population[22] and is responsible for over 100,000 annual childhood deaths[17]. Zinc deficiency is most prevalent in the developing world (Figure 1) and has the most negative effects on women and small children[23].

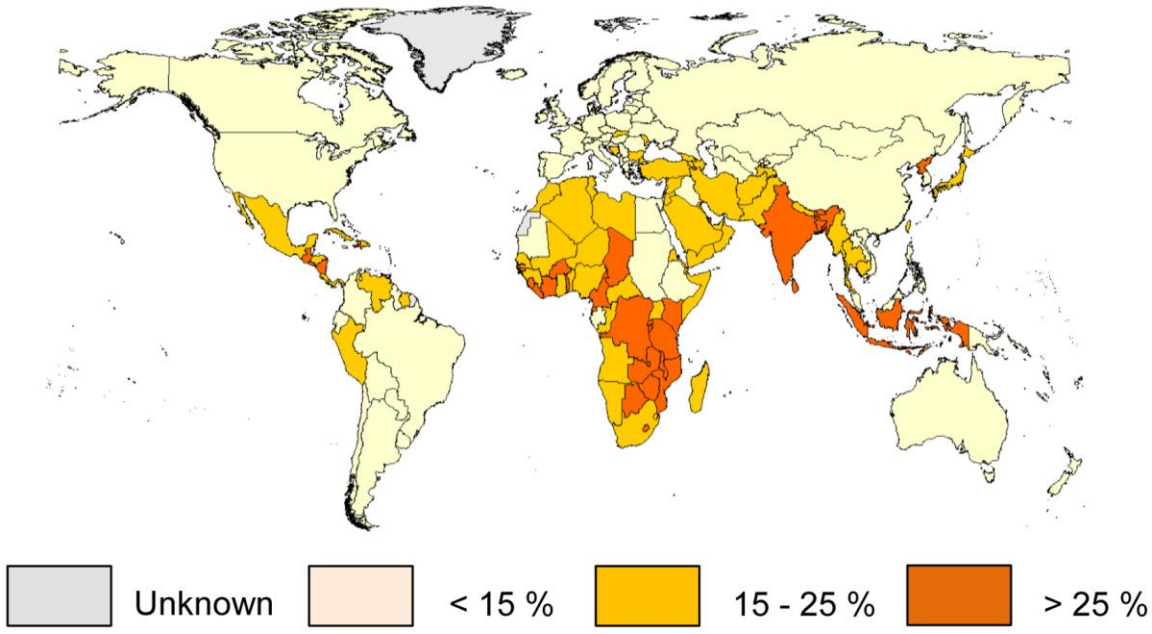

Figure 1: Estimated country-specific prevalence of inadequate zinc intake. Reproduced from Wessells and Brown, *Plos One* 2012[22].

The most reliable biomarker for zinc deficiency is plasma or serum zinc concentration. However, plasma zinc still has several disadvantages as a biomarker: it can vary based on food intake, time of day, and a variety of other factors that are decoupled from actual zinc deficiency. This variation makes plasma zinc an unreliable marker of individual zinc status, but an adequate marker of population zinc levels[21]. The threshold

for healthy plasma zinc is between 57 and 74 μg/dL[21], or between 8.7 and 11.3 μM, with physiological zinc concentrations ranging between 2 and 30 μM[24].

Currently, assessment of serum zinc levels requires sample shipment, extensive sample processing, and analysis with advanced analytical equipment. To avoid red blood cell lysis and artificial increase of plasma zinc levels from the resulting influx of zinc, samples must be shipped under constant refrigeration, a process referred to as "cold chain" shipment. For analysis, serum samples must be acid-digested at high pressure and then measured with atomic absorption spectrometers (AAS) or inductively coupled plasma mass spectrometers (ICP-MS). Isolated academic studies have had the resources to support this analysis process, but the costs and logistical challenges of maintaining cold chain and the costs of current testing methods have prevented population-level assessment of zinc status at the scale needed to effectively treat zinc deficiency.

1.3 Previous work towards a whole-cell zinc biosensor

A bacteria-based biosensor could fill the need for a field-friendly zinc test, and could be potentially expanded to assess other micronutrients. As obligate consumers of micronutrients, bacteria have the cellular machinery to sense and respond to varied micronutrient concentrations in their extracellular environments. Our group has already created a preliminary *E. coli* zinc sensor by harnessing zinc-responsive transcription factors to control production of pigmented metabolites[25,26]. However, these initial sensor cells are far from being field-deployable. These sensor cells always produce some pigment, which necessitates that the cells be grown from a very small inoculum so that coloration due to initial cell mass is minimal. This requirement leads to overnight assay times, which are far

longer than the four-hour threshold set for use in a DHS survey. Further, these sensor cells respond to zinc concentrations outside of the physiologically relevant range. To make the device more field-friendly, it is vital to reduce the time to coloration and tune the response range.

1.4 Metabolic pigments for visual test interpretation

In our group's continued effort to develop a biosensor for zinc deficiency, we have used pigmented metabolites as the sensor's output because of their advantages in enabling equipment-free test interpretation. Commonly used reporters all require equipment to interpret: fluorescent proteins are often not visible to the naked eye, necessitating use of a fluorimeter; and while commonly used enzymatic reporters (such as β-galactosidase) cleave substrates into visibly colored products, test interpretation requires measuring intensity of color production, which cannot be easily done by eye and thus necessitates use of a spectrophotometer. By using multiple pigment reporters, we can engineer discrete color changes, which can enable the user to interpret test output as easily as reading a litmus test and can minimize the subjectivity inherent to quantifying color intensity. We have previously used the pigments violacein, lycopene, and β-carotene as reporters to indicate relative low, medium, and high levels of extracellular zinc[25,26].

Violacein is a pigment produced by the bacterium *Chromobacterium violaceum*, and metabolic engineering of violacein has been extensively investigated[27-33] because of its medical potential: it has been demonstrated to have antibiotic, antiviral, and antitumor activity[28]. Additionally, the complexity and pigmented intermediates of the violacein biosynthesis pathway (Figure 2A) make it a useful testbed for the development and

validation of novel metabolic engineering strategies[29,31,34]. Lycopene and β-carotene are pigments in the carotenoid pathway (Figure 2B) and have also been targets of metabolic engineering efforts[35-40]. Two different pathways produce the precursors needed for carotenoid synthesis: the non-mevalonate pathway, which naturally occurs in bacteria, and the mevalonate pathway, which can be heterologously expressed in bacteria. Both pathways have been used to overproduce the metabolic precursors both for carotenoids and for other medical and commercial products[41-43].

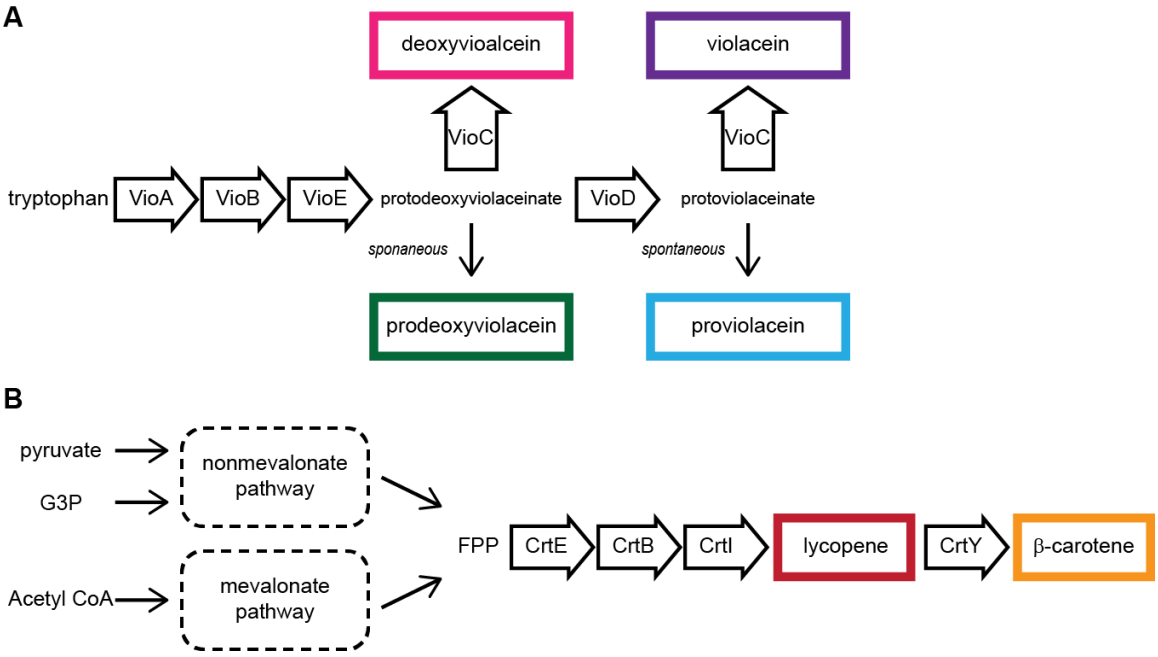

Figure 2: Pigment production pathways, with different pigmented metabolites indicated by colored boxes.
(A) Violacein synthesis pathway. Five enzymes convert tryptophan to the purple pigment violacein, and different enzyme combinations can produce different colored pigments. (B) Carotenoid synthesis pathway. Both the nonmevalonate and mevalonate pathways produce FPP, which is the immediate precursor to the carotenoid pathway. Three enzymes are required to convert FPP into lycopene, and a single enzyme converts lycopene into β-carotene.

Engineering cells to produce metabolites (such as pigments) requires more complex cell engineering than what is required for protein overproduction. Metabolites are produced through multi-enzymatic pathways that draw precursors from naturally-occurring cell metabolism. Overexpressing these pathways can deplete vital metabolites from the cell, cause cofactor imbalances, and lead to accumulation of toxic pathway intermediates, all of which lead to low cell viability and construct stability[44]. Optimization of enzyme expression levels can help to balance flux and prevent buildup of intermediates, but as the number of enzymes in a pathway increases, the potential design space dramatically increases, and combinatorial assessment becomes intractable without high-throughput assembly and screening processes. Metabolite-responsive control methods offer a more rational approach to balancing metabolic flux. Metabolite-responsive promoters can control production of downstream enzymes so that the cell produces more enzymes as substrates accumulate[45,46]. However, since this approach requires the presence of a regulator that responds to the target metabolite, it is limited to pathways that have transcription factors that respond to pathway intermediates.

Engineering cells to not just produce pigments but to *selectively* produce certain pigments in response to *specific* inputs poses even further engineering challenges. Sensor cells must be able to produce visible pigment in a reasonable time period, but more importantly, they must maximize selectivity of pigment production so that only the desired pigment is produced[47]. For such an application, cells must be able to flexibly respond to different signals and then tightly control cell output to fully repress metabolic flux through competing pigment pathways. Previous metabolic engineering work has demonstrated the difficulty of fully repressing pigment production: when the lycopene production pathway

was controlled by an inducible promoter, lycopene yields were higher when cells were grown *without* the inducer, meaning that enough baseline protein was produced to catalyze lycopene production in the uninduced state[40].

Dynamic metabolic control strategies have been successfully used to separate cell growth and metabolite production phases[48,49], but these have primarily focused on maximizing final overall yields (rather than response selectivity). Metabolite valves redirect metabolic flux from central carbon metabolic pathways to competing production pathways[50,51], and effectively shift the bulk of metabolic flux upon recognition of a target molecule. However, these still permit some baseline expression through competing pathways, which can actually be beneficial for overall performance. For situations where complete control of metabolic flux is required (such as a pigment-based biosensor), this minimal leakage can lead to visible levels of pigment production that can completely confound sensor interpretation.

In previous work developing a responsive sensor, our group has demonstrated the difficulty of using pigmented metabolites as outputs and has also begun to develop engineering tools to harness metabolism for sensor output. We used a zinc-responsive promoter to control production of CrtY, a single enzyme that converts lycopene to β-carotene, and found that uninduced, baseline expression of CrtY converted all lycopene to β-carotene, preventing a lycopene-only state. A combination of translational and post-translational control was necessary to compensate for leaky expression and enable discretely red and orange sensor cells[25]. Creation of a field-deployable zinc sensor requires

even more complex regulatory systems, and will likely require layered regulation to precisely control pigment production.

1.5 Cell-free expression systems for diagnostic applications

While whole biosensors have the potential to meet many of the ASSURED requirements for point-of-care tests, a cell-free device has the potential to be even more field-friendly. Cell-free expression (CFE) systems use bacterial proteins, rather than whole cells, for protein production. Removing the cell membrane creates an open system, giving the user more control over substrate addition and reaction conditions. It additionally removes the requirement for cell survival and growth, enabling better allocation of resources to target protein production.

Cell-free systems have been increasingly used in biotechnology for high-yield protein production, circuit characterization, and metabolic pathway prototyping. Cell-free systems can be classified into two general categories: those made with purified protein components[52-54] and those made with crude cell lysate[55,56]. Both types of systems are commercially available from scientific vendors, but limitations in yield, volume, reaction rate, and cost per reaction have motivated exploration of different extract preparation methods.

Cell-free expression systems that use crude cell lysate have been created with protein extract from a wide variety of cell types, including bacterial cells, rabbit reticulocytes, insect cells, and wheat germ cells[57]. For expression of most proteins, bacterial-based cell-free systems are the preferred choice, as they have the highest protein yields, the shortest preparation time, and the lowest production costs. While *E. coli* is the

most commonly used bacterial strain for lysate production, other bacterial species have recently been used for extract preparation in efforts to decrease extract production time, increase protein yield, and increase extract robustness and versatility[58-60]. Eukaryotic cell extracts are useful for producing proteins that are insoluble in bacterial systems or proteins that require post translational protein modifications such as glycosylation. Of the eukaryotic expression systems, wheat germ extract has been the most widely studied and has the highest protein yield, but the extract preparation method is quite time consuming, and protein yields are still lower than what can be achieved using bacterial extracts[57].

All bacterial extract preparation methods follow the same general process, with modifications based on the target application. Bacterial strains optimized for protein expression are grown in rich media and isolated in exponential phase. Cells are then lysed, and lysate is centrifuged to remove the cell wall and genomic DNA. Effective cell lysis is critical to obtaining high lysate function and protein yields. Homogenizers have traditionally been used in extract preparation[61], but high equipment cost and variability has motivated exploration of alternative systems, such as bead beating[62] and sonication[63]. For all methods, it is critical to achieve an energy-input optimum to fully lyse cells without deactivating enzymes. Subsequent lysate incubation and dialysis can increase expression from native bacterial promoters[64].

Once the cell lysate is prepared, protocols for running cell-free reactions are similar. The most widely used expression protocols require addition of components that mimic the physiological conditions of the bacterial cytoplasm, through addition of salts, energy sources, and crowding reagents[65]. The final reactions consist of protein extract, the plasmid encoding the target proteins or regulatory elements, nucleotide triphosphates, amino acids,

tRNA, crowding reagents, cofactors, and a high-energy phosphate source, such as phosphoenolpyruvate (PEP) or 3-phosphoglycerate (PGA).

Beyond fast protein production, a primary advantage of bacterial cell-free systems is their utility in rapid prototyping. Implementing circuits in whole-cell systems generally requires cloning all genes and regulatory elements onto the same plasmid and then varying promoter and RBS strengths are varied to tune relative expression. Combinatorial exploration of expression levels thus requires cloning dozens or even hundreds of constructs. In cell-free reactions, relative protein expression levels can be easily modulated through gene dosage (adding different relative amounts of each plasmid), which eliminates the need for extensive cloning and thus facilitates rapid testing of complex circuits[66-68]. To make this process even faster, linear DNA can be used instead of plasmids[69], which further reduces the design-build-test cycle from multiple days (for standard cloning procedures) to under eight hours[70]. Similar approaches can be used to prototype metabolic pathways in a high-throughput fashion, which can then inform bacterial strain design for metabolic engineering applications[71,72].

Cell-free systems have already been used to create diagnostic tools with global heath applications: RNA-based cell-free sensors rapidly detect Ebola and Zika viruses[15,16], and related CRISPR-based diagnostics detect pathogens with attomolar sensitivity[73-75]. Allosterically regulated transcription factors[15,76,77] and riboswitches[78] can also control output in cell-free systems, potentiating the expansion of cell-free diagnostics to diseases and conditions that require assessment of diverse types of biomarkers.

1.6 Contribution of this thesis

In this dissertation, I develop methods to quantify biomarker levels in an equipment-free fashion using bacterial-based biosensors. I create tunable whole-cell and cell-free sensors that produce different colored outputs based on biomarker concentration. Tests semi-quantitatively measure biomarkers in real human serum, and test interpretation is as easy as reading a litmus test. I create a complete system for diagnosis of zinc deficiency and show that the diagnostic platform can be easily expanded to quantify other clinically-relevant biomarkers.

CHAPTER 2. ENGINEERING PIGMENTS FOR USE AS REPORTER OUTPUTS

Portions of this chapter are reproduced from my publication "Precise control of lycopene production to enable a fast-responding, minimal-equipment biosensor"[79] in *Metabolic Engineering*.

2.1 Introduction

The use of pigments as biosensor readouts holds great promise for emerging biosensor applications. When substituted for widely-used fluorescent reporters, pigment readouts can be interpreted without advanced equipment because they are visible to the naked eye, making them useable even in resource-poor settings. While there have been isolated examples of the use of colors as biosensor readouts[15,16], this approach is yet to be widely adopted.

One would expect the use of pigmented reporters to be a straightforward task given the breadth and depth of knowledge about pigment biosynthesis. Pigmented molecules are a common metabolic engineering target, whether due to their intrinsic value, their value as precursors, or just as a testbed for metabolic engineering techniques that enable simple screening[29,30,33,34,80]. However, using metabolites as reporters requires more precise control than what is necessary for most metabolic engineering applications, since small amounts of enzyme can produce visible amounts of pigment and overproduction of certain metabolites can be toxic to the cell.

In our group's previous work towards a whole cell-biosensor for zinc assessment, we engineered cells that produce one of three pigmented metabolites—violacein (purple), lycopene (red), or β-carotene (orange)—based on extracellular zinc concentrations[25,26]. In our initial zinc sensor prototype, the sensor cells always produced some pigment, a design selected for simplicity and to minimize ambiguity in readouts. However, this approach necessitates that the cells be grown from a very small inoculum so that coloration due to initial cell mass is minimal – thus requiring overnight assay times. To make the device more field-friendly, an important goal is to reduce the assay's time to coloration, which we are attempting to do by engineering cells that completely repress pigmentation during growth and quickly produce the appropriate pigment upon induction. This will enable sample addition to concentrated pre-cultured cells, making time to coloration only dependent on pigment production rates rather than coupled to the time required to grow a sufficiently large mass of cells.

In our previous work, we focused on the widely-studied and widely-engineered carotenoid pathway, which produces the red pigment lycopene. Overproduction strategies — including gene knockouts[36,39,81], precursor supplementation[40-42,82-84], and dynamic regulation of pathway genes[38,85] — have greatly improved lycopene yields and titers in previous metabolic engineering efforts. However, to use lycopene as a reporter in a biosensor, the primary goal must shift from maximizing yields and titers to maximizing response specificity.

To be effectively used as reporters, pigment production must be able to be turned completely off and on based on the state of the system. Here, we aimed to completely repress pigment production before inducing the biosynthetic pathway for downstream

biosensor readout. Previous metabolic engineering work has demonstrated the difficulty of fully repressing lycopene production – a goal that is critical for biosensing applications. When the enzymes that produce lycopene were expressed from an IPTG-inducible promoter, high lycopene yields and titers were achieved without any IPTG induction, meaning that enough protein was produced even in the uninduced state to catalyze lycopene production[40]. In fact, IPTG induction actually reduced both cell growth and lycopene production, proposed to be due to toxicity effects. Since maximum pigment production does not correspond with maximum protein production, precise control of the induced expression level is thus necessary to completely control pigment production.

To deal with the known difficulties in controlling lycopene production, we sought to investigate the abilities of different transcriptional and translational control mechanisms to enable both complete repression of lycopene when uninduced as well as fast production of visible amounts of lycopene upon induction. We chose to explore three commonly used promoter systems — the Lac, Ara, and T7 systems — that are all considered very inducible (at least in terms of dynamic range) but have varying levels of uninduced leaky expression, though Ara is widely considered to be tightly repressible and not leaky[86,87]. We sought to characterize the levels of unwanted protein expression in these promoter systems and reduce this unwanted expression by manipulating *cis* regulatory elements. Once systems were developed that could fully repress lycopene, we compared the time to response of the three different promoter systems. Finally, we explored the effect of metabolic precursor supplementation on the time to visible lycopene production upon induction.

This chapter presents approaches that ultimately enabled full repression of lycopene in the absence of an inducer while also enabling production of visible amounts of lycopene

within two hours of induction, a reduction of over an order of magnitude compared to the previously reported strategy. Promoter engineering, RBS strength modification, and pathway engineering were all explored, and the effectiveness of each approach is evaluated.

2.2 Materials and Methods

2.2.1 Materials

T4 DNA ligase, T5 exonuclease, Taq ligase, Phusion polymerase, Q5 polymerase, and restriction endonucleases were purchased from New England Biolabs (Ipswich, MA, USA). E.N.Z.A. Plasmid Mini Kits were purchased from Omega Bio-tek (Norcross, GA, USA), and QIAquick PCR Purification Kits and QIAquick Gel Extraction Kits were purchased from QIAGEN (Valencia, CA, USA). A lycopene standard was purchased from Millipore Sigma (St. Louis, MO). Sudan I (95%) was purchased from TCI America (Portland, OR, USA).

2.2.2 Strains and plasmids

Escherichia coli K-12 DH10B (New England Biolabs, Ipswich, MA) was used for plasmid assembly and for all protein and metabolite production. The plasmid pSB3T5, with a p15A origin, was taken from the Standard Registry of Biological Parts. To better enable colony selection based on antibiotic resistance during construct assembly, we made variations of the pSB3T5 plasmid by replacing the tetracycline resistance gene with either a kanamycin or chloramphenicol resistance gene. Consistent protein expression across plasmids was verified with fluorescence (data not shown), and these plasmids were used

for all heterologous protein production. The plasmid pSB6A1, which is a derivative of the pBR322 plasmid, was obtained from the Standard Registry of Biological Parts and used for expression of the mevalonate genes.

2.2.3 Cloning and construct assembly

All constructs were assembled with either Gibson assembly[88] or restriction endonuclease digestion of components and subsequent ligation and transformation following the BioBricks idempotent standard assembly[89]. For fluorescent characterization, *mRFP* was obtained from the Registry of Standard Biological Parts (bba_E1010), and the barcode downstream of the coding sequence was removed. The genes *crtE*, *crtB*, and *crtI* were amplified from Part bba_k274100 of the Registry of Standard Biological Parts and were originally isolated from *Pantoea ananatis*.

Mevalonate pathway experiments used genes from the plasmid pJBEI-6409[83], which was obtained from Addgene (Cambridge, MA, USA). Mevalonate pathway genes were amplified from this plasmid, a ribosomal binding site with a putative translation rate of 500 as determined by the RBS calculator[90] was added to each gene, and genes were placed under control of the arabinose-inducible promoter pBad and cloned into the plasmid pSB6A1.

2.2.4 Promoter Assembly

The promoters P_{Bad} (bba_I0500) P_{Lac} (bba_R0011) were obtained from the Registry of Standard Biological Parts and used as templates for promoter modifications. P_{Lac} is a P_{λ} -based promoter with two operator sites for LacI repression. $P_{Lac,weak}$ was purchased as a

gene fragment from IDT (Coralville, IA). $P_{Lac,weak,2}$ was assembled by adding an additional lac operator site to $P_{Lac,weak}$ through Gibson assembly. All T7 promoters were assembled with Gibson assembly. The T7 RNA polymerase was taken from the Registry of Standard Biological Parts (bba_K145001) and placed under control of $P_{Lac,weak}$. In all Lac-controlled constructs, LacI was constitutively expressed from the promoter $P_{\lambda r}$ (bba_R0051).

2.2.5 Cell culture

For RFP expression, freshly transformed DH10B colonies were inoculated in triplicate into 5 mL LB medium and grown at 37°C and 180 rpm for 18 hours. 1 μL of each culture was then added to 150 μL of medium containing the appropriate concentration of inducer (either IPTG or arabinose) in a 96-well plate, and the plate was incubated at 37°C and 180 rpm for 18 hours and then analyzed. For time course fluorescence experiments, 15 μL of overnight cultures was added to 135 μL of fresh media, and plates were incubated in a Biotek Synergy H4 plate reader at 37°C with medium-strength shaking and analyzed every 20 minutes.

For lycopene expression, freshly transformed DH10B colonies were inoculated in triplicate into 5 mL LB medium containing the appropriate inducer and grown at 37°C and 180 rpm for 18 hours. For time-course experiments, overnight cultures were diluted to an OD of 0.15 in 50 mL of fresh medium, the appropriate inducer was added, and the sample was aliquoted into culture tubes corresponding to different time points. OD and lycopene content were measured at the time of inoculation, every hour for six hours, and at 18 hours.

LB medium composed of 10 g/L NaCl, 5 g/L yeast extract, and 10 g/L tryptone was

used in all experiments. Either IPTG or arabinose was used for induction, and the following antibiotics were used for appropriate selection: tetracycline (15 μg/mL), chloramphenicol (33 μg/mL), kanamycin (30 μg/mL), and carbenicillin (100 μg/mL).

2.2.6 Measurement of optical density and fluorescence

Optical density of samples was quantified by measuring the absorbance at 600 nm either in a ThermoFisher Genesys 20 spectrophotometer with a 10 mm path length or in a Biotek Synergy H4 plate reader. 1 mL of culture was used for spectrophotometer measurements, and 150 μL of culture in a 96 well plate was used for plate reader measurements. Calibration curves were made for each instrument and used for uniform reporting of optical density. All optical densities reported correspond with those taken in the spectrophotometer. For RFP quantification, fluorescence at 585 nm excitation and 610 nm emission was measured on a Biotek Synergy H4 plate reader. All reported fluorescence values are background-subtracted and normalized to optical density.

2.2.7 Lycopene extraction and HPLC analysis

Either 250 μL, 500 μL, or 1 mL of bacterial culture was pelleted at 18,000 rcf for 5 minutes. Cell pellets were resuspended in 50 μL of ultrapure water. Lycopene was extracted with 1 mL of acetone at 50°C for 20 minutes. A heat block was used to maintain temperature, and extractions were vortexed every 5 minutes. Cellular debris was pelleted at 18,000 rcf for 5 minutes, and 500 μL of supernatant was removed for analysis. Sudan I was used as an internal standard[91] and added to the acetone used for extractions at a concentration of 1 μg/mL.

All HPLC analysis was conducted on a Shimadzu Prominence UFLC using an Agilent C18 4.6 mm x 50 mm column with a 5 μm particle size and a Shimadzu photodiode array detector. A solvent ratio of 50:30:20 acetonitrile:methanol:isopropanol was used as the mobile phase[92] and run at a flow rate of 1 mL/min with a 25 μL sample injection volume. Absorption was detected at 471 nm. Retention times and peak intensities were compared to analytical standards spiked into control extractions from DH10B cells, and the internal standard Sudan I was used to account for acetone evaporation during the extraction protocol and for instrument drift.

2.3 Results

2.3.1 Standard inducible promoter systems cannot repress lycopene production

Three inducible promoter systems were tested for their ability to control lycopene production: P_{Lac}, P_{Bad}, and P_{T7}. The promoter P_{Lac} is a synthetic P_{λ}-based promoter with two operator sites for LacI repression, and the promoter P_{Bad} was originally isolated from the *E. coli* genome. LacI was constitutively expressed from the promoter $P_{\lambda r}$, and AraC was expressed from its native promoter that promotes transcription in the opposite direction of P_{Bad}. To confirm the inducibilty of P_{Bad} promoters, each was used to control RFP production (Figure 3A). The P_{Lac} and $P_{Bad,weak}$ systems were then used to control the *crtEBI* genes, which code for the enzymes that produce lycopene. Successful clones of the P_{T7} system controlling *crtEBI* could not be isolated, which may have been due to toxicity caused by higher baseline levels of *crtEBI*.

In both the P_{Lac} and P_{Bad} systems, cells had clearly visible lycopene production when no inducer was present (Figure 3B). The P_{Bad} system had a significant increase in

lycopene production at $1x10^{-4}$ percent arabinose, but lycopene production decreased with further addition of inducer. The P_{Lac} system had consistent specific lycopene production at all inducer concentrations, though with an insignificant downward trend (Figure 3C). Both promoter systems exhibited reduced cell growth with addition of inducer: compared to the uninduced state, fully induced cultures had 50% fewer cells with P_{Bad} -regulated lycopene production and 98% fewer cells with P_{Lac} -regulated lycopene production (Figure 3D). DH10B cells with negative control P_{Lac} and P_{Bad} vectors showed only slight decreases (about 15%) in terminal OD when fully induced and produced no detectable lycopene.

Inability to repress lycopene and cell toxicity upon lycopene induction is consistent with previous reports of *crtEBI* expression from a Lac-inducible promoter[40]. These limitations and constraints pose a significant challenge to using lycopene as a reporter, motivating efforts to engineer more repressible promoter systems.

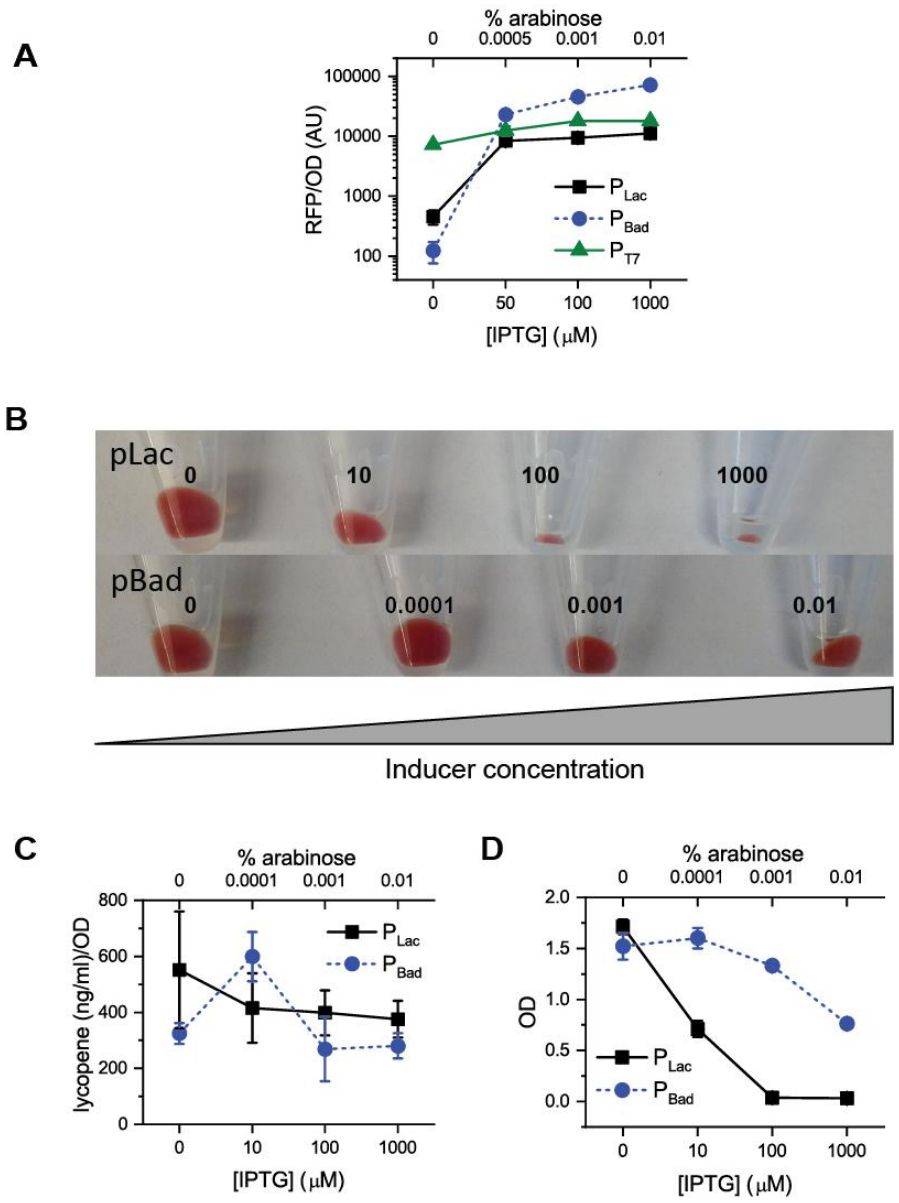

Figure 3: Standard inducible promoters cannot adequately control lycopene production.

(A) Inducibility of P_{Lac}, P_{Bad}, and P_{T7} promoters. Normalized RFP production from the P_{Lac}, P_{Bad}, and P_{T7} promoters when induced with varying concentrations of IPTG (P_{Lac} and P_{T7}) or arabinose (P_{Bad}). Error bars represent standard deviation. (B) Cells expressing *crtEBI* from either P_{Lac} or P_{Bad} that were grown for 18 hours in different concentrations of inducer. P_{Lac} (top) and P_{Bad} (bottom) show visible lycopene production in the uninduced state. Terminal cell densities decrease with increasing inducer concentration, and cells in all states are visibly red. Numbers correspond to μM of IPTG for P_{Lac} and % arabinose (w/v) for P_{Bad}. (C) Lycopene production normalized to cellular density. P_{Lac}-regulated production is constant at all concentrations of IPTG. P_{Bad}-regulated production increases only at 0.0001%

arabinose. (D) Optical density at 18 hours of cultures with *crtEBI* expressed from either P_{Lac} or P_{Bad}. Cell density decreases with increasing concentration of inducer. All error bars represent standard deviation.

2.3.2 Promoter engineering decreases leaky protein expression

Variants of three common promoter systems—Lac, Ara, and T7—were constructed with the goal of decreasing lycopene production in the uninduced state. The P_{Lac} and P_{Bad} promoters used previously were modified to create weaker versions by changing the -10 and -35 σ_{70} RNAP binding domains to those of J23113, a very weak promoter. An additional P_{Lac} variant was constructed by adding a third operator site for LacI downstream of the -10 RNAP binding domain. T7 promoter variants were built by adding operator sites for LacI downstream from the consensus T7 sequence. In all T7 constructs, T7 RNA polymerase was expressed on the same plasmid from the Lac-inducible promoter $P_{Lac,weak}$. Table 1 contains the description and sequences for all promoters constructed.

Table 1: Description and sequences of inducible promoters tested.
The -10 and -35 RNAP binding domains for P_{Lac} and P_{Bad} variants and the T7 RNAP consensus sequence for the P_{T7} variants are highlighted in bold. Operator sites for LacO are underlined.

Promoter	Description	Sequence
P_{Lac}	promoter with -10 and -35 elements from λ phage and 2 operator sites for LacI	AATTGTGAGCGGATAACAA**TTGACAT**TGTGAGCGG ATAACAA**GATACT**GAGCACA
$P_{Lac,weak}$	modified P_{Lac} with weak -10 and -35 elements from J23113	AATTGTGAGCGGATAACAA**CTGATGG**TGTGAGCGG ATAACAA**GATTAT**GAGCACA

Table 1, continued

$P_{Lac,weak,2}$	modified $P_{Lac,weak}$ with additional operator site for LacI downstream from -10 site	AATTGTGAGCGGATAACAA**CTGATGG**TGTGAGCGGATAACAA**GATTAT**GAGCACAAATTGTGAGCGGATAACAA
P_{Bad}	standard P_{Bad} promoter	ACTTTTCATACTCCCGCCATTCAGAGAAGAAACCAATTGTCCATATTGCATCAGACATTGCCGTCACTGCGTCTTTTACTGGCTCTTCTCGCTAACCAAACCGGTAACCCCGCTTATTAAAAGCATTCTGTAACAAAGCGGGACCAAAGCCATGACAAAAACGCGTAACAAAAGTGTCTATAATCACGGCAGAAAAGTCCACATTGATTATTTGCACGGCGTCACACTTTGCTATGCCATAGCATTTTTATCCATAAGATTAGCGGATCCTAC**CTGACG**CTTTTTATCGCAACTCTC**TACTGT**TTCTCCATACCCGTTTTTTTGGGCTAGC
$P_{Bad,\ weak}$	modified P_{Bad} with weak -10 and -35 elements from J23113	ACTTTTCATACTCCCGCCATTCAGAGAAGAAACCAATTGTCCATATTGCATCAGACATTGCCGTCACTGCGTCTTTTACTGGCTCTTCTCGCTAACCAAACCGGTAACCCCGCTTATTAAAAGCATTCTGTAACAAAGCGGGACCAAAGCCATGACAAAAACGCGTAACAAAAGTGTCTATAATCACGGCAGAAAAGTCCACATTGATTATTTGCACGGCGTCACACTTTGCTATGCCATAGCATTTTTATCCATAAGATTAGCGGATCCTAC**CTGATGG**TTTTTATCGCAACTCTC**GATTAT**TTCTCCATACCCGTTTTTTTGGGCTAGC
P_{T7}	standard T7 promoter	**TAATACGACTCACTATAGG**
P_{T7LacO}	standard T7 promoter with one downstream operator site for LacI	**TAATACGACTCACTATAGG**AATTGTGAGCGGATAACAA
$P_{T7LacO2}$	standard T7 promoter with two downstream operator sites for LacI	**TAATACGACTCACTATAGG**AATTGTGAGCGGATAACAAGATTATAATTGTGAGCGCTCACAATT

Each promoter was used to control RFP, and fluorescence was measured in both the uninduced and fully induced states (Figure 4A). Decreasing the strength of the RNA polymerase binding domains reduced uninduced protein expression by about an order of

magnitude in both the Lac and Ara systems. Addition of operator sites for LacI reduced uninduced protein expression in the T7 system by orders of magnitude but had no significant effect on uninduced protein expression from $P_{Lac,weak,2}$ compared to $P_{Lac,weak}$.

Modifications to P_{Bad} made the promoter both more repressible and increased its dynamic range. P_{Bad} is already considered one of the most repressible promoters, and $P_{Bad,weak}$ is over 30 times more repressible than P_{Bad}. Despite this dramatic difference, induced expression from pBad was only 3 times higher than from $P_{Bad,weak}$, which is likely because AraC recruitment of RNA polymerase largely compensates for the polymerase's decreased affinity for the -10 and -35 RNAP binding domains. $P_{Bad,weak}$ has a dynamic range of over 5000, which is over ten times greater than any of the other promoters characterized.

The most repressible promoter from each category was tested for its ability to repress lycopene (Figure 4B and Figure 4C), and lycopene repression and induction generally did not follow the fluorescent induction trends in Figure 3A. $P_{Bad,weak}$ enabled repression and induction of lycopene, a marked improvement over P_{Bad}'s constitutive expression of lycopene. However, when uninduced, cells with *crtEBI* controlled by $P_{Bad,weak}$ still had slight, but visible, lycopene production. Cells with *crtEBI* controlled by $P_{Lac,weak}$ and $P_{T7LacO2}$ had obviously visible lycopene in the uninduced state, no change in OD normalized lycopene production with induction, and visible reductions in cell growth upon induction. Though promoters were engineered to be 10 times more repressible than commonly used inducible promoters, only one ($P_{Bad,weak}$) was able to repress lycopene production, and even then the repression was incomplete.

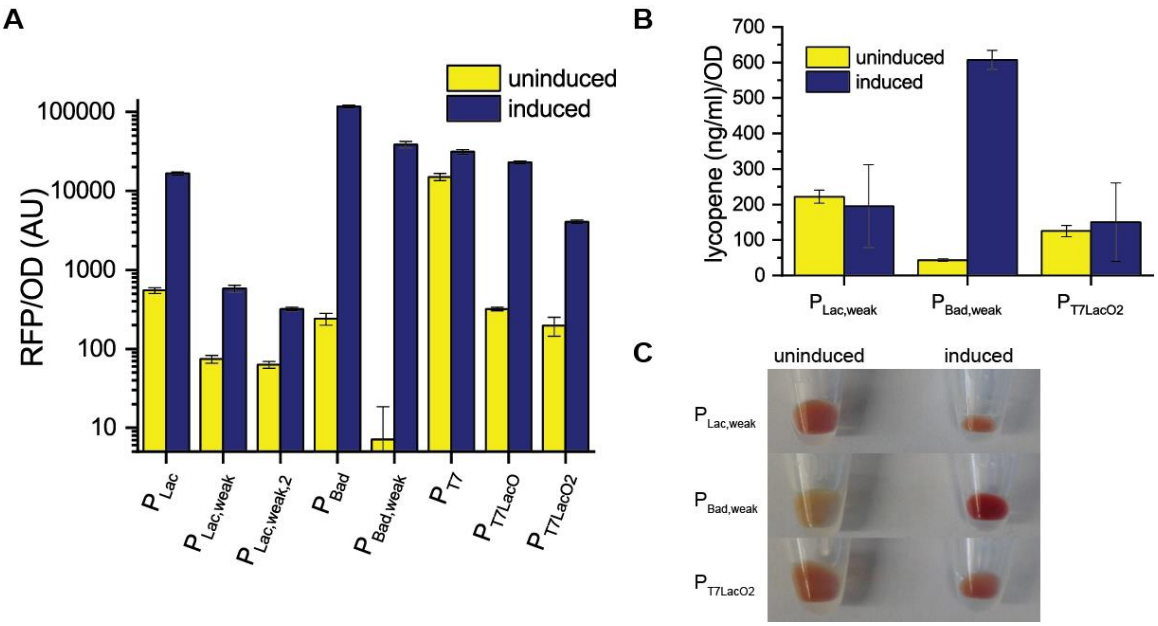

Figure 4: Discrepancy between fluorescent protein production and lycopene production from engineered promoter systems
(A) Normalized RFP production from the variants of the Lac, Ara, and T7 promoter systems described in Table S1. (B) Lycopene concentration normalized to cellular density. The most repressible promoter systems were used to control *crtEBI*, and lycopene was quantified. Only $P_{Bad,weak}$ shows increased lycopene production with induction, likely due to $P_{Bad,weak}$'s very low levels of uninduced protein expression. (C) Cells expressing *crtEBI* from either $P_{Lac,weak}$, $P_{Bad,weak}$, or $P_{T7LacO2}$. Cells were grown for 18 hours with or without inducer. In the uninduced state, $P_{Bad,weak}$ is the least colored, but still produces visible amounts of lycopene. In all experiments, cells were induced with either 1 mM IPTG (for the P_{Lac} and P_{T7} constructs) or with 0.01% (w/v) arabinose (for the P_{Bad} constructs). All error bars represent standard deviation.

2.3.3 Qualitative and quantitative evaluation of visible lycopene

Since the goal of our work is to have colorless cells that can be induced to be clearly colored, we needed to carefully consider our definition of what qualifies as "colorless" and "red". For example, is the uninduced lycopene production of $P_{Bad,weak}$ in Figure 4C sufficiently low to call it colorless? To minimize potential subjectivity, we set thresholds for lycopene visibility based on the OD normalized lycopene concentration of cells considered universally "colorless" and universally "red" in a survey that asked 10 different

people to match the perceived "redness" of ten different samples to different colors on a spectrum (Figure 5). The lycopene levels of samples unanimously considered either "colorless" or "red" were then set as the thresholds: samples with OD normalized lycopene concentrations < 10.6 (ng/mL)/OD are considered colorless, and samples with OD normalized lycopene concentrations > 195 (ng/mL)/OD are considered fully red. These thresholds will likely have to be adjusted to fit the final form factor of a biosensor device, since the media used (ie: LB vs. M9), culture volume, and cell density all affect the apparent "redness" of a sample, even if the lycopene concentration values are the same. However, these thresholds are useful for evaluating the effects of different genetic modifications and will be used throughout this work to quantify lycopene visibility.

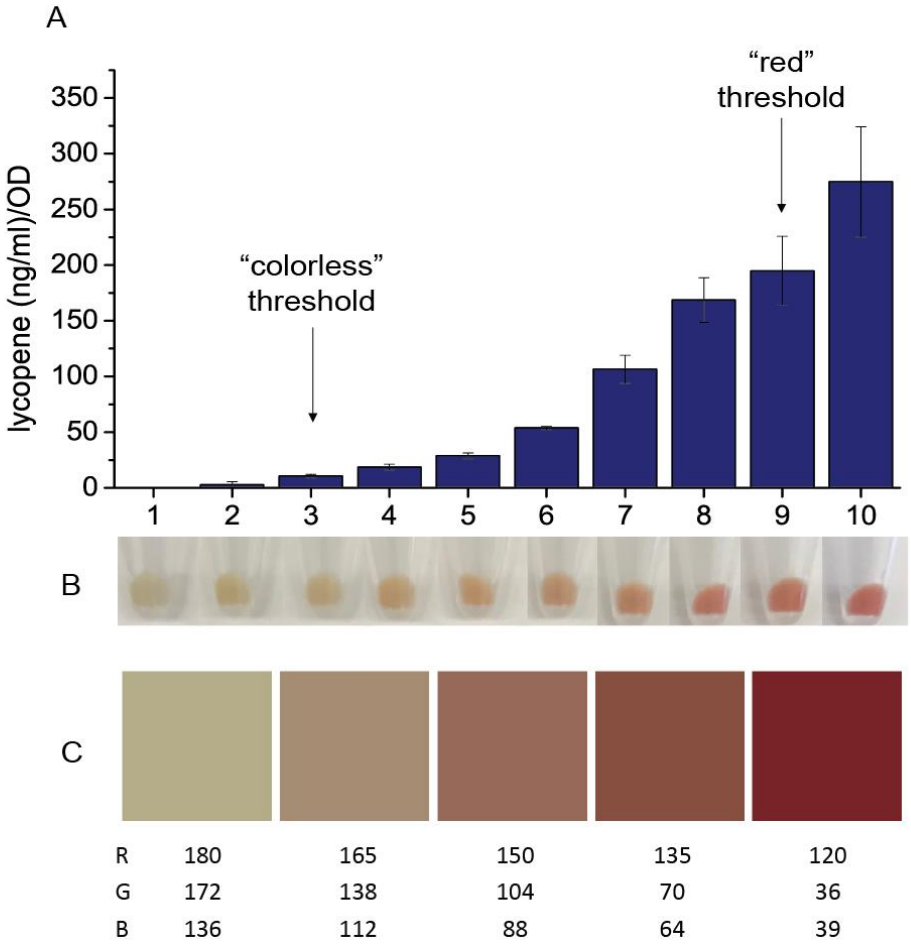

Figure 5: Evaluation of "colorlessness" and "redness" in cells producing different amounts of lycopene.
Ten strains expressing different levels of lycopene (A and B) were presented to ten different people one at a time in a random order, and each person was asked to match the perceived "redness" of each sample to different colors on a spectrum (C). The "red" end of the spectrum was set as the color of the cells expressing P_{Lac} *crtEBI* (Figure 3A) using the image shown and RGB quantification, and the "white" end of the spectrum was set as the color of DH10B cells alone. Three RGB intermediates were then linearly interpolated evenly over the "red" and "white" colors. All people polled said that samples 9 and 10 matched the furthest red end of the spectrum and that samples 1-3 matched the furthest white end of the spectrum. The lycopene values of samples 3 and 9 were thus set as the thresholds for colorless and red, respectively: Samples with OD normalized lycopene concentrations < 10.6 (ng/mL)/OD are considered colorless, and samples with OD normalized lycopene concentrations > 195 (ng/mL)/OD are considered fully red.

2.3.4 Reduced RBS strength enables full lycopene repression and proper induction

Since rational promoter engineering was unable to prevent unwanted lycopene production, reduction in ribosomal binding site (RBS) strength was explored as another way to decrease uninduced protein expression. The *crtEBI* genes used here have been widely used elsewhere; they were originally taken from the Registry of Standard Biological Parts (bba_k274100) and already contained RBSs that were added to create a composite part. The RBS calculator[90] was used to determine the strength of the RBS on each gene, and the predicted strengths were comparable (on the same order of magnitude) to the predicted strength of bba_B0034 (B34), a commonly used strong RBS from the Registry of Standard Biological Parts. Since a strong RBS amplifies the effect of any unwanted transcription, reduction in RBS strength was considered a viable option for reduction of unwanted protein. As an initial proof of principle, repressible promoter systems were used to control RFP production with weaker RBSs, which reduced uninduced fluorescence to below the level of detection (Figure 6A), thus supporting RBS strength reduction as a viable strategy for reducing unwanted protein and pigment production.

RBSs with a range of strengths were then tested for their ability to control lycopene production. Operons were assembled with a promoter from each group controlling the *crtEBI* genes with either the medium strength RBS bba_B0032 (B32) or the weak RBS bba_B0033 (B33) on all genes. The most repressible promoter from each group was chosen to control *crtEBI*, with the exception of the P_{Lac} variants: P_{Lac} was used for testing instead of $P_{Lac,weak}$ or $P_{Lac,weak,2}$ because of their very low dynamic ranges (less than 10). Cells were grown with different concentrations of inducer from small inocula, and levels of lycopene were determined both quantitatively and qualitatively after 18 hours. With RBSs of B32 and B33 on the *crtEBI* genes, cells contained no visible lycopene when uninduced

(lycopene < 10.6 (ng/mL)/OD) and produced increased amounts of lycopene with addition of inducer. $P_{Bad,weak}$ and $P_{T7LacO2}$ with the RBS B32 had the greatest dynamic ranges, maintaining white cells when uninduced and dark red cells (lycopene > 450 (ng/mL/OD) at full induction (Figure 6B, Figure 6C).

When a strong RBS is on the *crtEBI* genes, the P_{Lac} and $P_{T7LacO2}$ systems are unable to induce lycopene production. These samples also have a lower final cell density, which suggests that overproduction of the CrtEBI proteins, lycopene, or an intermediate metabolite places some stress on the cell that reduces cell growth and prevents further lycopene production. In the $P_{T7LacO2}$ system with a strong RBS and to a lesser extent in the P_{Lac} system with the medium-strength RBS, lycopene production increases with partial induction (10 μM IPTG) but then decreases with further induction. This peak at low levels of induction, combined with decreased cell growth at higher induction levels further supports that overproduction of lycopene can be toxic to the cell.

The induction profiles of RFP and lycopene showed notable differences. Though maximum RFP production varied by orders of magnitude across promoter systems (Figure 6A), maximum lycopene production in all promoter systems was similar (~600 (ng/mL)/OD). Differences in maximum RFP production could be attributed to variations in either promoter strength or effective RBS strength within a promoter system. Because of such drastic variation in protein production from each system, as represented by RFP levels, it is surprising that maximum lycopene production is so similar across promoter systems. The comparable amounts of lycopene produced suggest that either fluorescent proteins are not adequate indicators of the amounts of CrtEBI proteins actually produced, or that there is an upper limit on the amount of lycopene that cells can accumulate, and

increased protein production does not necessarily correspond with increased lycopene production.

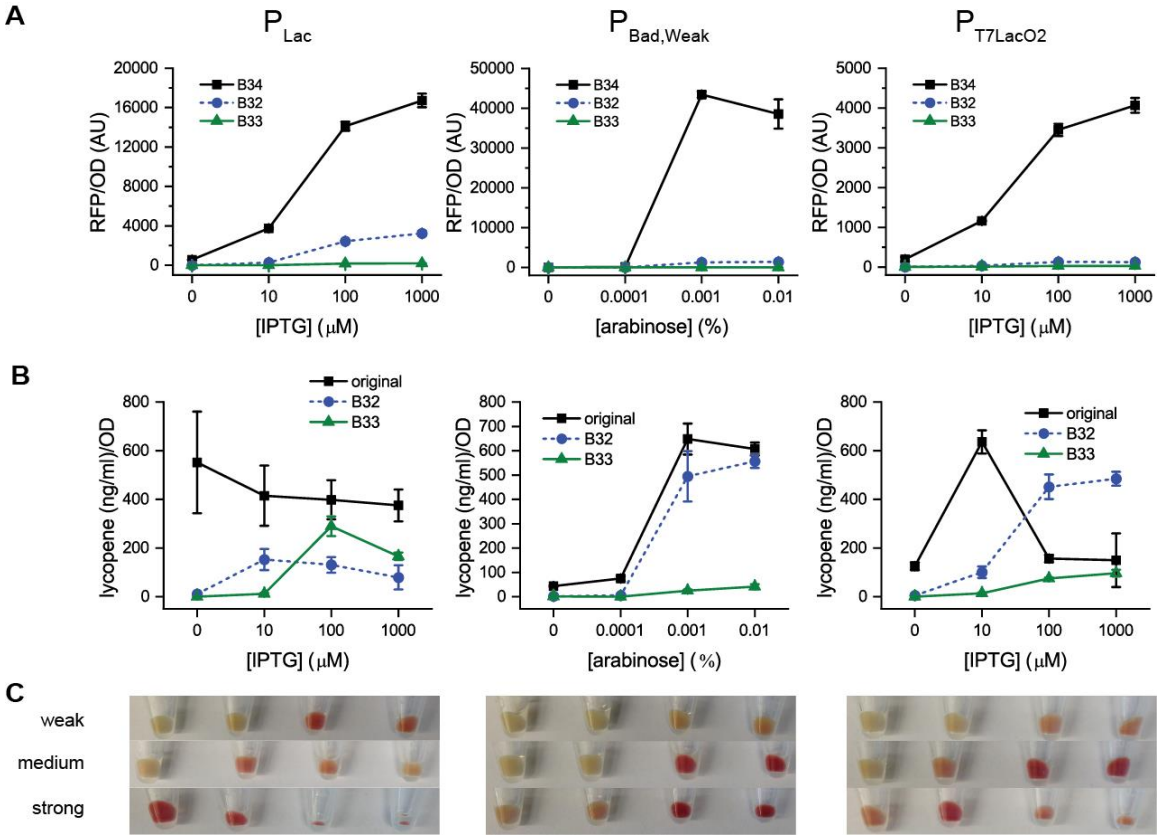

Figure 6: Effect of RBS strength on lycopene production across different promoter systems.
(A) Lycopene production from each promoter system with three different RBSs on the *crtEBI* genes: original (strong), B32 (medium), and B33 (weak). Weakening the RBS decreases uninduced lycopene production. The effect of RBS strength on induced lycopene production varies by promoter system. The P_{Lac} system has maximal lycopene production (in terms of dynamic range) when B33 is on the *crtEBI* genes, and the $P_{Bad,weak}$ and $P_{T7LacO2}$ systems has maximal dynamic range when B32 is on the *crtEBI* genes. Error bars represent standard deviation. (B) Cells expressing *crtEBI* with different RBSs and inducer concentrations. In all systems, when B32 and B33 were on the *crtEBI* genes, uninduced cells are colorless. The visible redness upon induction corresponds with the lycopene production in panel B.

2.3.5 The P_{Lac} system produces visible lycopene most quickly

By enabling full repression of pigment production, the time to visible pigmentation is determined by the rate of pigment production upon induction, rather than the time for growth of large numbers of cells. The RBS and promoter modifications were thus next tested for their time to lycopene production upon induction.

The three different promoter systems, each with the medium-strength RBS B32 on the *crtEBI* genes, were tested for their time to visible lycopene production upon induction. All systems reached the previously established threshold for visible lycopene within four hours, and the P_{Lac} system had slightly higher lycopene levels than the $P_{Bad,weak}$ and $P_{T7LacO2}$ systems at all time points (Figure 7A).

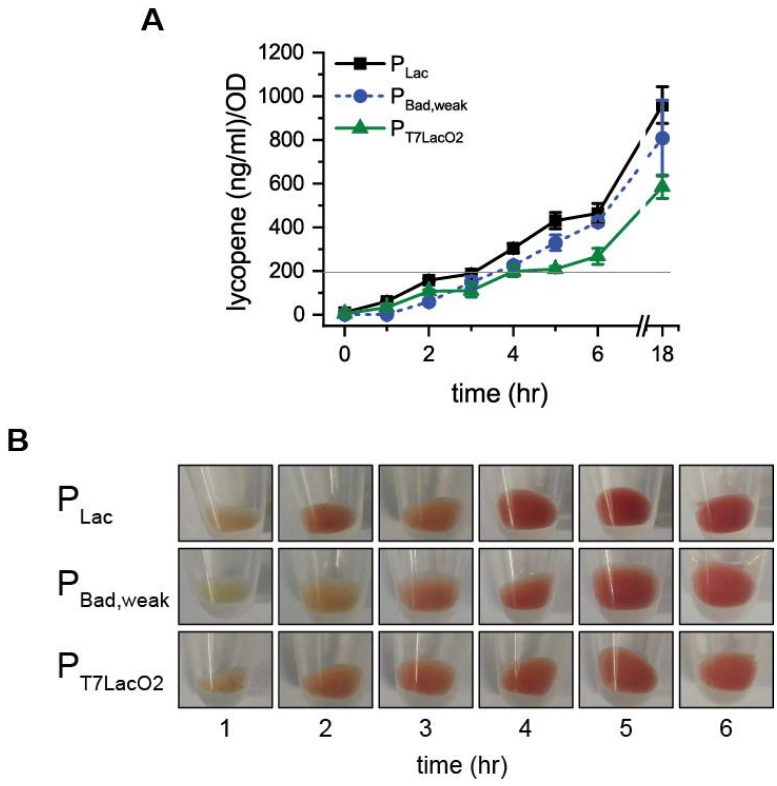

Figure 7: Time to response of three different promoter systems.
(A) Lycopene produced from each promoter system with respect to time. All systems reach the 195 (ng/mL)/OD threshold (marked with gray line) within four hours, and

the P_{Lac} system reaches it the most quickly. Error bars represent standard deviation. (B) Cells from each system at different time points.

The P_{Lac} system produced the most lycopene at all time points, with a final lycopene production of 950 (ng/mL)/OD (Figure 7A), ten times more than what was produced after 18 hours when a small inoculum was used (Figure 6B), which prompted exploration of the effects of different inoculum densities. Cultures were inoculated to starting optical densities between 0.01 and 0.4 and induced. Cultures inoculated with more cells had higher final lycopene levels, though the effects plateaued above an initial inoculum density of OD 0.05 (Figure 8). Cultures inoculated to optical densities above 0.05 all reached the threshold for visible lycopene at approximately the same time (Figure 8).

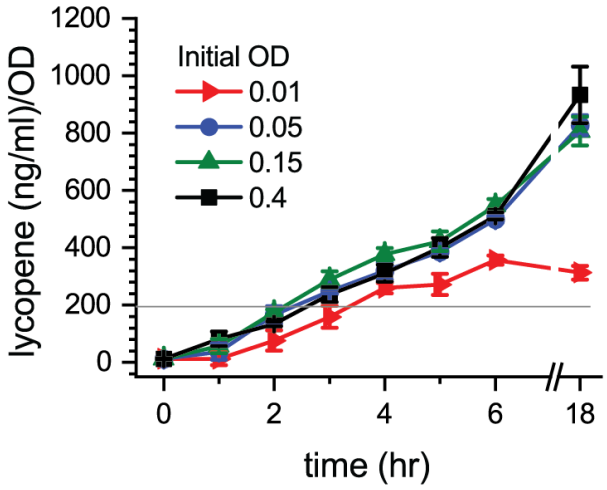

Figure 8: The effect of inoculation density on lycopene production.
Fresh media was inoculated with cells expressing *crtEBI* from P_{Lac} to different starting optical densities, and 1 mM IPTG was added. Cultures inoculated to an OD above 0.05 reached the threshold for visible lycopene production at approximately the same time (about 2.5 hours). The faster response time compared to other experiments (Figure 7) can be attributed to a decrease in the number of temperature excursions in the incubator during the experiment.

2.3.6 Precursor supplementation reduces time to visible lycopene

To attempt to further decrease the time to visible lycopene production, metabolic precursor supplementation was explored. Farnesyl diphosphate (FPP) is the substrate for CrtE, the first enzyme in the lycopene-production pathway, and FPP is produced by either the nonmevalonate (dxp pathway) or the mevalonate pathway. The dxp pathway naturally occurs in *E. coli*, and the mevalonate pathway can be heterologously expressed in *E. coli*. We have previously shown that addition of the mevalonate pathway increases end-point lycopene production by a factor of three[25], and we hypothesized that its addition could decrease the time to visible lycopene.

The fastest responding system (the P_{Lac} crtEBI system) was cotransformed with either a plasmid containing the mevalonate genes under P_{Bad} control (P_{Bad} -MEV) or an empty control vector (P_{Bad} ∅). P_{Bad} -MEV supplementation decreased the time to visible lycopene (lycopene > 195 (ng/mL)/OD) to about 1.5 hours (Figure 9A). Interestingly, the cells produced lycopene faster and produced more total lycopene when the mevalonate pathway was induced at the same time as the *crtEBI* pathway, rather than when the mevalonate pathway was induced during the growth stage to potentially accumulate precursors ready for induction of *crtEBI*. Of note, cells cotransformed with an empty vector had a longer time to visible lycopene production than when just the P_{Lac} crtEBI vector was transformed (about 5.5 hours compared to 3 hours), suggesting that maintenance of a second plasmid can significantly decrease pigment production from the first plasmid.

Though mevalonate supplementation decreased the time to visible lycopene, it also increased the amount of unwanted lycopene in the uninduced state. When P_{Bad} -MEV was induced in the growth stage, cells contained about 14 times more lycopene compared to cells without P_{Bad} -MEV, and even when P_{Bad} -MEV was repressed in the growth stage,

cells still contained over 3 times more lycopene, pushing the lycopene concentration just over the preferred threshold for colorless cells (Figure 9B).

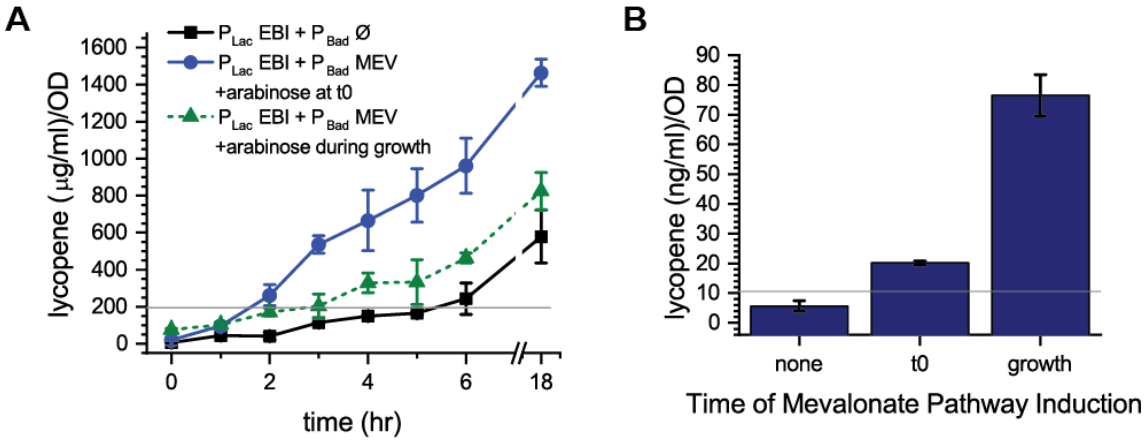

Figure 9: Effects of precursor supplementation on lycopene production.
(A) Normalized lycopene production from the P_{Lac} system cotransformed with either an empty vector (P_{Bad} ∅) or P_{Bad} -MEV, with arabinose induction either during the growth phase or at the time of IPTG induction. Addition of the mevalonate pathway decreases the time to visible lycopene to 1.5 hours, with the greatest reduction occurring when the mevalonate pathway is repressed during the growth stage and induced at the same time as the *crtEBI* pathway. The gray line marks the threshold for visibility. (B) Lycopene produced in the growth stage for each system. In the uninduced state (no IPTG), lycopene production increases with the presence of P_{Bad} -MEV and further increased when P_{Bad} -MEV was induced with arabinose. The gray line marks the threshold for perceived colorlessness. All error bars represent standard deviation.

2.4 Discussion

In this work, we engineered metabolic pigment pathways to harness them for use in a fast-responding whole cell biosensor. Using pigments as reporters can better enable sensor use in low-resource settings, since sensor output can be interpreted by the naked eye, without any equipment. By engineering cells to be initially colorless, a large inoculum of precultured cells can be added to the sample, and the time to pigmentation will be determined by the rate of metabolite production rather than the rate of cell growth.

However, fully repressing pigment production to achieve an initial "off" state poses unique challenges, since small amounts of unwanted protein can catalyze the production of large, visible amounts of pigment. Commonly used inducible promoter systems could not adequately repress lycopene, which necessitated exploring engineering modifications at the transcriptional and translational levels to eliminate unwanted pigmentation. When exploring transcriptional modifications, we generated a mutated P_{Bad} with 30 times lower uninduced levels and a 10 times greater dynamic range, which could be of use in a broad range of applications.

When characterizing the effects of genetic modifications on RFP and lycopene production, we repeatedly encountered the problem that low levels of fluorescent protein expression did not correspond with visibly low levels of pigment production. Reducing fluorescence by orders of magnitude still yielded promoters with visible uninduced lycopene and induced lycopene levels that changed by much smaller factors. The systems that could adequately repress lycopene had uninduced fluorescent levels below the plate reader's limit of detection, emphasizing the need for much tighter regulation when using pigments instead of fluorescent reporters. When using fluorescent reporters, the value of the baseline "off" level is inconsequential as long as the "on" value is distinctly higher. However, when using pigment reporters, the enzymatic amplification of low levels of expression in the "off" state can confound sensor output, which necessitates focusing on reduction of absolute (rather than relative) protein expression. Transcriptional modifications made modest improvements in decreasing uninduced lycopene expression, but only when the RBS strength of the *crtEBI* genes was reduced could each system

adequately control lycopene production. This suggests that translational modifications are perhaps the best starting point in combatting unwanted expression.

Differences in RFP and fluorescent induction profiles accentuate the limitations in using fluorescent reporters to characterize metabolic pathways. In many systems, as inducer was added, RFP production increased (as expected), but lycopene production decreased. This reduction in lycopene production upon induction is likely because of the added complexities of using metabolite reporters, specifically metabolic precursor limitations and toxicity effects at high levels of induction. These differences necessitate that when using metabolites as outputs or reporters, all final levels of tuning and system characterization must be performed with the final metabolite of interest as the reporter. However, despite the limitations of fluorescent reporters, they are useful for first approximations of system behavior, especially when assaying for metabolite levels is time-intensive and costly.

Lycopene production varied greatly based on the inoculum density: higher initial inocula resulted in higher final titers of lycopene. Previous work in the area of dynamic metabolic engineering has demonstrated the usefulness of separating the growth stage and metabolite production stage[50,51,93]. Many of the approaches used in dynamic metabolic engineering[48,49] can be applied to our biosensor design, since cells must switch from a growth to a production phase. However, the requirement of a completely colorless preculture necessitates elimination of baseline or leaky pigment expression during the growth stage, which is often permitted and can even be beneficial in dynamic metabolic engineering efforts.

When optimizing time to visible lycopene upon induction, we encountered a tradeoff between low levels of lycopene during the growth stage and fast production of lycopene upon induction. The P_{Lac} system reached the visibility threshold the most quickly; however, the P_{Lac} system also had the highest level of uninduced lycopene at the time of induction, which may partly account for the faster time to visible pigmentation. Similarly, supplementation of metabolic precursors further reduced the time to visible lycopene production, but also further increased unwanted lycopene produced during the growth stage to a level above the colorless threshold. Though these effects could likely be somewhat mitigated by using a more repressible promoter to control the mevalonate pathway genes (i.e.: $P_{Bad,weak}$ instead of P_{Bad}), since the P_{Lac} system already has uninduced lycopene levels just below the color threshold, it is likely that any level of precursor supplementation will push uninduced levels past the threshold.

In exploring the effect of metabolic precursor supplementation, we expressed the *crtEBI* genes and the mevalonate pathway genes on separate plasmids. Just by addition of a second plasmid (an empty control plasmid), the rate of lycopene production significantly decreased, suggesting that addition of a second plasmid places a stress on the cell that can alter protein and metabolite production. When the mevalonate genes were expressed on the second plasmid, lycopene production dramatically increased despite the limitations of a two plasmid system, which emphasizes the power of precursor supplementation. Combining the two pathways onto one plasmid would likely further improve the effects of precursor supplementation.

Though the systems developed should be useful in any biosensing application that uses lycopene as a reporter, we acknowledge that the *crtEBI* genes used in this study are

not the only ones used in metabolic engineering applications. In all of our experiments, we used *crtEBI* genes isolated from the bacterium *Pantoea ananatis*. Most previous work to engineer *E. coli* cells to produce lycopene use either these genes or those from *Pantoea agglomerans*. Though some of the problems we encountered—specifically, high levels of uninduced expression and toxicity effects at high levels of induction—could be specific to the *P. ananatis* proteins, work using *P. agglomerans* genes[40] has demonstrated similar problems. We also recognize that the visibility thresholds used will likely need to be changed based on the form factor of the final application device, but similar approaches can be used to develop systems that meet the visibility requirements of different devices.

Here we have improved the response time of a previously reported biosensor framework by an order of magnitude. We have demonstrated ways to control production of the metabolite lycopene, and the approaches used should be generalizable to any other metabolite of interest. As the applications of metabolic engineering expand beyond traditional chemical production, tight control of output in response to the external environment will be necessary. Cells are already being engineered to specifically deliver drugs to tumors[10,11,94] and to produce different drugs based on what is needed in low-resource settings [95,96]. For both of these applications, it is necessary that cells produce the desired compound only in the desired condition—specificity of response based on environment is critical. Here, we have demonstrated the ways that transcriptional and translational control can be used in combination to engineer response specificity and the ways that pathway engineering can increase the rate and intensity of the metabolite produced in the "on" state. These same approaches can be used to control production of

other metabolites and will likely help to broaden the scope of metabolic engineering applications.

CHAPTER 3. DESIGN OF A FAST-RESPONDING, TUNABLE ZINC SENSOR

3.1 Introduction

The previous chapter detailed our efforts to completely decouple growth from pigment production to decrease the time required to see a visible response upon sample addition. Through transcriptional, translational, and metabolic engineering approaches, we created cells that fully repress lycopene in the absence of an inducer and produce visible lycopene within four hours of sample addition. While this laid the foundation for a fast-responding whole-cell biosensor, the resulting cells respond only to a standard chemical inducer, not to a physiologically relevant compound. To make a usable biosensor, sensor cells must be able to respond to different analyte concentrations upon induction. In the context of a pigment-based zinc biosensor, this entails engineering cells to be colorless in the absence of inducer, and then upon addition of inducer, produce different pigments based on the concentration of extracellular zinc. Further, the cells need to respond to physiologically relevant zinc concentrations so that they can provide useful clinical data. In this chapter, we expand on the inducible systems developed in Chapter 2 by incorporating zinc-responsive elements, adding additional pigment pathways, and tuning the engineered circuits to respond to specific zinc concentrations.

In our group's previous work developing a zinc biosensor, we repeatedly encountered difficulties tuning the sensor to respond to clinically relevant zinc concentrations, which is an absolute requirement to making a usable sensor. Most sensors

that use bioprospected components respond to concentrations dictated by the natural sensor-analyte affinity, which often fall out of the desired response range. The initial version of zinc-responsive sensor cells responded to zinc concentrations orders of magnitude lower than clinically relevant zinc concentrations. While there are synthetic biology tools available to tune sensor response, most are not broadly applicable. Currently, the most effective approaches to shift the response curve require extensive protein engineering[4] or the use of multiple receptors with varied binding affinities for the target analyte[97,98], which can necessitate bioprospecting for other proteins that bind the target or protein engineering to alter the affinity of available receptors. Further, addition of the repeated sequences necessary for expression of multiple receptors can destabilize genetic constructs[99], making plasmids expressing burdensome metabolic pathways much more prone to mutations that harm sensor performance.

Here, we describe the development of a fast-responding whole-cell zinc biosensor that accurately quantifies clinically relevant concentrations of zinc in human serum. We designed and engineered a library of novel, dual-stimulus-responsive promoters that allowed us to decouple pigment metabolism from cell growth and thus produce pigment output within four hours of sample addition. We then used transcriptional, translational, post-translational, and metabolic control methods to tune which zinc concentrations activate different pigment pathways, ultimately shifting the threshold zinc concentrations by nearly an order of magnitude compared to our previous proof of principle and into the clinically relevant range. The resulting cells can be used to assay unprocessed human serum, producing one of three different visible pigments within four hours based on the concentration of serum zinc. This work is a major step towards a field-deployable

micronutrient biosensor that would impact the treatment of millions of people, and demonstrates generalizable strategies for the development of robust and tunable sensor cells.

3.2 Materials and Methods

3.2.1 Materials

T4 DNA ligase, T5 exonuclease, Taq ligase, Phusion polymerase, Q5 polymerase, and restriction endonucleases were purchased from New England Biolabs (Ipswich, MA, USA). E.N.Z.A. Plasmid Mini Kits were purchased from Omega Bio-tek (Norcross, GA, USA), and QIAquick PCR Purification Kits and QIAquick Gel Extraction Kits were purchased from QIAGEN (Valencia, CA, USA). Lycopene (98%) was purchased from Cayman Chemical (Ann Arbor, MI, USA). Sudan I (95%) was purchased from TCI America (Portland, OR, USA).

3.2.2 Strains and plasmids

Escherichia coli K-12 DH10B (New England Biolabs, Ipswich, MA) was used for plasmid assembly. Lambda red recombination[100] was used to make a DH10BΔZur strain, which was used for all protein and metabolite production. The plasmid pSB3T5, with a p15A origin, was taken from the Standard Registry of Biological Parts and used as the backbone vector for all plasmids used in the final analysis. The plasmid pSB6A1, which is a derivative of the pBR322 plasmid, was obtained from the Standard Registry of Biological Parts and used for expression of the mevalonate genes.

3.2.3 Cloning and construct assembly

All constructs were assembled with either Gibson assembly[88] or restriction endonuclease digestion of components and subsequent ligation and transformation following the BioBricks idempotent standard assembly[89]. LB medium composed of 10 g/ L NaCl, 5 g/L yeast extract, and 10 g/L tryptone was used for all cell growth during cloning steps. The following antibiotics were used for appropriate selection: tetracycline (15 µg/mL), chloramphenicol (34 µg/mL), kanamycin (30 µg/mL), and carbenicillin (100 µg/mL).

The genes *zur* and *zntR* were isolated from previously assembled zinc-responsive plasmids[47]. The coding sequence for Zur from *B. subtilus* (zur_{Bs}) was codon-optimized for expression in E. coli, and the gene was synthesized by Eurofins (Louisville, KY). The lycopene expression cassette (crtEBI) was amplified from a previously assembled vector[79] that uses the genes from part bba_k274100 of the Registry of Standard Biological Parts. The violacein genes *vioA*, *vioB*, *vioC*, *vioD*, and *vioE* were amplified from Part bba_k274002 of the Registry of Standard Biological Parts. A previously assembled arabinose-inducible plasmid expressing the mevalonate pathway[79] used genes from the plasmid pJBEI-6409[83], which was obtained from Addgene (Cambridge, MA, USA).

Lambda red recombination[100] was used to make DH10B*ΔZur*, and this strain was used for all experiments that assessed response to zinc.

3.2.4 Cell culture

For all protein and pigment expression experiments, a modified M9 medium was used. A 5× salts solution consisted of 22.5 g/L NaCl, 8.2 g/L KCl, 5 g/L NH_4Cl, 19.5 g/L MES, 10 g/L β-glycerophosphate and was pH adjusted to 7.4 with 2 M KOH. To remove

trace amounts of zinc, each 1 L batch of salts was treated with 1g of Chelex-100 resin. The mixture was vigorously stirred for 1 hour, and resin was removed through filtration with a 0.2 µm filter. The final medium consisted of 1× salts, 2 mM $MgSO_4$, 0.1 mM $CaCl_2$, 0.01% thiamine, 1.92 g/L of SC-Ura amino acid mixture (Sunrise Science), and 0.4% of either dextrose or glycerol. Medium was sterilized through filtration with a 0.2 µm filter.

For GFP expression, freshly transformed DH10B colonies were inoculated in triplicate into 4 mL of modified M9 medium and grown at 37°C and 220 rpm for 24 hours. For pigment expression in the absence of serum, freshly transformed DH10B colonies were inoculated in triplicate into 5 mL of modified M9 medium containing the appropriate antibiotic, and grown at 37°C and 220 rpm for 18 hours. Cells were concentrated through centrifugation and used to inoculate cultures that contained the fresh media with the appropriate inducer and zinc concentrations. Each 4 mL culture was inoculated to an OD of 0.1 and grown at 37°C and 220 rpm for 4 hours. OD, carotenoid content, and violacein content was measured at 4 hours.

For pigment expression in serum, freshly transformed DH10B colonies were inoculated in triplicate into 3 mL of modified M9 medium containing the appropriate antibiotic and grown at 37°C and 220 rpm for 8 hours. This culture was used to inoculate a 300 mL culture of modified M9 medium containing the appropriate antibiotic, and the 300 mL culture was grown at 37°C and 220 rpm for 18 hours. Cells were concentrated through centrifugation and used to inoculate cultures that consisted of 25% serum, 75% modified M9, and the appropriate antibiotics, inducers, and supplemented zinc. Unless otherwise specified, 1 mL cultures were inoculated to an OD of 3.0 and grown at 37°C and

220 rpm for 4 hours. OD, carotenoid content, and violacein content were measured at 4 hours.

3.2.5 Serum processing and zinc measurement

Pooled human serum was purchased from Corning (Corning, NY). Zinc was removed from serum through Chelex-100 treatment. 1g of Chelex 100 resin was added to 100 mL of serum, and the mixture was vigorously stirred for 2 hr. Zinc concentration was measured at the University of Georgia Laboratory for Environmental Analysis. Samples were digested with concentrated acid and analyzed on an ICP-MS according to EPA method 3052.

3.2.6 Measurement of optical density and fluorescence

Optical density of samples was quantified by measuring the absorbance at 600 nm either in a ThermoFisher Genesys 20 spectrophotometer with a 10 mm path length or in a Biotek Synergy H4 plate reader. When necessary, cultures were diluted to ensure that the reading fell within the linear range of the instruments. 1 mL of culture was used for spectrophotometer measurements, and 150 µL of culture in a 96 well plate was used for plate reader measurements. Calibration curves were made for each instrument and used for uniform reporting of optical density. All optical densities reported correspond with those taken in the spectrophotometer.

For GFP quantification, fluorescence at 485 nm excitation and 510 nm emission was measured on a Biotek Synergy H4 plate reader. All reported fluorescence values are background-subtracted and normalized to optical density.

3.2.7 Pigment extraction and quantification

For carotenoid analysis, either 1 mL or 250 µL of bacterial culture was pelleted at 18,000 rcf for 5 minutes. Cell pellets were resuspended in 50 µL of ultrapure water. Carotenoids were extracted with 1 mL of acetone at 50°C for 15 minutes. A heat block was used to maintain temperature and extractions were vortexed every 5 minutes. Cellular debris was pelleted at 18,000 rcf for 5 minutes, and 500 µL of supernatant was removed for analysis. Carotenoid content was analyzed on a Shimadzu Prominence UFLC using an Agilent C18 4.6 mm x 50 mm column with a 5 µm particle size and a Shimadzu photodiode array detector. A solvent ratio of 50:30:20 acetonitrile:methanol:isopropanol was used as the mobile phase[92] and run at a flow rate of 1 mL/min with a 25 µL sample injection volume. Absorption was detected at 471 nm. Retention times and peak intensities were compared to analytical standards spiked into control extractions from DH10B cells.

For violacein analysis, either 1 mL or 300 µL of bacterial culture was pelleted at 18,000 rcf for 5 minutes. Cell pellets were resuspended in 50 µL of ultrapure water. Violacein was extracted with 40 µL of water-saturated butanol. The mixtures were vortexed for 5 minutes at room temperature and then centrifuged at 18,000 rcf for 5 minutes. The butanol layer was removed and recentrifuged at 18,000 rcf for 5 minutes. 15 µL of the butanol extraction was removed for analysis and added to a 384 well plate. Absorbance at 585 nm was measured on a Synergy H4 plate reader. All reported values are background subtracted, using a butanol extraction of non-engineered *E. coli* cells as the blank.

3.2.8 Protein mutagenesis experiments

For undirected mutagenesis of zur, error-prone PCR was used to introduce mutations at a target rate of 2 amino acids/coding sequence using the protocol described in Wilson and Keefe[101] with magnesium and manganese concentrations adapted to be 2 mM $MgCl_2$ and 0.25 mM $MnCl_2$. 15 cycles were run with a denaturation step of 30 sec at 95°C, an annealing step of 60 sec at 51°C, and an extension step of 5 min at 68°C. Mutated sequences were inserted into a GFP expression plasmid through Gibson assembly, and plasmids were transformed into DH10B*ΔZur* cells and grown on modified M9-agar plates with 1 μM zinc at 37°C. After 24 hours, plates were visually inspected, and green colonies were streaked onto modified M9-agar plates containing 20 μM zinc and incubated at 37°C. After 18 hours, plates were analyzed, and cells that were visibly green on 1 μM plates and visibly colorless on 20 μM plates were inoculated. Plasmids were isolated from these cells, sequenced, and used for a more thorough analysis of zinc response.

For site-directed mutagenesis of Zur, eight residues were chosen for saturation mutagenesis based on their proximity to the zinc-binding residues or role in the dimer interface. Using primers for NNK mutagenesis (Eurofins) of the specified residue, a GFP-expression plasmid was assembled, transformed into DH10B*ΔZur* cells, plated on modified M9 plates, and grown at 37C for 18 hours. 96 individual colonies were inoculated into 150 μL of modified M9 containing 1 μM zinc in a 96 well plate and grown at 180 rpm and 37°C. After 12 hours, fluorescence and OD were measured, and 7.5 μL of each culture was added to 140 ul of modified M9 media containing 20 μM zinc. After 6 hours, GFP and OD were measured.

3.3 Results

3.3.1 Synthetic promoters to separate chemical production from cell growth

Our previous efforts to engineer diagnostic zinc sensor cells were plagued by long assay times, construct instability, and poor test interpretability, which needed to be overcome in order to make a potentially deployable diagnostic. To accomplish this goal, we sought to decouple pigment production from cell growth by using a small molecule inducer as a master regulator to control expression of all pigment pathways. During the pre-assay inoculum production stage (in the absence of inducer), cells would be colorless, which would decrease the metabolic burden on cells during the growth phase and thus improve cell viability and genetic circuit construct stability[48,50,79,93,102]. A large inoculum of these cells could then be added to the sample, and a standard inducer (such as IPTG or arabinose) would turn the color synthesis system "on", leaving zinc-responsive elements to control pigment production. The assay time would then depend only on the pigment biosynthesis rate (Figure 10), and not the time needed for generation of visible biomass from a small (colored) inoculum as in our proof-of-principle work. This would also improve test interpretation (since colorless cells will indicate an incomplete or nonfunctional test).

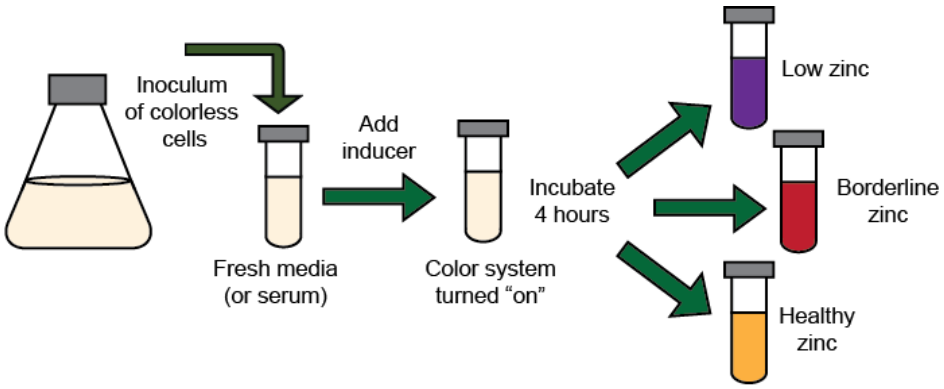

Figure 10: Schematic illustrating the overall design of a dual-input system that decouples cell growth from pigment production.

A large culture of colorless cells is grown to saturation. These cells are added to fresh medium or to a serum sample at a density high enough that cells are visible, and a small-molecule inducer is added to activate the color-response circuit. After a short incubation (approximately 4 hours), different pigments are produced to indicate different zinc concentrations

To engineer a system in which pigment production is controlled by both a standard inducer and zinc, we designed dual-input synthetic promoters with operator sites for both the inducer's cognate transcriptional regulator (such as LacI) and for the zinc-responsive repressor Zur. During the pre-assay inoculum production stage, LacI (for example) binds to its cognate operator and prevents expression of downstream pigment production genes. IPTG addition should alleviate this repression, with gene expression then solely controlled by Zur, a repressor that binds to its cognate operator in the presence of zinc. Ideally, expression from this promoter would only occur at very low zinc concentrations (Figure 11A). The transcriptional regulators AraC and T7 RNA polymerase have different regulatory mechanisms, but could enact the same logical function (Figure 11B,C).

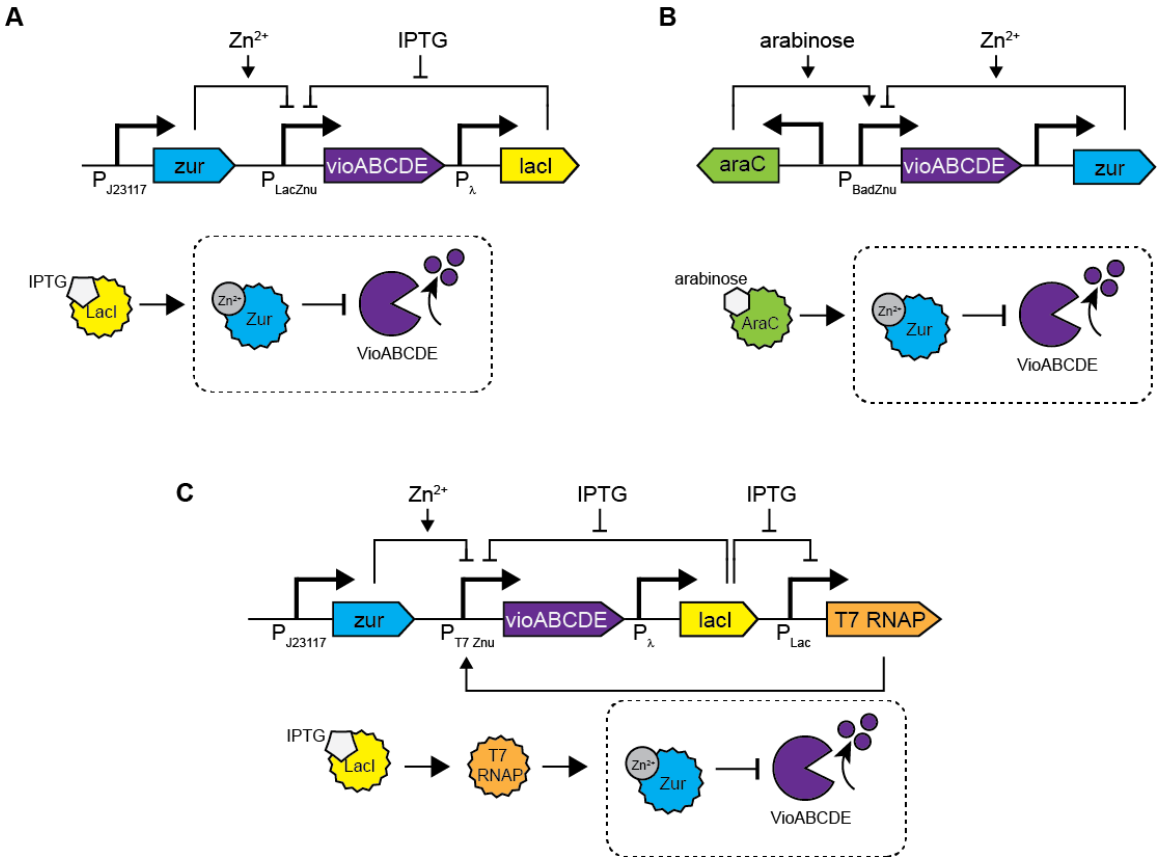

Figure 11: Circuit diagrams and schematics depicting the design of a dual-input promoters to regulate production of the violacein pathway genes.

(A) LacI/IPTG controlled circuit. During the pre-assay culture stage, LacI represses pigment production. IPTG is added as an inducer to alleviate LacI repression, and the pathway genes are then controlled by Zur. Zur is a transcriptional repressor that is only active when bound to zinc; thus violacein will only be produced in low zinc conditions. (B) AraC/arabinose controlled circuit. During the pre-assay culture stage, AraC represses pigment production. Arabinose is added as an inducer to activate AraC (switching AraC from a repressor to an activator), and the pathway genes are then controlled by Zur, which binds to its operator in the presence of zinc. (C) T7 RNAP/LacI/IPTG controlled circuit. During the pre-assay culture stage, LacI represses expression of both T7 RNA polymerase and any leaky expression from the synthetic promoter. IPTG is added as an inducer to alleviate LacI repression, and T7 RNAP is produced. Pathway genes are then controlled by Zur, which binds to its operator in the presence of zinc.

We created a first generation of dual-input promoters (referred to as $P_{LacZnu,1}$, $P_{BadZnu,1}$, and $P_{T7Znu,1}$), by adding a single Zur operator site downstream of a standard inducible promoter (Figure 12A, Table 2). Addition of operator sites has been successfully

used in previous efforts to make promoters controlled by two inputs[45,46,103,104], and while fluorescent characterization showed that these first-generation hybrid promoters all respond to both IPTG and zinc, all promoters showed high levels of baseline, uninduced protein expression (Figure 12B). Zur's operator sequence includes a -10 σ_{70} RNA polymerase binding domain that is heavily conserved across Zur-regulated promoters[105], so this leakiness is likely caused by unintentional introduction of a promoter element. To decrease this unwanted expression, we engineered a second generation of P_{Lac}- and P_{T7}-based promoters that included additional LacI operators downstream of the Zur operator (Figure 12A, Table 2). The second generation of hybrid promoters all showed decreased uninduced expression and improved dynamic range (Figure 12B).

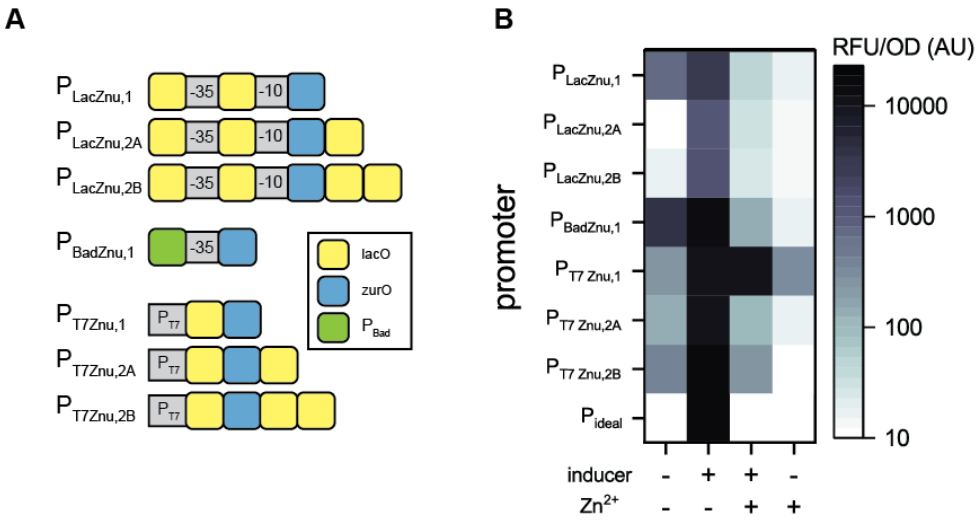

Figure 12: Design and characterization of synthetic dual-input promoters.
(A) Promoter architecture for the library of novel promoters. The -10 and -35 σ_{70} binding domains are marked, and lac and zur operator sites are shown in yellow and blue, respectively. For the P_{BadZnu} promoter, the -10 binding domain is not explicitly marked because it is embedded in the Zur operator site, and the green box indicates the entire P_{Bad} promoter sequence that is upstream of the -35 binding domain. For the P_{T7} variants, the consensus T7 RNAP binding domain is marked in gray. Table 2

contains annotated promoter sequences for all constructed promoters. (B). Fluorescent characterization of all engineered promoters. Engineered promoters were used to control production of eGFP. Ideally, eGFP should only be produced in the +inducer/-zinc state, as indicated by the P_{ideal} values. Labels on the vertical axis correspond with the promoters depicted in (A). IPTG was used to induce both the P_{Lac}- and P_{T7}-based circuits, arabinose was used to induce the P_{Bad}-based circuit, and when indicated, zinc was added to a concentration of 20 µM.

Table 2: Sequences of all dual-input promoters used in this study.
The sequences are color coded according to the schematic in Figure 12. Lac operator sites are highlighted in yellow; the sequence of AraC- P_{Bad} promoter is highlighted in green; Zur operator sites are highlighted in blue, and the -10 σ_{70} binding site is underlined and italicized. For all P_{Lac} and P_{Bad} variants, the -10 and -35 σ_{70} binding sites are bolded and underlined. For all P_{T7} variants, the consensus T7 promoter sequence is bolded and underlined.

Promoter	Sequence
$P_{LacZnu,1}$	AATTGTGAGCGGATAACAA**TTGACAT**TGTGAGCGGATAAC AA**GATACT**GAGCACAGAAGTGTGA*TATTAT*AACATTT
$P_{LacZnu,2A}$	AATTGTGAGCGGATAACAA**TTGACAT**TGTGAGCGGATAAC AA**GATACT**GAGCACAGAAGTGTGA*TATTAT*AACATTTAAT TGTGAGCGGATAACAA
$P_{LacZnu,2B}$	AATTGTGAGCGGATAACAA**TTGACAT**TGTGAGCGGATAAC AA**GATACT**GAGCACAGAAGTGTGA*TATTAT*AACATTTAAT TGTGAGCGGATAACAAGACTGAATTGTGAGCGCTCACAAT T
$P_{BadZnu,1}$	...GCAGAAAAGTCCACATTGATTATTTGCACGGCGTCAC ACTTTGCTATGCCATAGCATTTTTATCCATAAGATTAGCG GATCCTAC**CTGATG**ATGAATATGAGAAGTGTGA**TATTAT**A ACATTT
$P_{T7Znu,1}$	**TAATACGACTCACTATAGG**AATTGTGAGCGGATAACAAAA TTGTGAGCGGATAACAA
$P_{T7Znu,2A}$	**TAATACGACTCACTATAGG**AATTGTGAGCGGATAACAAAA TTGTGAGCGGATAACAAAATTGTGAGCGCTCACAATT
$P_{T7Znu,2B}$	**TAATACGACTCACTATAGG**AATTGTGAGCGGATAACAAAA TTGTGAGCGGATAACAAAATTGTGAGCGGATAACAAGACT GAATTGTGAGCGCTCACAATT

We determined the best-responding promoter of each class by calculating the relative change in fluorescence caused by inducer and zinc addition (Table 3), and then used these selected promoters to control production of the violacein production pathway. A starter culture of uninduced cells that had been grown overnight was used to inoculate tubes containing fresh medium, the appropriate inducer, and different concentrations of zinc. Though all systems showed some level of induction, the P_{Lac}-based system outperformed the others, as it had visually undetectable violacein production in the overnight culture and the highest level of induced violacein production (Figure 13).

Table 3: Fold change of all characterized promoters in response to the inducer and to zinc.

Promoter	Response to inducer (fold change)	Response to zinc (fold change)
$P_{ZnuLac,1}$	6.31	77.0
$P_{ZnuLac,2A}$	188	24.8
$P_{ZnuLac,2B}$	73.7	52.1
$P_{BadZnu,1}$	3.10	107
$P_{T7Znu,1}$	25.0	0.867
$P_{T7Znu,2A}$	85.37	143
$P_{T7Znu,2B}$	53.7	75.4

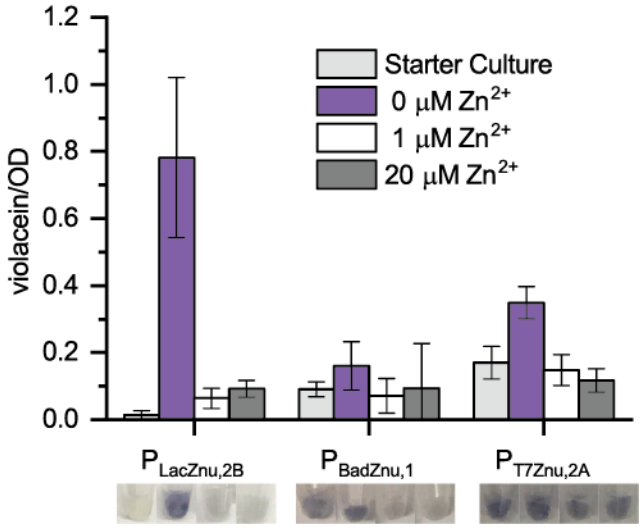

Figure 13: Violacein production from the best-responding hybrid promoters.
The best-responding promoter from each group was selected to control production of the violacein pathway genes. A starter culture was grown without any inducer or zinc, and then used to inoculate cultures that contained the appropriate inducer and different concentrations of zinc. Error bars indicate standard deviations. Images below the graph show representative cell pellets from each condition.

3.3.2 A multi-colored, fast-responding zinc sensor

Using the optimized P_{Lac}-based violacein circuit, we constructed multi-color zinc-responsive sensor cells by incorporating metabolic pathways from the carotenoid pathway, specifically those to produce the red pigment lycopene and the orange pigment β-carotene. We used LacI/IPTG to control expression of the lycopene production pathway and the zinc-responsive activator ZntR to control expression of the enzyme CrtY, which converts lycopene into β-carotene (Figure 14A). Upon IPTG induction, cells will always produce lycopene, but cells should only appear red at intermediate zinc concentrations: at low zinc concentrations, the more intense pigment violacein overwhelms lycopene and cells appear purple, while at high zinc concentrations CrtY converts all lycopene into β-carotene and cells appear orange. The mevalonate pathway genes (which produce the precursor to the

carotenoid pathway) were expressed from P_{Bad} to increase the rate and intensity of carotenoid production.

As designed, the implemented engineered cells turn one of three colors based on the zinc concentration. After overnight growth (with no inducer), cells are visibly colorless and have no detectable violacein or carotenoid. When these cells are used to inoculate medium containing IPTG and different concentrations of zinc, cells appear visibly purple, red, or orange (Figure 14B) after four hours of culture.

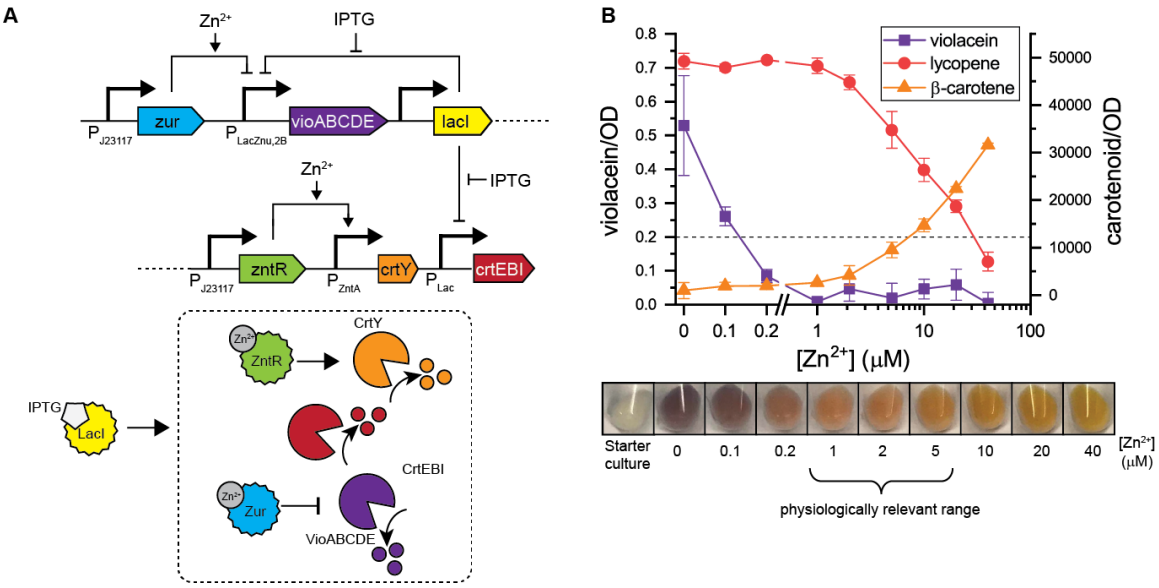

Figure 14: Initial multi-color sensor cells.
(A) Circuit diagram and schematic depicting the design of the three-color circuit. During the pre-assay culture stage, LacI represses all pigment production by repressing $P_{LacZnu,2B}$ (which controls violacein production) and P_{Lac} (which controls lycopene production). IPTG alleviates LacI repression, activating the pigment production module indicated by the dashed box in the schematic. The *crtEBI* genes, which control lycopene production, are produced at all zinc concentrations. In low zinc concentrations, violacein is produced, overpowering lycopene production and leading to visibly purple cells. At intermediate zinc concentrations, Zur binds zinc and represses violacein expression, leading to visibly red cells. At high zinc concentrations, ZntR also binds zinc and activates production of CrtY, which converts lycopene to β-carotene, leading to visibly orange cells. (B) Pigment quantification and visualization of sensor cells that were induced with IPTG and

grown for four hours. At low zinc concentrations, cells produce violacein and lycopene and appear visibly purple. Cells grown in zinc concentrations between 0.2 and 10 μM are visibly red. At high zinc concentrations, β-carotene production overpowers lycopene production, and cells appear visibly orange. The dotted line indicates the threshold for visible violacein. Error bars indicate standard deviations. The bracket indicates the range of physiologically relevant zinc concentrations corresponding with cells grown in 25% human serum. Ideally, cells should appear three different colors within this bracketed concentration range.

To better enable objective color assessment, we set thresholds for color classifications. We surveyed ten people to ask how they would classify the colors of cells that contained different levels of violacein, lycopene, and β-carotene (Figure 15). Based on these results, cells that contained OD-normalized violacein > 0.2 are considered purple, and cells that contain OD-normalized violacein < 0.2 are classified based on the dominating carotenoid: either red or orange, based on whether cells contain primarily lycopene or primarily β-carotene, respectively.

Though the initial sensor cells respond to a wide variety of zinc concentrations, the concentration range is far wider than the clinically relevant range of zinc concentrations. To meet the requirements for in-field nutrition testing, an assay should require both small amounts of serum and minimal sample processing, so we aimed to run our test in a 25% serum sample. Population data show that serum zinc concentrations fall between 2 and 20 μM[24], so a test run in 25% serum must produce distinct colors across a range of 0.5 to 5 μM zinc. Across this range, all sensor cells produced primarily lycopene and are classified as red according to predetermined color thresholds. To make a field-deployable sensor, we thus needed to shift both the zinc concentration that triggers the purple-to-red color transition and the concentration that triggers the red-to-orange color transition, overall narrowing the response range by an order of magnitude.

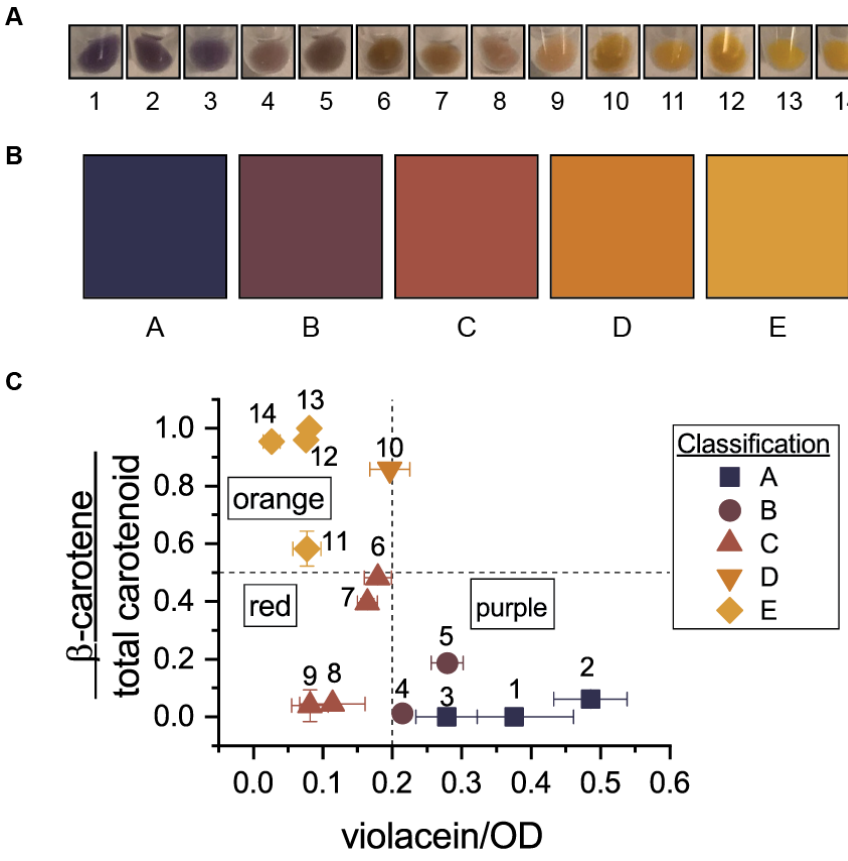

Figure 15: Color classification of cells with different pigment concentrations.
(A) Fourteen strains expressing different levels of violacein, lycopene, and beta-carotene were presented to ten different people one at a time in a random order, and each person was asked to match the perceived color of the each samples to different colors on a spectrum. (B) The color spectrum used in the survey to assess color. RGB quantification of cell pellets expressing only violacein, only lycopene, and only β-carotene was used to set the far left (A), middle (C), and far right (E) colors, respectively. The intermediate color (B) was set by averaging the RGB values of (A) and (C), and the intermediate color (D) was set by averaging the RGB values of (C) and (E). Each sample was classified as one of five colors based on the overall survey consensus. We deemed cells classified as (A) or (B) as "purple", cells classified as (C) as "red", and cells classified as (D) or (E) as "orange". (C) Pigment quantification of the fourteen strains and determination of quantitative color thresholds. Cell pellets contain pooled samples from biological triplicates. OD-normalized concentrations of violacein, lycopene, and β-carotene were quantified. To better enable color thresholds, we reduced carotenoid quantification into a single variable: the fraction of total carotenoid produced that is β-carotene. Error bars indicate the standard deviation. Symbol colors and shapes indicate survey results. We used these data to set quantitative color thresholds. Cells with OD-normalized violacein > 0.2 are considered "purple". Cells with OD-normalized violacein < 0.2 are considered "red"

if the fraction of β-carotene is < 0.5, and "orange" if the fraction of β-carotene is > 0.5.

3.3.3 Rational tuning of color switch points

We first focused on shifting the purple-to-red response point so that higher zinc concentrations are required to shut down violacein production. Both colorimetric and fluorescent characterization show that expression of $P_{LacZnu,2}$ shuts off by 200 nM, and we aimed to shift this by an order of magnitude to a concentration between 1 and 3 μM.

We explored several strategies to increase the threshold concentration that activates the purple to red color transition. We first tested whether reducing the amount of Zur in the system could shift the transition point to higher concentrations. Decreasing Zur expression through ribosomal binding site (RBS) modifications on Zur had little to no effect on Zur's switch point and instead led to increased protein production at all zinc concentrations (Figure 16).

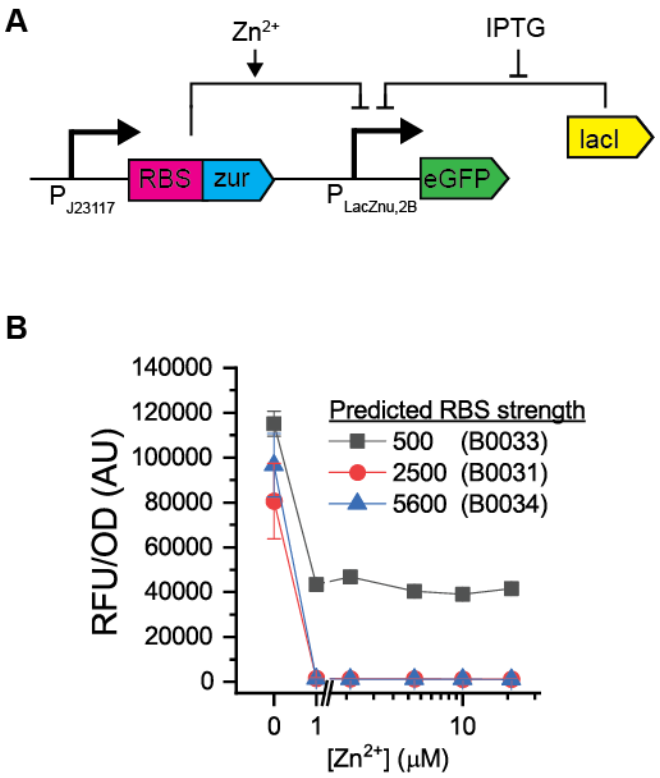

Figure 16: Effect of Zur levels on zinc response.
(A) Genetic circuit used to test the effect of RBS modulation on response to zinc. Zur is constitutively expressed from the promoter P_{J23117}, and the RBS of Zur is varied. (B) Fluorescent characterization showing the effect of Zur levels on expression from $P_{LacZnu,2}$. Compared to the baseline Zur with an RBS strength of 2500, Zur with a decreased RBS strength of 500 leads to higher eGFP production at all zinc concentration and minimal decrease between 1 and 20 µM zinc. Increasing the RBS strength to 5600 had no apparent effect on $P_{LacZnu,2}$ expression. RBS sequences were taken from the standard registry of parts, and their relative strengths were quantified with the RBS calculator[90].

We next attempted to use a heterologous zinc-responsive repressor taken from *Bacillus subtilis* (termed Zur_{Bs}) to control expression of two *B. subtilis* promoters that demonstrate different *in vitro* responses to zinc depletion[106]. We placed these operator sites downstream of a standard *E. coli* promoter, and fluorescent characterization shows that Zur_{Bs} fully repressed expression from both tested promoter sequences before 1 µM zinc (Figure 17).

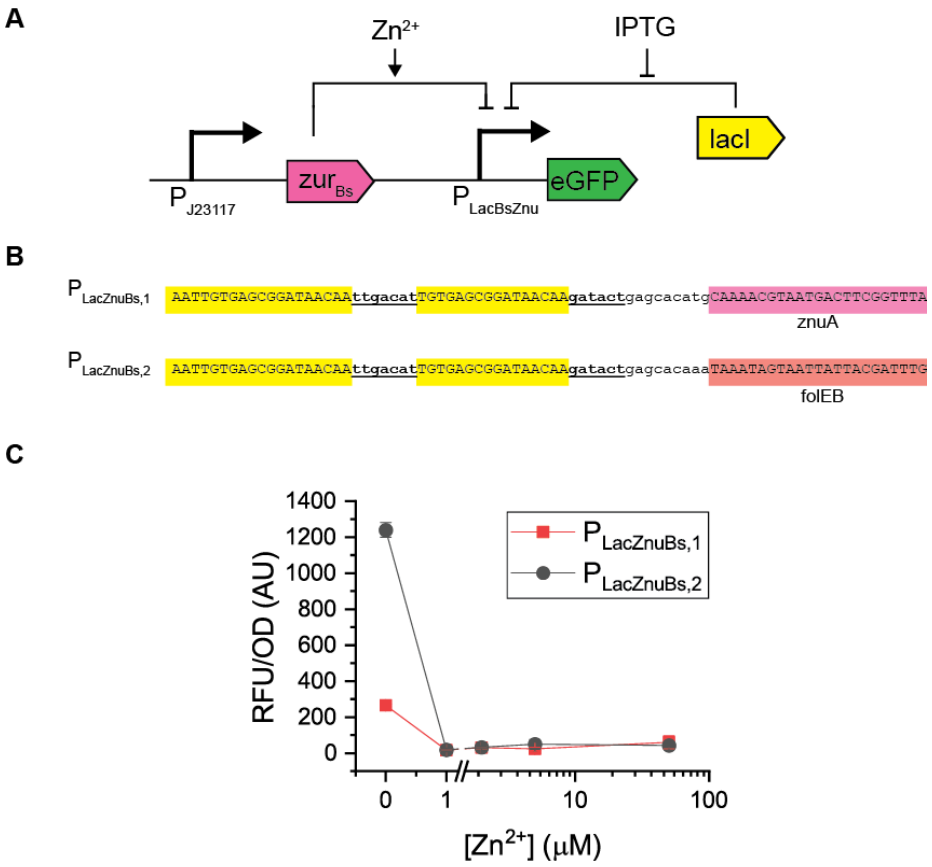

Figure 17: Response of heterologous Zur to added zinc.
(A) Genetic circuit and schematic depicting regulatory mechanism of *B. subtilis*'s Zur (Zur_{Bs}). Zur_{Bs} is constitutively expressed from the promoter P_{J23117}, and when Zur_{Bs} is bound to zinc, it binds to its cognate operator site to repress transcription. (B) Sequences of promoters that controlled by Zur_{Bs}. Two different Zur_{Bs} operator sites, taken from either the P_{znuA} or P_{folEB} of *B. subtilus*, were cloned downstream of a Lac-inducible promoter. (C) Fluorescent characterization of Zur_{Bs} regulation. Expression from both Zur_{Bs}-responsive promoters shuts off by 1 µM zinc.

We then explored protein engineering strategies to engineer an *E. coli* Zur mutant with a decreased affinity for zinc that maintained a high dynamic range (Figure 18). We mutagenized Zur through both error-prone PCR (EP-PCR) of the entire gene and through saturation mutagenesis of rationally-selected residues near Zur's zinc-binding pockets and dimerization domains. The best-responding mutants had relatively high GFP production at 1 µM zinc, but had only 2-3 fold differences in expression between 1 and 30 µM zinc, far

lower than the nearly 100-fold expression differences between 0 and 1 µM zinc characteristic of wild-type Zur.

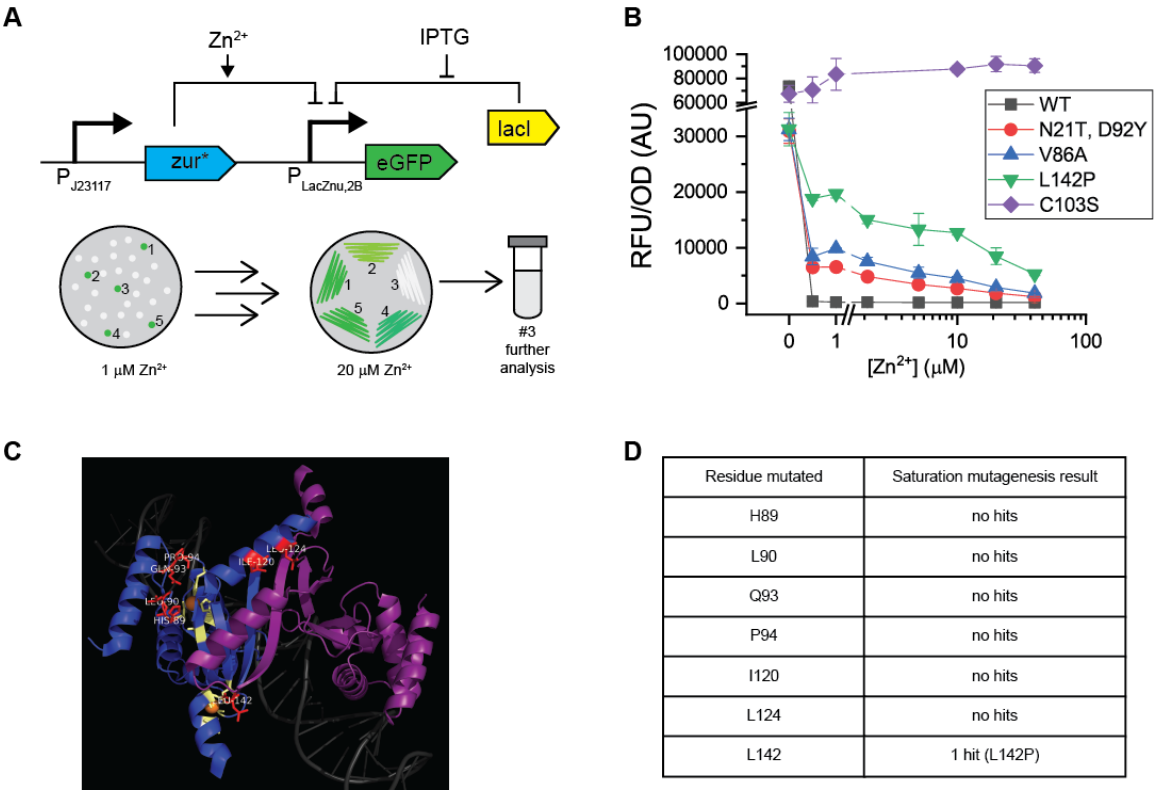

Residue mutated	Saturation mutagenesis result
H89	no hits
L90	no hits
Q93	no hits
P94	no hits
I120	no hits
L124	no hits
L142	1 hit (L142P)

Figure 18: Zur mutagenesis to move Zur response point.
(A) Plan for untargeted Zur mutagenesis and screening. Error-prone PCR was used to introduce mutations into the coding sequence of Zur, as indicated with the asterisk. Transformants were plated on M9-agar plates that contained 1 µM zinc and grown overnight. Visibly green colonies were selected and streaked onto M9-agar plates containing 20 µM zinc. Visibly white colonies were then selected for further screening. (B) Fluorescent characterization of mutagenesis "hits". Of the over 10,000 colonies screened, plasmids were isolated from the three initial "hits", sequenced, and more thoroughly characterized. All mutants showed decreased expression between 1 and 30 µM zinc, but the fold changes were relatively small. The previously characterized mutant C103S[105] cannot bind zinc and was used to control for decreased expression caused solely by addition of zinc. (C) Target residues for site-directed mutagenesis of Zur. Using a crystal structure of Zur bound to DNA (PDB ID 4MTD)[105] and PyMol software[107], seven amino acid residues were selected for saturation mutagenesis, based on either their proximity to the zinc-binding domains or their role in the protein dimerization domain. For each residue, 96 colonies were inoculated into minimal media containing 1 µM zinc and grown overnight. Then, this starter culture was used to inoculate media with 20 µM zinc and grown for 12 hours. We set thresholds for

"hits" if the OD-normalized eGFP fluorescence of cells grown in 1 μM zinc was both two-fold higher than cells grown in 30 μM zinc and ten-fold greater than the autofluorescence of untransformed cells. (D) Results of mutagenesis. Of all mutants formed, only a single colony met the requirements specified in (C). This mutant was sequenced, and the mutation (L142P) was the same mutation found in the EP-PCR mutagenesis experiments.

Redesigning regulatory circuit architecture proved much more effective and enabled us to successfully move Zur's effective response point. Instead of altering Zur's activity, we engineered a system such that Zur is only produced (and thus only available for repression) when zinc is present. Building off of a previously described "inverter"[26], we used the zinc-responsive activator ZntR to control Zur expression from the promoter P_{zntA}, creating a system that produces more Zur at higher zinc concentrations (Figure 19A). Thus, even if Zur is effectively all bound to zinc by 0.2 μM and thus in a repressive mode, by modulating the amount of Zur present we can control how much repression of $P_{LacZnu,2}$ there is. Expression from $P_{LacZnu,2}$ should thus decrease more slowly with added zinc, and at some threshold zinc concentration, expression from $P_{LacZnu,2}$ should be fully repressed. This threshold zinc concentration can be rationally tuned by varying the RBS and ssrA degradation tag on Zur: systems with low levels of Zur will require more transcription from P_{zntA} and thus more zinc to shut off violacein expression.

We made a library of sensor cells with this circuit design that turn off expression from $P_{LacZnu,2}$ at varied zinc concentrations while also maintaining high dynamic ranges. We designed RBSs with varied strengths using the RBS calculator[78] and used ssrA degradation tags with different relative degradation rates[108]. Fluorescent protein characterization shows that variation in expression of Zur from P_{zntA} enables systems that fully repress expression from the $P_{LacZnu,2B}$ promoter at zinc concentrations between 0 and

30 μM (Figure 19B). Cells show up to 200-fold expression differences between 1 and 20 μM, far higher than the 3-fold changes seen in the best-responding Zur mutants. When these systems control violacein production, threshold zinc concentrations are slightly lower than the threshold concentrations seen in fluorescent characterization, but the Zur "off" point still ranges between 0 and 5 μM zinc (Figure 19C, Figure 19D). We chose the circuit that shut off violacein expression between 2 and 5 μM as the best-responding system and used this for all further testing.

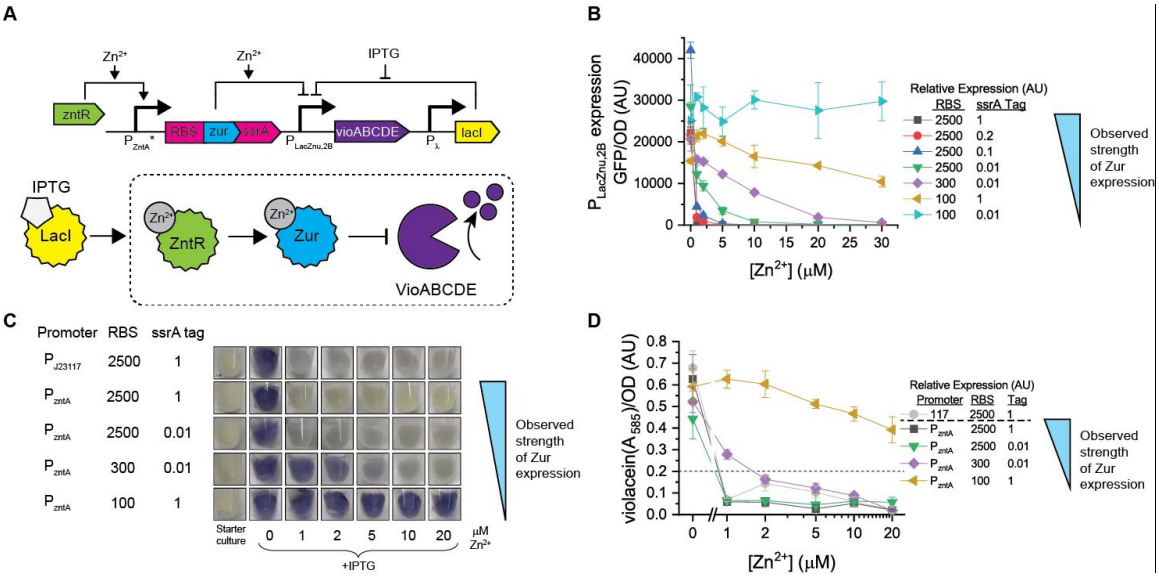

Figure 19: Tuning color thresholds with an inverter.
(A) Circuit diagram and schematic depicting "inverter" method to modulate $P_{LacZnu,2B}$ expression. During the pre-assay culture stage, LacI represses all pigment production. Upon IPTG addition, the activator ZntR controls expression of Zur: increasing concentrations of zinc correspond with increased amounts of Zur, which leads to decreasing expression from $P_{LacZnu,2B}$. The RBS and ssrA tag modulate the amount of Zur produced and thus the amount of zinc needed to activate full Zur repression. (B) Fluorescent characterization of Zur inverter circuits. A library of circuits was assembled with different relative levels of Zur. RBS values are the predicted relative RBS strength, and ssrA values indicate the relative amount of protein that remains (ssrA strength = 1 corresponds with no added degradation tag, and ssrA strength = 0.01 corresponds with the strongest degradation tag). Decreasing Zur expression levels correspond with cells that shut off expression at higher zinc concentrations. (C) Visual assessment of cells with tunable violacein expression. Overnight starter cultures were added to fresh media that contained IPTG and

specified zinc concentrations and grown for four hours. (D) Violacein quantification of inverter constructs. OD-normalized violacein was quantified for the cells depicted in Figure 3C. The dotted line indicates the threshold for visible violacein. Errors bars indicate standard deviation.

We incorporated the optimized violacein-control pathways into the three-color expression plasmids, and then tuned the red-to-orange transition point by varying the expression levels of CrtY, the enzyme that converts lycopene to β-carotene (Figure 20A). This tuning approach is analogous to the approach we used to tune the purple-to-red transition point, but we modulated expression levels of an enzyme, rather than a transcriptional regulator. Cells with lower expression levels of CrtY require a higher concentration of zinc to produce sufficient CrtY to mediate the red to orange color change and thus should appear red over a larger range of zinc concentrations.

Through these tuning approaches, we created a suite of three-color sensor cells with tunable zinc thresholds. We initially performed tests in media that contained glucose as the carbon source (Figure 20B), and in these cells, violacein largely overpowered carotenoid expression and created murky colored intermediates. When we instead used glycerol as the carbon source, cells show reduced violacein expression and increased carotenoid expression. They then appear distinctly purple, red, and orange (Figure 20C), and have purple "off" points between 1 and 2 μM zinc. Cells with the lowest CrtY expression do not turn orange over the range of zinc tested, and cells with the highest CrtY expression transition from red to orange between 0 and 1 μM zinc. The best responding cells, which have intermediate CrtY expression, turn from red to orange at approximately 5 μM zinc, enabling sensor cells that meet the defined criteria of producing three different colors between 0.5 and 5 μM zinc.

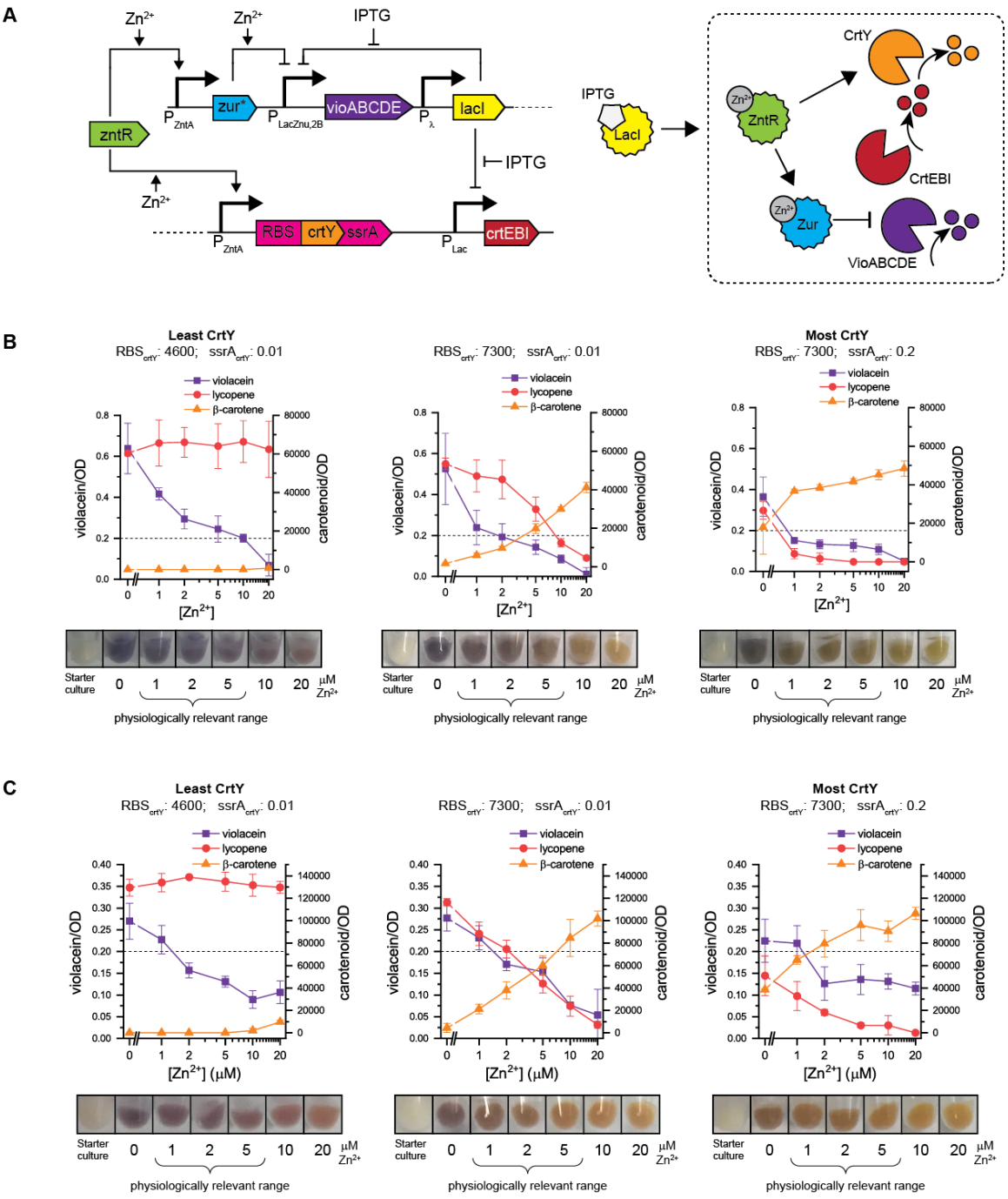

Figure 20: Multi-color sensor cells that respond to physiologically relevant zinc concentrations.

(A) Circuit diagram and schematic depicting the design of tunable sensor cells. During the pre-assay culture stage, LacI represses all pigment production. IPTG addition activates the pigment production stage, which is indicated by the dashed box. ZntR controls expression of both Zur and CrtY. At a threshold zinc concentration, Zur will repress expression of the violacein pathway, leading to cells that are red at

intermediate zinc concentrations. Increasing amounts of zinc also lead to increased amounts of CrtY, which converts lycopene to beta-carotene. Modulation of the RBS and ssrA tag on CrtY can be used to tune the red to orange transition point. (B) Pigment quantification and visualization of three-color sensor cells grown in minimal medium containing glucose. All sensor cells have tunable color transition points, but high baseline violacein production and low overall carotenoid expression leads to murky-looking cells. (C) Pigment quantification and visualization of sensor cells grown in minimal medium containing glycerol. All sensor cells have violacein "off" points between 1 and 2 µM, and the lycopene to β-carotene transition points vary based on the expression levels of CrtY. The best performing sensor cells have moderate CrtY expression and are visibly purple, red, and orange across a physiologically relevant range of zinc concentrations. The dotted line indicates the threshold for visible violacein.

3.3.4 Assessment of physiologically relevant zinc concentrations in human serum

We next used these cells to assess zinc concentration in real human serum. We first used an inducible lycopene circuit to show that cells are metabolically active in serum as long as they are inoculated to a sufficiently high OD (Figure 21).

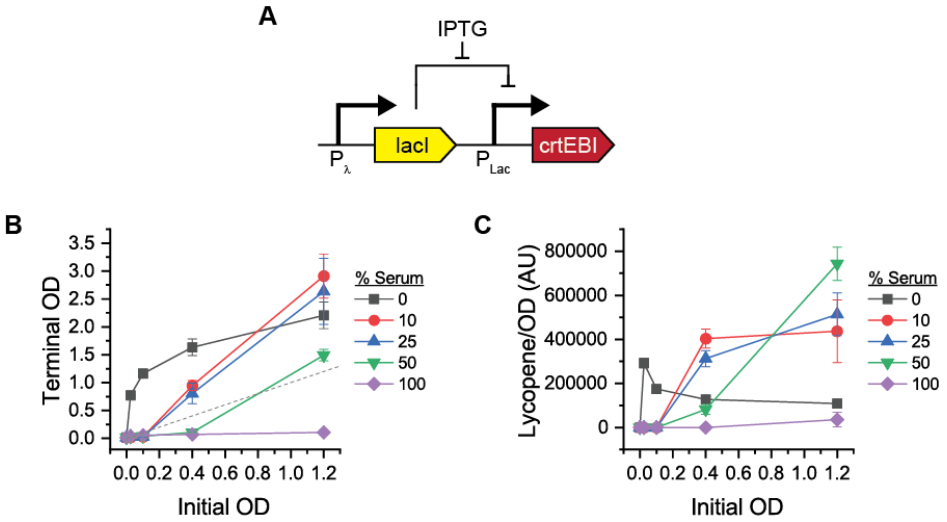

Figure 21: Effect of serum percentage and inoculation density on cell growth and pigment production.
(A) Circuit diagram of construct used to test metabolic activity. The *crtEBI* genes, which produce the red pigment lycopene, are controlled by an IPTG-inducible promoter. (B) Effect of serum percentage and initial inoculation density on terminal OD. For cells to grow in increasing amounts of serum, cultures must be inoculated to

higher starting densities. Data points falling below the dotted gray line indicate that cells had negative changes in OD, which could indicate cell lysis. (C) Effect of serum percentage and initial inoculation density on terminal lycopene production. When grown in serum, if cultures are inoculated to a sufficiently high initial OD, cells produce more OD-normalized lycopene than cells grown without serum.

Based on preliminary experiments (data not shown) that showed stronger color production at even higher inoculation densities, we inoculated a very high concentration of the initial sensor cells ($OD_{initial}$ = 3.0) into media containing 25% human serum that had different zinc concentrations. Cells produced different pigments based on the concentration of zinc in the sample, turning either purple, red, or orange across a physiologically relevant range of zinc concentrations (Figure 22).

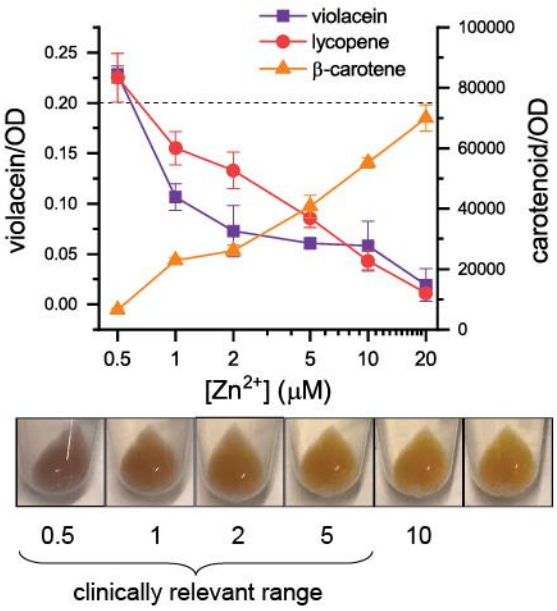

Figure 22: Pigment quantification and visualization of sensor cells grow in 25% serum with IPTG and specified zinc concentrations.
Assessment was performed four hours after inoculation. Cells are visibly purple, red, or orange across a range of physiologically relevant zinc concentrations. The dotted line indicates the threshold for visible violacein.

Though we focused on equipment-free test interpretation, cell color results could also be assessed quantitatively, which would eliminate potential subjectivity and variability and could enable more precise and reliable assessment of serum zinc values. Using the RGB values from the color bar used in the survey to assess color thresholds (Figure 15), we developed linear relationships between RGB values and perceived color. We then quantified the RGB values of photos of cell pellets and calculated a "color score" that indicates the cell's relative color (with purple = 0 – 1.5, red = 1.5 – 2.5, and orange = 2.5 – 4) (Figure 23 A-C). Color scores increase with increasing zinc concentrations, and based on set thresholds, cells grown in the physiologically relevant concentration range of 0.5 – 5 μM zinc are either purple, red, or orange (Figure 23D). Though we used color scores only for classification of colors into one of three bins, a calibration curve that relates color score to zinc concentrations could enable more precise zinc quantification.

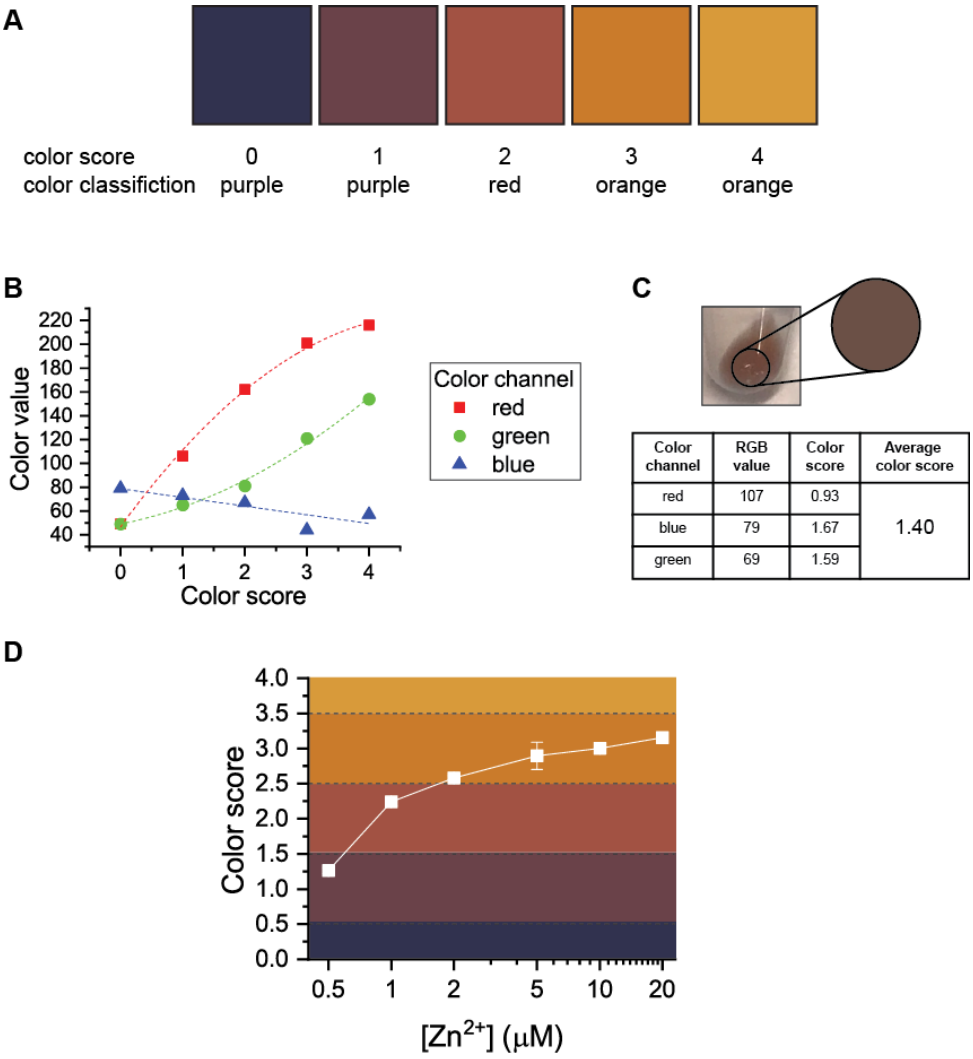

Figure 23: Quantitative color assessment of cells grown in human serum.
(A) Colors and color scores that correspond with purple, red, and orange cells. Color classifications are based on the color spectrum shown in Figure 15. (B) Plot of the RGB values corresponding with the color bar shown in (A). From these data, we determined relationships to relate the raw color value of each channel to the color score that describes whether cells are purple, red, or orange. The x-axis represents color, with 0 and 1 corresponding with purple cells, 2 corresponding with red cells, and 3 and 4 corresponding with orange cells. (C) Example of photo processing pipeline. The average RGB values of each cell pellet are determined with Adobe Photoshop. For each of the red, blue, and green values, a color score is calculated using the correlations shown in (B). These three numbers are averaged to produce a single overall color score. (D) Quantitative color assessment of sensor cells. Using RGB values taken from images of cell pellets, a color score was calculated for cells grown in each zinc concentration. Data points show the average of three biological replicates, and error bars indicate standard deviation.

3.4 Discussion

We have demonstrated significant steps in the development of a pigment-based biosensor for micronutrient testing and have developed generalizable strategies to decrease the time to response, increase cell stability, and tune the response range that can be applied to the development of other responsive microbial systems. The final sensor cells turn either purple, red, or orange to indicate whether a sample has dangerously low, borderline, or healthy levels of serum zinc. The test can be interpreted visually by matching colors to a color bar or quantitatively by simply taking a picture of the cells and determining RGB values. Compared to previous proof-of-principle work, we reduced assay time by nearly an order of magnitude, meeting a critical requirement for in-field micronutrient assessment. We also tuned the sensor response point by an order of magnitude, reducing the colorimetric response range to a clinically relevant range of 0.5 – 5 μM.

The developed sensor cells can serve as the foundation of a zinc diagnostic that meets the requirements for a field-deployable micronutrient assay[18]. Tests produce results quickly (within the typical time allocation for an in-home visit during a nutritional survey campaign), require minimal equipment, and require minimal sample processing. Serum could be isolated from blood with a low-cost, portable, paper-based centrifuge[109], and added to lyophilized sensor cells. After a four-hour incubation, the user could assess test results visually or with a camera phone that contains a simple photo processing program. This test would allow zinc assessment to be incorporated into standard public health surveys and thus provide governments and aid organizations with the information needed to efficiently implement zinc supplementation programs.

More broadly, the sensor cells we created can serve as a platform for the development of other sensor cells that produce chemical outputs. In the final sensor cells, a single transcription factor mediates multiple metabolite production pathways: ZntR directly mediates production of β-carotene and indirectly mediates production of violacein by controlling expression of Zur, which is effectively a constitutive repressor. By replacing P_{zntA} with a different metabolite-responsive promoter, one could easily make a pigment-based biosensor for a different target metabolite. *E. coli* has a host of metabolite-responsive promoters[46], enabling easy production of sensors for a range of metabolites. Transcription factors and regulatory pathways from other organisms can also be expressed in *E. coli*, further broadening the scope of biosensor development. For applications outside of pigment-based biosensing, other metabolic pathways could replace the pigment expression pathways to enable production of a desired chemical upon sensing a threshold concentration analyte.

Recently developed prototyping tools can help facilitate easy incorporation of new metabolic pathways into this sensing framework. Cell-free expression (CFE) systems, which use bacterial protein extract to implement genetic networks, can be used to rapidly prototype metabolic pathways to determine the optimal relative expression levels of each pathway enzyme[71,72]. While CFE systems have garnered attention for use as biosensors[16,110], for applications that require sustained and scalable chemical production, living cells are the more advantageous chassis, and CFE systems are most useful as tools to rapidly explore the design space.

While we were able to effectively shift Zur's response point, our tuning strategy sacrificed Zur's original sharp, step-like response (which would have enabled more

discrete color changes) for a linear response over the concentration range of interest. Incorporation of positive feedback loops and more extensive protein engineering efforts could be used to create systems that have both shifted response thresholds and cooperative, switch-like responses. Further optimization could also involve redesigning the system to allow more orthogonal control of expression levels of specific proteins. To alter levels of both Zur and CrtY, we used protein degradation tags because of their effectiveness in decreasing protein levels. However, using degradation tags to control multiple regulator proteins could introduce competition for proteases and thus inadvertently couple expression levels of the two proteins. Alternative approaches for more precise, orthogonal tuning could rely solely on modulating RBS strength.

As the applications of biosensing expand to include not just sensors, but living therapies, engineering cells to deliver diverse types of payloads upon sensing target molecules will be critical. Responsive bacterial therapies have already been developed for treatment of cancer[10,11], metabolic disorders[12,13], and inflammation[14], and cells that produce complex chemicals upon target recognition could have an even greater impact on disease treatment. The presented approaches for incorporating chemical production into biosensors in a robust and tunable fashion can help to enable a new generation of bacterial sensors to meet the need for responsive chemical delivery.

CHAPTER 4. POINT-OF-CARE BIOMARKER QUANTIFICATION IN CELL-FREE DIAGNOSTICS

4.1 Introduction

The previous two chapters described our efforts towards a field-deployable whole-cell biosensor for in-field zinc assessment. We created a biosensor that produces multiple pigments that correspond with different concentrations of serum zinc, and the tests are interpretable within four hours of sample addition. However, engineering a field-deployable test still requires developing protocols for cell lyophilization, packaging, reconstitution, and point-of-care incubation. Cell-free systems, which use bacterial protein extract for transcription and translation, have already been demonstrated to be field-deployable: they can be lyophilized on paper and rehydrated in the field, they produce colored outputs quickly, and they require very small reaction volumes. Because of these advantages, we explored whether we could use cell-free expression systems to create a more field-friendly zinc sensor.

In recent years, cell-free expression (CFE) systems have dramatically expanded the scope and applications of synthetic biology[56]. CFE systems have brought drug manufacturing, vaccine production, and disease diagnoses from labs and clinics into the field, where production or testing can be performed on-demand and on-site[15,110]. Low cost, ease of use, and ability to be stably stored and shipped make CFE systems appealing for use in low-resource settings. CFE systems have been particularly useful in the development of fast and sensitive diagnostic tools for infectious diseases, including Ebola and Zika

viruses[16], with other technologies expanding on these advances[74,75,111]. However, to date, low-resource CFE diagnostics have been limited to diseases that have nucleic acid biomarkers.

Differences in levels of other biomarkers, such as ions, metabolites, and proteins, indicate a wide variety of important diseases and conditions, including micronutrient deficiencies[112-114]. Unlike diagnosing infectious diseases, which requires determining only whether a specific pathogen is present, diagnosing these conditions can necessitate discriminating biomarker levels across a small range of concentrations. The ability to sense small molecules and ions in cell-free reactions[76-78] suggests that the benefits of CFE diagnostics could extend beyond infectious diseases. However, the potential applications of low-resource CFE measurement of biomarkers in relevant samples (such as serum) are limited to detection, rather than quantification, in large part because equipment-free quantification methods (i.e., the ability to read measurements with the naked eye) do not exist. Moreover, variability in the components of samples can affect the readouts of even sophisticated analytical instrumentation, a phenomenon known as "matrix effects". These matrix effects can cause inaccurate or irreproducible results, and are prominent in CFE reactions, thus precluding the use of defined reference standards (e.g., pure chemical standards or pooled plasma), which by definition are not in the exact matrix of the test sample. While we have made efforts to address some of these challenges in the development of a whole-cell zinc biosensor, we sought to develop a related semi-quantitation method for CFE diagnostics.

Here, we present a CFE diagnostic platform capable of semi-quantitatively measuring serum zinc levels in an equipment-free fashion. The key innovation is the

development of a standardization approach that allows equipment-free quantitation in assays consisting of 25-100% human serum. To account for both general matrix effects of serum as well as inter-individual donor matrix variation, the standardization scheme is designed so that the serum sample to be analyzed is added both to the test reaction and to a set of standard reference reactions. Analogous to a litmus test, the color of the test can be matched to the colors of the reference reactions so that the user can easily determine the sample concentration. The test reliably quantifies clinically relevant zinc concentrations and is a significant step towards a low-cost, field-deployable test for zinc deficiency. We demonstrate the generalizability of our semi-quantitation method by applying it to a sensor that uses an established toehold switch. The developed test is the first CFE assay to provide equipment-free biomarker quantification in a complex matrix, and the platform developed can be readily expanded to quantify other molecules in cell-free expression reactions.

4.2 Materials and Methods

4.2.1 Construction of zinc-responsive circuit

Three plasmids were assembled through Gibson assembly: one in which the transcription factor ZntR was under the control of a standard T7 promoter, one in which P_{ZntA} controlled GFP production, and one in which P_{ZntA} controlled LacZ production. ZntR and P_{ZntA} were amplified from a previously described circuit[26]. LacZ was amplified from BL21(DE3) genomic DNA, and sfGFP was amplified from the plasmid pJL1. All operons were cloned into a plasmid containing a ColE1 origin and a kanamycin resistance cassette. All plasmids were purified with EZNA midiprep columns and sequence confirmed.

4.2.2 Construction of knockout strains

Lambda red recombination was used to make all knockout strains[100]. Two knockout strains were constructed: a Lac knockout strain was constructed as previously described[76] to make BL21(DE3) *ΔLac*, and a dual knockout strain in which ZntR was deleted was also constructed: BL21(DE3) *ΔLac ΔZntR.* For the dual knockout strain, ZntR was first knocked out and selected for through antibiotic resistance. Then, the Lac operon was knocked out, and blue-white screening was used to determine successful knockouts.

4.2.3 Preparation of cellular lysate

Cellular lysate for all experiments, excluding toehold switch experiments, was prepared as previously described[63]. BL21(DE3) *ΔLac ΔZntR* cells were grown in 2x YTPG medium at 37°C and 180 rpm to an OD of 2.0, which corresponded with the mid-exponential growth phase. Cells were then centrifuged at 2700 rcf and washed three times with S30 buffer. S30 buffer contains 10 mM Tris-acetate (pH 8.2), 14 mM magnesium acetate, 60 mM potassium acetate, and 2 mM dithiothreitol (DTT). After the final centrifugation, the wet cell mass was determined, and cells were resuspended in 1 mL of S30 buffer per 1 g of wet cell mass. The cellular resuspension was divided into 1 mL aliquots. Cells were lysed using a Q125 Sonicator (Qsonica, Newton, CT) at a frequency of 20 kHz, and at 50% of amplitude. Cells were sonicated on ice with three cycles of 10 seconds on, 10 seconds off, delivering approximately 180 J, at which point the cells appear visibly lysed. An additional 4 mM of dithiothreitol was added to each tube, and the sonicated mixture was then centrifuged at 12,000 rcf and 4°C for 10 minutes. The supernatant was removed, aliquoted, and stored at -80°C for future use.

Cellular lysate for toehold switch experiments was prepared as previously described in Sun, et al[115]. BL21 Star (DE3) Δ*Lac* cells were grown in 2x YTP medium at 37˚C and 220 rpm to an OD of 2.0. Cells were centrifuged at 2700 rcf and washed three times with S30A buffer (50mM of Tris, 14 mM magnesium glutamate, 60 mM potassium glutamate, 2 mM dithiothreitol, pH corrected to 7.7 with acetic acid). Wet cell mass was determined after the third centrifugation step, the cells were resuspended in 1 mL of S30A buffer per 1 g of wet cell mass and sonicated using the same method described above, though with a sonication output of approximately 400 J. Following the centrifugation of the sonicated cellular mixture, the supernatant was removed, divided into 0.5 mL aliquots, and incubated at 37˚C and 220 rpm for 80 minutes. After this runoff reaction, the cellular lysate was centrifuged at 12,000 rcf and 4˚C for 10 minutes. The supernatant was removed and loaded into a 10 kDa MWCO dialysis cassette (Thermo Fisher). Lysate was dialyzed in 1L of S30B buffer (14 mM magnesium glutamate, 60 mM potassium glutamate, 1 mM dithiothreitol, pH-corrected to 8.2 with Tris) at 4˚C for 3 hours. Dialyzed lysate was removed and centrifuged at 12,000 rcf and 4˚C for 10 minutes. The supernatant was removed, aliquoted, flash frozen in liquid nitrogen, and stored at -80˚C for future use.

4.2.4 Cell-free reactions: constitutive expression and zinc-sensing

Cell-free reactions for all experiments, excluding toehold switch reactions, were run as previously described[65]. Each cell-free reaction contained 0.85 mM each of GTP, UTP, and CTP, in addition to 1.2 mM ATP, 34 μg/mL of folinic acid, 170 μg/mL *E. coli* tRNA mixture, 130 mM potassium glutamate, 10 mM ammonium glutamate, 12 mM magnesium glutamate, 2 mM each of the 20 standard amino acids, 0.33 mM nicotine adenine dinucleotide (NAD), 0.27 mM coenzyme-A (CoA), 1.5 mM spermidine, 1 mM

putrescine, 4 mM sodium oxalate, 33 mM phosphoenol pyruvate (PEP), 27% cell extract, and the specified concentration of plasmids. In all reactions producing LacZ, CPRG was added to a final concentration of 0.6 mg/mL. All chemicals were purchased from Sigma Aldrich. In reactions containing human serum, RNase inhibitor (NEB) was added to a concentration of 0.6 U/μL.

In all reactions producing GFP, plasmids were added to reactions at a final concentration of 20 ng/μL. Plasmid dosage of LacZ and ZntR expression plasmids (pLacZ and pZntR) was optimized so that color change would be observable at approximately 60 minutes. In reactions without serum, pLacZ was added at a concentration of 1.0 ng/μL when ZntR was pre-expressed, and at a concentration of 1.5 ng/μL when ZntR was co-expressed. When ZntR was co-expressed in reactions without serum, pZntR was added to reactions at a concentration of 0.5 ng/μL. In all reactions with serum, pLacZ was added at a concentration of 15 ng/μL, and pZntR was added at a concentration of 2.5 ng/ul.

In experiments in which ZntR was pre-expressed and added to the reaction, ZntR was first produced overnight in a cell-free reaction. Reactions were carried out in 1.5 mL microcentrifuge tubes, and the reaction volume in each tube was 50 μL. A plasmid expressing ZntR was added at 20 ng/μL, and a plasmid expressing a ZntR-GFP fusion protein was added at 1 ng/μL. Reactions were incubated at 30°C for 16 hours. Reactions were then centrifuged at 12,000 rcf and 4°C for 10 minutes, and the supernatant was removed and subsequently used. To measure fluorescence, each reaction was diluted by a factor of 10 in DNAse-free ultrapure water. 10 μL was added to a well of a 384 well plate, and the fluorescence was measured with a plate reader (Synergy4, BioTek). Excitation and emission for sfGFP were 485 and 528 nm, respectively. Fluorescence values were used to

account for batch-to-batch variations so that a constant amount of ZntR was added to each reaction. Unless otherwise specified, the overnight ZntR reaction was added to fresh reactions at a concentration of 1% (+/- variations of less than 0.05% determined through fluorescent quantification measurements).

CFE reactions were run in 8 μL volumes in 384 well small volume plates (Greiner Bio-One), and a clear adhesive film was used to cover the plate and prevent evaporation. Fluorescence of GFP was quantified as described above. LacZ activity was monitored by measuring absorbance at 580 nm. For time course experiments, plates were incubated at 37°C, and either fluorescence or absorbance was measured every two minutes. For end-point experiments, plates were incubated at 37°C, and fluorescence was measured after 22 hours.

4.2.5 Cell-free reactions: toehold switches

For experiments involving toehold switches, cell-free reactions were run according to the protocol described in Sun, et al[115]. Each reaction contained 1.5 mM of ATP and GTP, 0.9 mM of CTP and UTP, 0.2mg/mL *E. coli* tRNA mixture, 0.33 mM of NAD, 0.26 mM of CoA, 0.75mM cyclic adenosine monophosphate (cAMP), 0.068 mM of folinic acid, 1 mM of spermidine, 30mM of 3-phosphoglyceric acid (3-PGA), 50mM of HEPES, 1.5mM each of the 20 standard amino acids, 4 mM of magnesium glutamate, 100 mM of potassium glutamate, 2% PEG-8000, 33% cell extract, 0.6 mg/mL CPRG, and DNA expression plasmids. Toehold switch was expressed from the plasmid pSwitch. Unless otherwise specified, the concentration of pSwitch in reactions was 2.5 nM. Trigger RNA was produced from 40 ng/μL linear DNA template in an *in vitro* transcription reaction using T7

RNA Polymerase (NEB), following the manufacturer's protocol. Synthesized RNA was treated with DNase to remove the DNA template and then purified using a Zymo RNA Clean and Concentrator kit (R1014), according to the manufacturer's protocol. The concentration of trigger RNA added varied across experiments. Time course reactions were run as described above.

4.2.6 Determination of best-fit reactions and predictive standard reactions

In determining which standard reference reaction best fit each zinc concentration, sum of squared error (SSE) minimization was used. The difference between each standard and test reaction was calculated at all time points between 30 and 90 minutes. The SSE was calculated over this time frame, and the standard reaction that had the lowest SSE was determined to be the best-fit reaction and thus the optimal regulator for that experimental run. When choosing what regulator concentration best predicts each potential biomarker concentration, we determined the overall optimal regulator concentration as the one closest to the average of the optimal matching regulator concentration across three runs.

4.2.7 Quantitative Error Metric Calculations

We defined a quantification error metric (QEM) to compare the absorbance readings of the test and standard reactions that should predict the test reaction. We first calculated the difference between prediction and absorbance readings at each time point..

$$\Delta A(i,j) = \left| A_{580,predicted}(i) - A_{580,actual}(j) \right| \quad (1)$$

$i =$ index of zinc prediction

$j =$ index of zinc test evaluated

Then, we calculated the normalized sum of squared error for the correct prediction readings for each zinc concentration. We defined this as the QEM of the correct predictions ($QEM_{correct}$). Ideally, the $QEM_{correct}$ should be zero to indicate identical absorbance curves between test reactions and the corresponding correct prediction.

$$QEM_{correct} = \frac{1}{n}\sum_{i=1}^{n}\left(\Delta A(i,i)\right)^2 \quad (2)$$

$n =$ number of zinc concentrations evaluated

$i =$ index of zinc concentration evaluated

We next calculated the normalized sum of squared error for the closest incorrect predictions and defined this as the $QEM_{incorrect}$. Ideally, the $QEM_{incorrect}$ should be very high to indicate substantial absorbance differences corresponding with incorrect predictions.

$$QEM_{incorrect} = \frac{1}{2(n-1)}\sum_{i=1}^{n-1}\left(\Delta A(i,i+1)\right)^2 + \left(\Delta A(i+1,i)\right)^2 \quad (3)$$

$n =$ number of zinc concentrations evaluated

$i =$ index of zinc concentration evaluated

In all evaluation of quantification error, we set a threshold of 0.0484, which is 0.22^2. Across all experiments, the average maximum A_{580} value was approximately 2.2, so 0.22 corresponds with one-tenth of the spectrum. Values below the threshold indicate indistinguishable differences, and values above the threshold indicate distinguishable differences.

4.2.8 Preparation of human serum

Pooled human serum was purchased from Corning. Chelex 100 (BioRad) was used to deplete zinc from the serum. 1 g of resin was added to 100 mL of serum, and serum was stirred for 2 hours. Resin was removed from serum through filtration.

In single donor experiments, blood was collected from donors as approved in IRB protocol number H17489. Venous blood was collected in 6 mL BD Vacutainer collection tubes for trace element testing, and tubes were left on ice for 30 minutes to clot. Blood was then transferred to a 50 mL conical tube and centrifuged at 2700 rcf, 4°C for 30 minutes. The serum was removed and either immediately frozen or treated with Chelex-100 resin. 80 mg of resin was added to 8 mL of serum, and the mixture was vigorously stirred for 2 hours. Resin was isolated from the samples through centrifugation, and serum was syringe filtered. All serum samples were aliquoted to minimize freeze-thaw cycles and stored at -20°C.

4.2.9 Zinc measurements

Zinc concentration of pooled serum was analyzed using an X-Ray Fluorescence spectrometer. 2 μL of serum was spiked with 1 ppm of a gallium internal standard, pipetted

onto a quartz disc, and atomic fluorescence emission spectra were collected. Zinc concentration in individual donor serum samples was measured at the University of Georgia Laboratory for Environmental Analysis. Samples were digested with concentrated acid and analyzed on an ICP-MS according to EPA method 3052.

4.2.10 Spectra analysis

To analyze the spectrum of chlorophenol red and reaction intermediates, a large batch of concentrated chlorophenol red was made by adding CPRG to a small amount of extract made from standard BL21(DE3) cells (which have high baseline LacZ activity). The spectrum of CPR was analyzed to ensure that all CPRG reacted to CPR by screening for absence of a detectable peak at 410 nm. Different combinations of CPRG and CPR were then added to solutions containing 27% bacterial cell extract (made from BL21(DE3) *ΔLac* cells), with or without serum. The final concentration of dye in each solution analyzed was 1.02 μM, which corresponds with addition of 0.6 mg/mL of CPRG.

When adding small molecules to the reaction, 10x stocks of each molecule were made. Penicillin, dicloxacillin, and naproxen were dissolved in water, ibuprofen was dissolved in ethanol, and sulfisoxazole was dissolved in chloroform. 3 μL of each stock was added to PCR tubes, and tubes were left open in a fume hood overnight so that solvents could evaporate. A 30 μL solution containing the specified amount of dye, protein extract, and serum was used to re-dissolve the small molecule. Concentrations reported are the final concentration of small molecule in the analyzed solutions.

The spectra of all solutions reported were measured in triplicate with a Nanodrop 2000. When analyzing reaction intermediates, spectrum height was normalized to a peak

at 280 nm. When further analyzing the peak corresponding with CPR, each spectrum was first height-normalized so that the maximum of the peak corresponding with chlorophenol red was the same for all spectra. Then, the wavelengths that correspond with 4 different absorbance intensities were determined and subtracted from the values of the control spectrum. The four differences were averaged to compute the overall wavelength shift. Reported averages are the average of the overall wavelength shift of the three initial replicates.

4.2.11 Color imaging and processing

All pictures were taken with a Panasonic Lumix camera in a light-controlled setting. All pictures in figures showing color results are of 8 μL reactions in 384 well plates. The centers of selected reaction wells were cropped using Adobe Photoshop and combined to make color arrays. A brightness filter was applied to photos to make them better resemble actual appearance.

4.2.12 Lyophilization

30 μL reactions were prepared in PCR tubes and flash frozen in liquid nitrogen. Frozen samples were removed from liquid nitrogen and added to a Labconco Fast-freeze flask that contained a small amount of liquid nitrogen. Care was taken to transfer samples quickly and keep samples cold throughout the transfer process. Flasks were connected to a LabConco benchtop freeze-drier and lyophilized at -50°C and 0.05 mbar for 3 hours. Samples were then removed and rehydrated on ice.

4.3 Results

4.3.1 Development of a cell-free zinc detection system

In developing a cell-free quantification method, we chose to use zinc as the model analyte because of its global health relevance[21] and our group's previous experience in developing whole-cell zinc biosensors[25,26,79]. To begin, we tested whether zinc-responsive elements could properly control output in a CFE reaction. We constitutively expressed the zinc-responsive activator ZntR, and used this transcription factor to control GFP expression from ZntR's cognate promoter P_{zntA} (Figure 24A). The system showed dose-dependent zinc response between 0 and 8 μM (Figure 24B), demonstrating that zinc can be detected in a cell-free system. Notably, the system also showed a dramatic decrease in protein production at higher zinc concentrations, which can likely be attributed to decreased expression from native *E. coli* σ_{70} promoters at high zinc concentrations (Figure 24C).

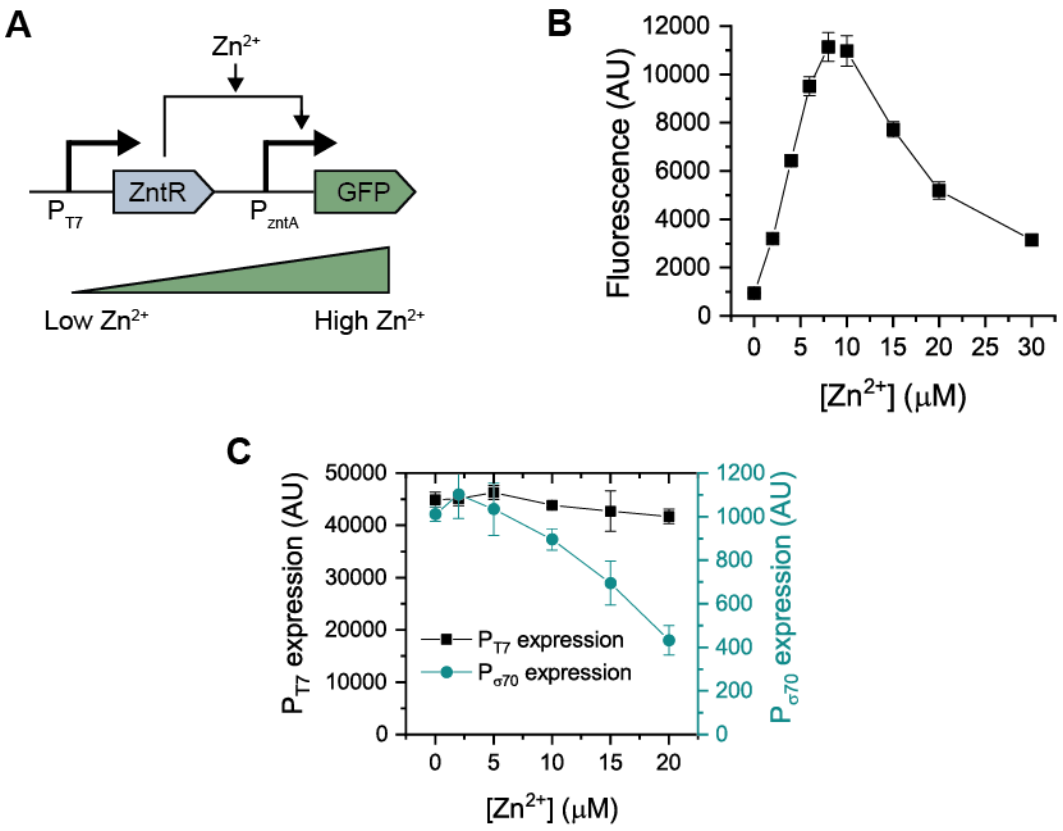

Figure 24: Cell-free expression systems respond to added zinc.
(A) Schematic of a zinc-responsive circuit used to control GFP production. ZntR is expressed from a T7 promoter, and GFP is expressed from the ZntR-activated promoter P_{zntA}. (B) Fluorescent output in response to zinc. (C) Effect of zinc on expression from constitutive promoters. Increasing amounts of zinc slightly decrease expression from T7 promoters and substantially decrease expression from σ_{70} promoters. GFP was used to measure protein expression. Error bars represent standard deviation.

To better enable equipment-free testing, we replaced the GFP reporter with beta-galactosidase (LacZ) to create a colorimetric output (Figure 25Figure 24A), using a bacterial extract with no LacZ or ZntR background activity. LacZ cleaves the yellow substrate chlorophenol red-β-D-galactopyranoside (CPRG) to the purple product chlorophenol red (CPR) and has previously been used in the development of low-resource diagnostic tools[15]. Colorimetric output can be quantified by measuring absorbance at 580

nm or assessed qualitatively by looking at reaction color. Different ratios of CPR to CPRG create a large spectrum of colors (Figure 25B) that directly correspond with absorbance readings.

Using this system, we engineered a colorimetric response to zinc concentrations (Figure 25C, Figure 25D). At early time points, there is no detectable LacZ activity, and all reactions look yellow. Between 50 and 80 minutes, the test clearly differentiates between zinc concentrations, with better differentiation of high zinc concentrations at earlier times and better differentiation of lower zinc concentrations at later times. At late reaction time points (90 minutes), almost all of the reactions have gone to completion (all tests with zinc concentrations over 2 μM look purple). As reactions proceed from yellow to purple, they pass through intermediate reaction phases that are different shades of orange and red.

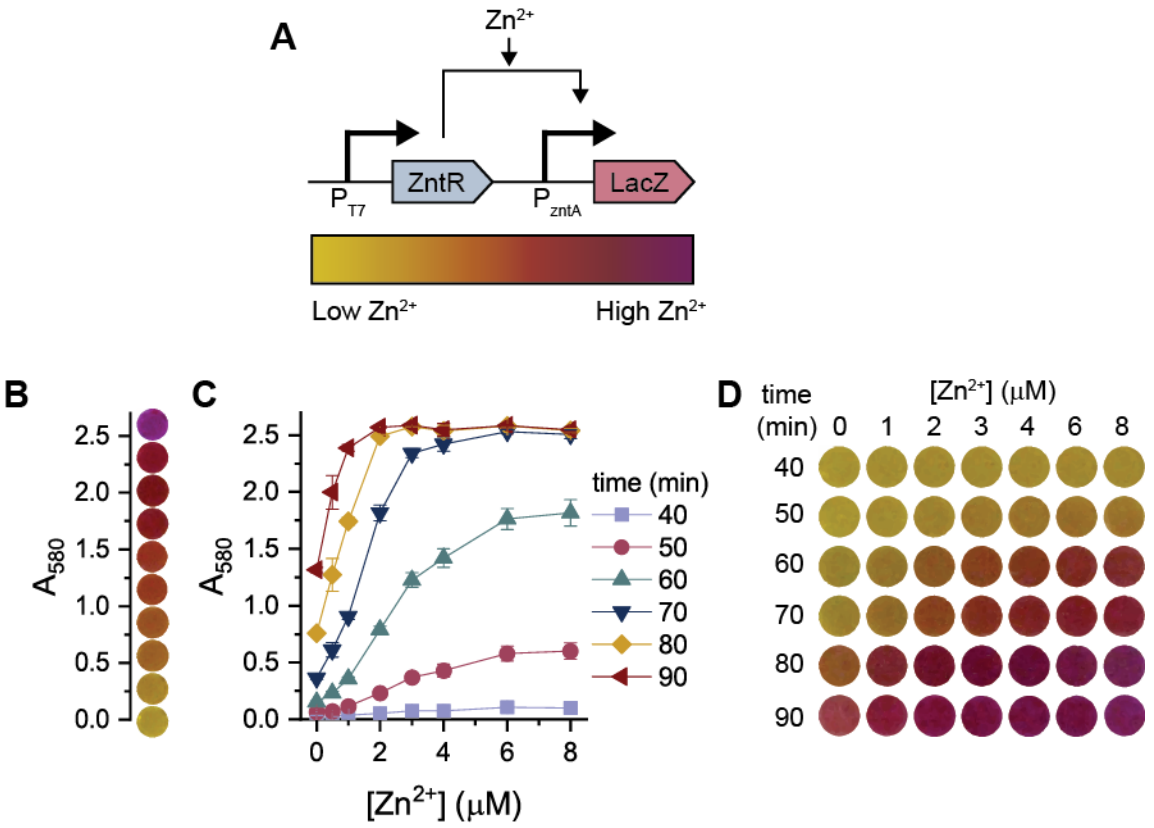

Figure 25: Colorimetric response to added zinc in CFE reactions.
(A) Schematic of a zinc-responsive circuit used to control LacZ expression. (B) Pictures of visible colors from reactions corresponding with different absorbance measurements. The lowest A_{580} readings correspond with yellow reactions, and as the A_{580} increases, the reaction color turns different shades of orange, red, and purple. (C) Quantitative colorimetric response to added zinc. At early time points, there is no detectable absorbance of the purple substrate CPR at tested [Zn^{2+}]. As the reactions proceed, they produce CPR at different rates based on the concentration of Zn^{2+} in the reaction, with maximal differences visible between 60 and 70 minutes. Ideal assay readout times would span a wide range of absorbances across as much of the [Zn^{2+}] range as possible. (D) Qualitative colorimetric response to added zinc. Reactions that were measured quantitatively in (C) were imaged at different time points. Between 60 and 80 minutes there is a clear color gradient based on zinc concentration.

To tune reaction timing for detection purposes, we modulated the concentration of reporter plasmid in the reaction. As expected, higher concentrations of the reporter plasmid (pLacZ) decrease the incubation time required for visible color, though they also decrease

the time frame in which a dose-dependent zinc response is detectable (Figure 26). Thus, plasmid dosage can be used to create tests that meet the necessary time parameters for a given application.

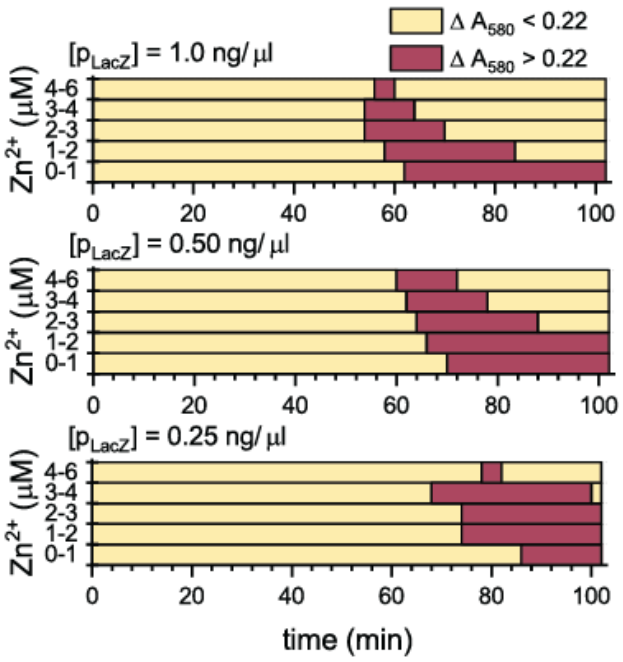

Figure 26: Effect of reporter plasmid concentration on ability to distinguish between different zinc concentrations.
Zinc concentrations were considered indistinguishable if the difference in A_{580} readings between two concentrations was less than 0.22. Times highlighted in red indicate that the absorbance difference between the two concentrations on the y-axis is above this threshold and thus the user can visualize colorimetric differences between the two concentrations.

Direct addition of the regulator ZntR to reactions (rather than simultaneous expression in the sensing reaction) could potentially improve sensor performance by simplifying the genetic circuitry in the reaction and reducing the number of added components. We showed that cell-free systems can detect zinc when the regulator ZntR is pre-expressed and subsequently added to the reaction at a fixed amount rather than being

co-expressed in the reaction. We overexpressed ZntR in an overnight CFE reaction and then added a small amount to a fresh sensing reaction. These reactions with pre-expressed ZntR show a reproducible zinc response (Figure 27) similar to the response when ZntR is simultaneously expressed in the reaction (Figure 25C) but show slight differences in range of detectable zinc. Though both tests show nearly linear changes in color output between 0 and 4 µM zinc, tests with co-expressed ZntR show further changes between 4 and 8 µM zinc, while tests with pre-expressed and added ZntR showed nearly identical output across this concentration range.

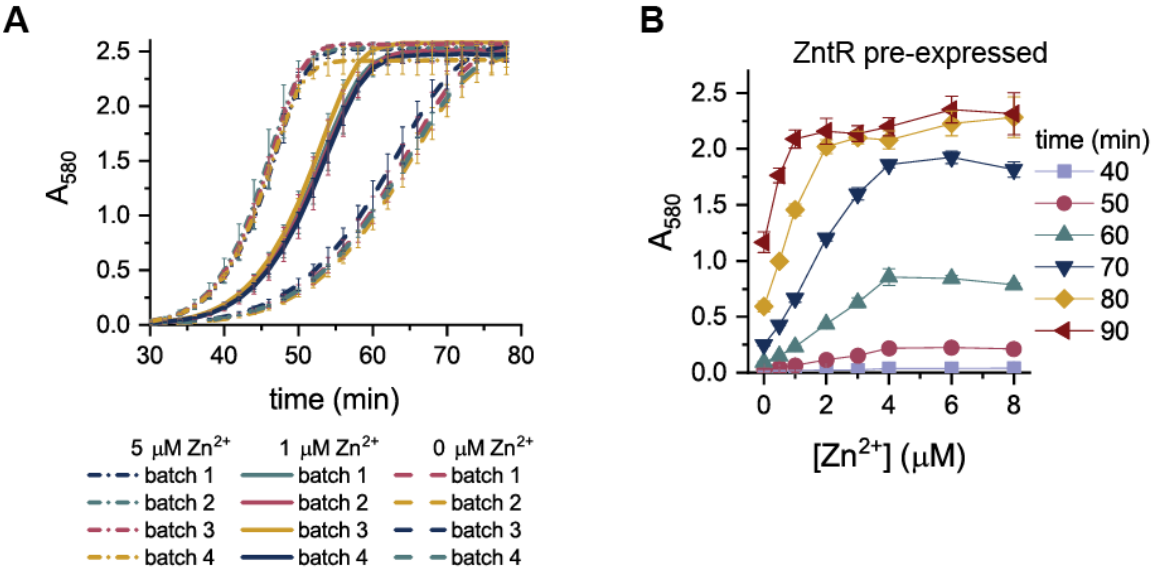

Figure 27: Direct addition of ZntR protein mediates a response to added zinc.
(A) Validation of ZntR protein addition to mediate CFE reactions. ZntR was expressed in 4 different batches, on different days and in different batches of cellular extract. When added to the reaction, each batch of ZntR mediated a nearly identical response to different concentrations of zinc. (B) Quantitative colorimetric response to zinc when ZntR is pre-expressed and added to the CFE reaction. Reactions controlled by pre-expressed ZntR respond similarly to reactions controlled by ZntR that is simultaneously expressed in the sensing reaction.

The developed test is compatible with field-friendly technologies. The CFE test with co-expressed ZntR was lyophilized and rehydrated in water with a range of zinc concentrations. Though the response is slightly slower than fresh reactions, the system shows a zinc response similar to that of reactions run without lyophilization (Figure 28), which demonstrates the potential for our zinc test to be field deployable.

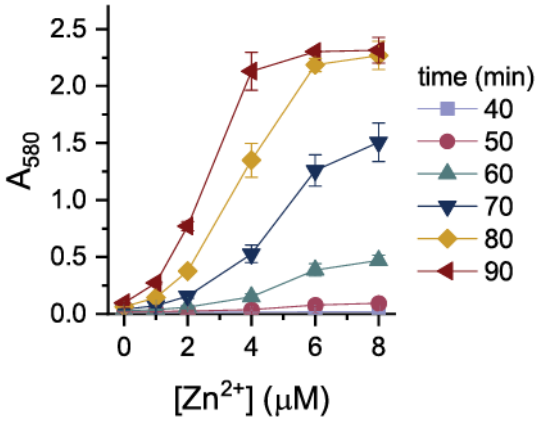

Figure 28: Quantitative colorimetric response to zinc of lyophilized reactions that were rehydrated in different zinc concentrations.
Zinc response is similar to that of fresh reactions. The incubation time required to observe color differences is slightly longer, but at intermediate and later time points (60 – 90 minutes), the color production varies between 0 and 8 μM Zn^{2+}.

4.3.2 CFE systems sense and respond to zinc in human serum

Since many biomarkers (including zinc) are measured in human serum or plasma, we next tested whether CFE systems could work in high serum concentrations. Previously developed CFE diagnostics amplify nucleic acids from a 10% serum matrix, but because of upstream processing steps, the final CFE reaction consists of less than 1% serum[16]. Similarly, minimal-equipment CRISPR-based diagnostics have only been shown to work in a 2% serum matrix[75]. Since an ideal in-field test would require minimal sample

processing and dilutions, we aimed to run the test in the highest possible concentration of serum.

We first showed that CFE reactions produce protein in a 25% serum matrix with addition of RNAse Inhibitor (Figure 29A). Because of the volume of necessary reaction components, 25% serum is the highest concentration that we could reasonably test using freshly assembled reactions. Though serum matrix effects reduce protein expression from both T7 and native *E. coli* promoters (Figure 29B), the observed expression levels still support the viability of running reactions in up to 25% serum.

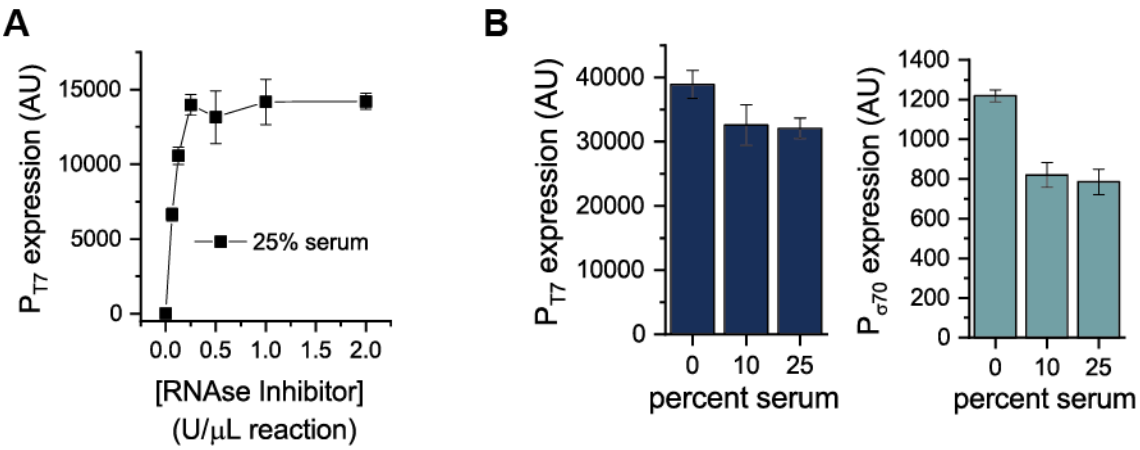

Figure 29: Protein production in high concentration of serum.
(A) Effect of RNAse inhibitor on CFE reactions in 25% serum. Inhibition of RNAse activity is necessary for protein expression in serum. In the absence of RNAse Inhibitor (RNAseI), reactions produce no detectable protein, and increased amounts of RNAseI enable expression. (B) Protein expression in reactions run in serum. The protein sfGFP was expressed from either a T7 or σ_{70} promoter. CFE reactions produce protein from both T7 and σ_{70} promoters in a matrix of up to 25% serum, which was the highest that could be tested in freshly assembled reactions.

To test whether the system could detect zinc in this matrix, we used Chelex 100 resin to remove zinc from pooled human serum, and confirmed that the concentration was reduced to 2.5 μM with X-Ray Fluorescence. We then added a range of zinc concentrations

to the treated serum. Reactions run in serum respond to a similar concentration range of zinc as reactions run in water, but reactions in serum have lower protein production at all zinc concentrations (Figure 30A). Because we wanted the colorimetric test to produce visible color quickly, we accounted for observed changes in overall protein production by adding a higher concentration of the LacZ reporter plasmid to reactions that contained serum (see Methods). Reactions run in 25% serum show colorimetric differences based on zinc concentration (Figure 30B)

Since an ideal low-resource test would not require any dilutions, we tested the function of lyophilized reactions that were reconstituted in pure serum. Reactions rehydrated in pure serum produce protein from both T7 and native *E. coli* promoters (Figure 30C) and regulate a response to a large range of zinc concentrations (Figure 30D). Reactions run in 100% serum produce differential color across the entire range of zinc concentrations tested (between 2.5 and 22.5 μM zinc), suggesting that not only is simplified testing with undiluted samples possible, but it may in fact provide a wider dynamic range for measurement.

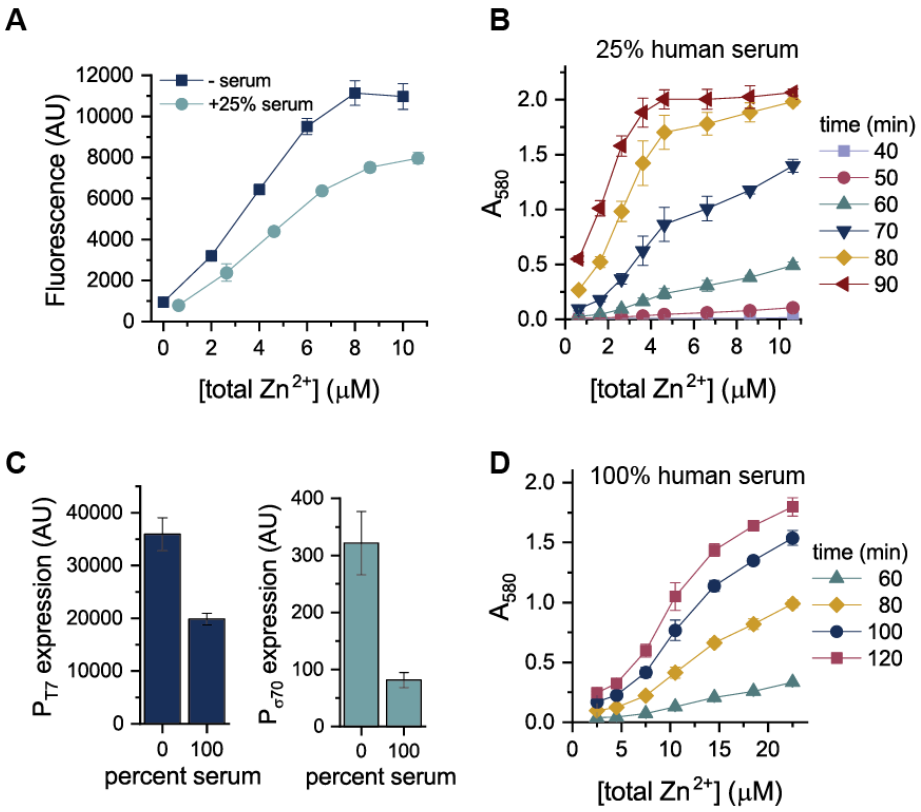

Figure 30: Zinc response in high concentrations of serum.
(A) Fluorescent response to zinc in 25% human serum. (B) Quantitative colorimetric response to zinc in 25% serum when ZntR is co-expressed in the CFE reaction. A higher concentration of LacZ plasmid was used so that color differences are visible between 60 and 80 minutes. (C) Protein expression in reactions run in 100% serum. CFE reactions expressing sfGFP from either a T7 or σ_{70} promoter were lyophilized and rehydrated in either water or serum. CFE reactions produce protein from both T7 and σ_{70} promoters in 100% serum, but expression is substantially lower than in reactions rehydrated with water. (D) Quantitative colorimetric response to zinc in lyophilized reactions rehydrated in different amounts of zinc. Color differences are apparent after 60 minutes, and the color output varies across the entire range of zinc tested (2 – 22 μM Zn^{2+}).

4.3.3 Development of parallelized calibration method

To make these measurements of serum field-friendly and equipment-free, we then developed a standardization method so that the color of the test reaction can be matched to an array of standard reactions run in the exact same sample matrix as the test reaction

(Figure 31). The standard reactions have saturated zinc concentrations and varying amounts of transcriptional regulator so that regulator concentration, rather than zinc concentration, controls colorimetric output. Importantly, the matrix effects of serum on CFE machinery will be identical in both the sample and the standards. Before testing this in the matrix of human serum, we first validated this approach in reactions that did not contain serum.

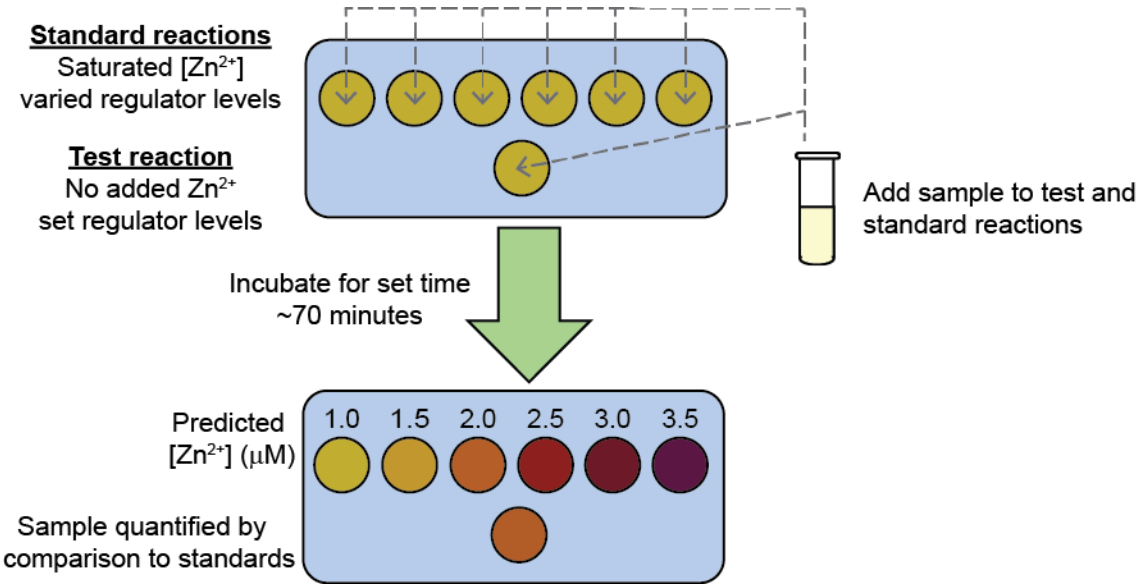

Figure 31: Matrix-specific quantification scheme for test standardization.
An array of standard reactions has saturated zinc concentrations and varied regulator concentrations. The test reaction will have a set regulator concentration and no added zinc. The sample to be analyzed will be added to both the standard and test reactions so that all reactions run in the same sample matrix. After a set incubation time, the color of the test reaction can be matched to the color of the standard reactions to determine zinc concentration in the test reaction.

For this approach to be valid, the colorimetric response must saturate and be identical over a range of zinc concentrations to account for the zinc in the sample being added to the already-saturated standard reactions. In this range of zinc concentrations, reaction output will only depend on regulator concentration. Early experiments with

fluorescent reporters showed that the system's zinc response is at a plateau by 8 µM and has decreased expression by 15 µM (Figure 24B). When we characterized this behavior at a finer resolution and with a colorimetric reporter, we found the output to be identical when reactions were run in zinc concentrations between 7 and 11 µM (Figure 32A). So, if 7 µM zinc is in each standard reaction and each raw sample has no more than 4 µM, then the final standard reactions will have between 7 and 11 µM of zinc, and thus have constant colored output. This enables the test to differentiate raw zinc concentrations between 0 and 4 µM, corresponding to a clinically relevant serum zinc range of 0 to 16 µM if reactions were run in a 1:4 sample dilution.

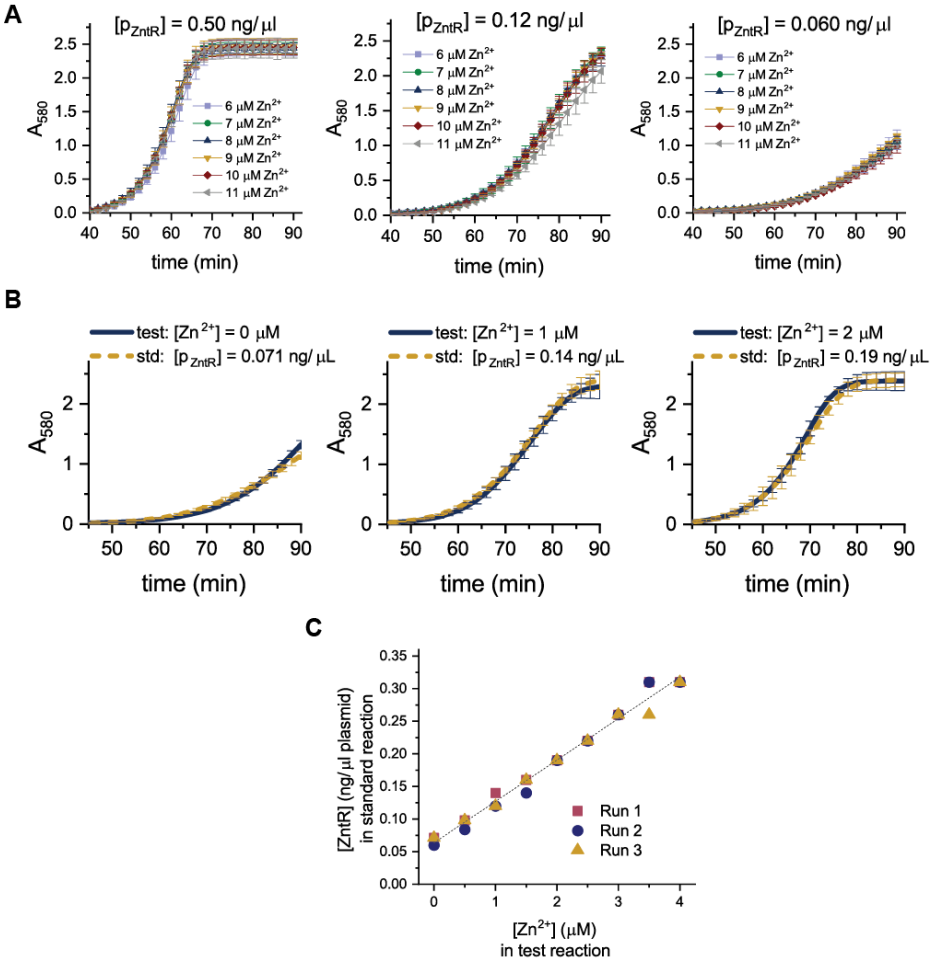

Figure 32: Development of matrix-specific quantification scheme for test standardization.
(A) Colorimetric response is identical across a range of zinc concentrations in reactions run without serum. Reactions with different regulator concentrations were run in a range of zinc concentrations. In all tests, colorimetric output is the same across the range of 7 to 11 µM zinc. (B) Selected time-course readings of test and standard reactions without serum. (C) Relationship between zinc concentration in the test reaction and the ZntR concentration in the standard reaction that most closely matches the test reaction.

We then determined what regulator concentrations in standard reactions would correspond to different zinc concentrations in test samples (all without serum). We ran a

large array of standard reactions with 8 μM zinc and a range of regulator concentrations in parallel with test reactions that had set regulator concentration and a range of zinc concentrations. We determined which standard reaction most closely matched each test reaction (assessed by sum of squares error across measurements at all time points). For each concentration of zinc tested, a standard reaction showed nearly identical colorimetric output (Figure 32B). The concentration of zinc in test reactions is highly correlated with the regulator concentration in the standard reactions that most closely matches the test output (Figure 32C), and correlations were consistent across experiments run on different days and in different batches of cell extract. Of the regulator levels that best matched each target zinc concentration for the three different runs, we used the regulator level closest to the average for the optimal set of regulator concentrations to correspond to each zinc concentration.

4.3.4 Parallel calibration reliably quantifies zinc concentrations

We assessed the accuracy of the test by comparing the absorbance of test reactions with the absorbance of predictive standard reactions (with the previously-identified regulator concentrations). When tests were evaluated at 70 minutes, all tests were appropriately classified into 1 μM raw concentration bins (Figure 33A).

To assess test prediction accuracy and specificity for all possible measured values across all time points, we defined a quantification error metric (QEM). The QEM captures the differences in absorbance, across all zinc levels, between the actual reaction for a given zinc level and a given predictive standard reaction (Methods). Ideally, the QEM of the correct predictions should be zero, and the QEM of the incorrect predictions should be

high. We set a QEM threshold that corresponds with the ability to differentiate between one-tenth increments of the color spectrum (Figure 25B). In all serum samples, the QEM of the correct predictions is substantially lower than the set threshold, and the QEM of the closest incorrect predictions is substantially higher than the threshold (Figure 33B), indicating unambiguous interpretability of test results. Tests can also be interpreted without equipment across the time course of the test, by comparing the color of the test reactions to the color of the predictive standard reactions (Figure 33C).

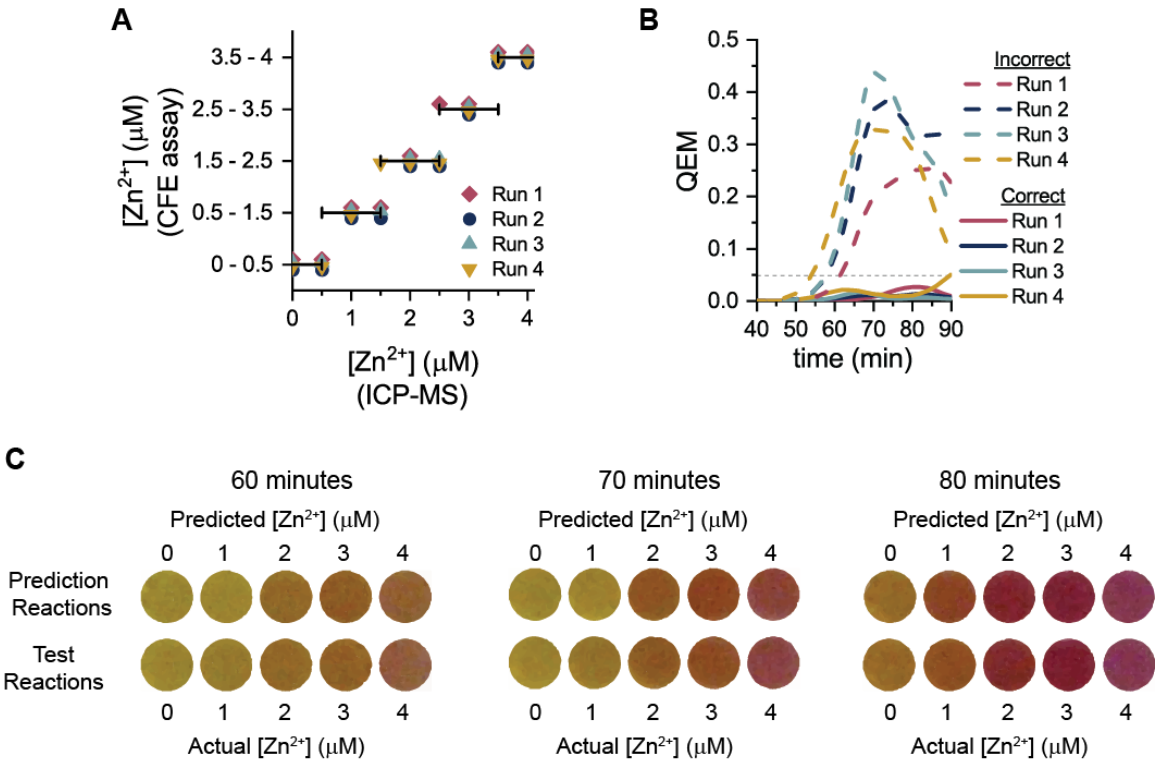

Figure 33: Quantification approach provides high prediction accuracy.
(A) Quantification of zinc concentrations for all four test runs, at 70 minutes. Runs 1-3 were used in initial calibration, and Run 4 was only used in test validation. Symbols falling inside the horizontal bars that correspond with the binned prediction ranges for each y-axis level indicate accurate predictions. (B) Error quantification of all test runs evaluate via the Quantification Error Metric (QEM). Low QEM for correct predictions and high QEM for incorrect predictions indicates unambiguously interpretable test results for a given time. (C) Visualization of reactions from Run 4. Pictures show test and predictive standard reactions at different time points.

We next evaluated how well the test predicts zinc concentrations when subject to variations in reaction conditions. Though optimal standards were chosen by correlations determined at 37°C, the test accurately quantifies zinc when run at both 34°C and 40°C. The QEM of the correct predictions is higher than when run at 37°C, but the QEM thresholds are still met for at least 20 minute intervals, and sometimes much longer, during the testing time, indicating that the classification is sufficiently good (Figure 34).

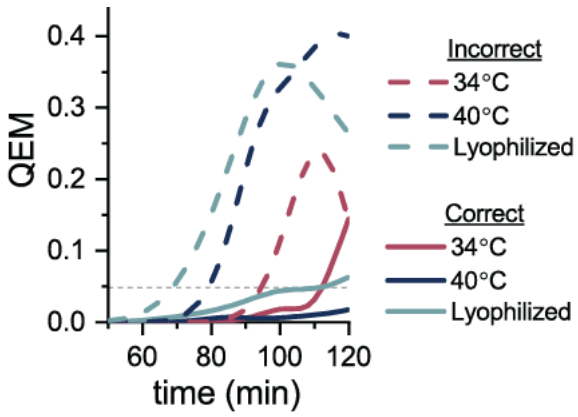

Figure 34: Quantification error for tests run in nonideal reaction conditions. The test accurately classifies zinc when run at varied temperatures and following lyophilization, as indicated by correct predictions falling below the threshold and incorrect predictions falling above the threshold.

The test can also predict zinc concentrations following lyophilization. Test reactions were assembled with no added zinc, and standard reactions were assembled with 8 μM added zinc. All reactions were lyophilized and then rehydrated in water (standard reactions) or in different zinc concentrations (test reactions). Rehydrated tests accurately predicted zinc concentration (Figure 34).

Because of the potential advantages of using pre-expressed protein to mediate test response, we used an identical calibration approach for test set-ups in which ZntR is

directly added. Tests can also accurately predict zinc concentrations when the regulator ZntR is pre-expressed and then added to the reaction (Figure 35).

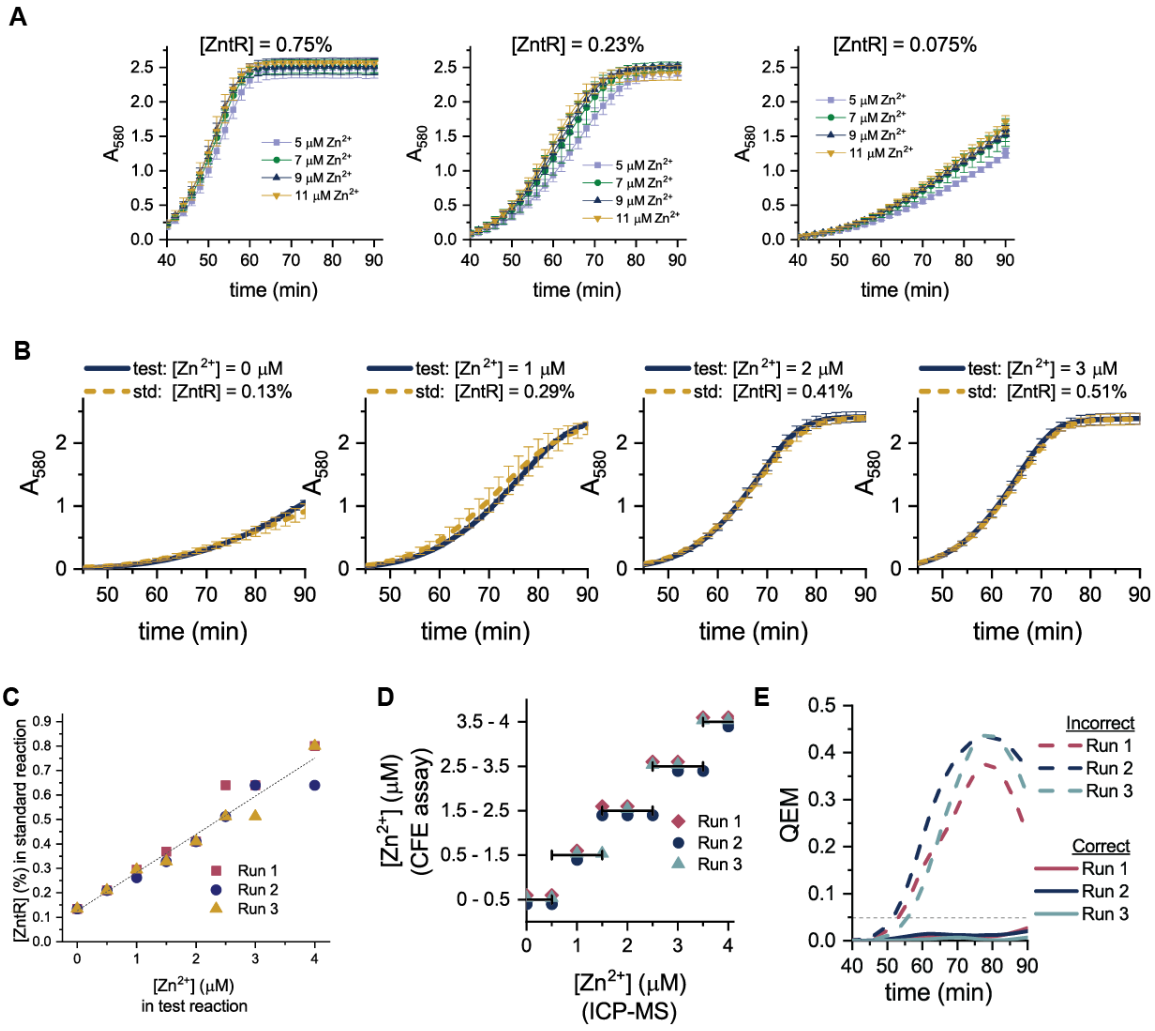

Figure 35: Validation of zinc quantification with direct protein addition.
(A) When ZntR protein is added directly to the reaction, the zinc response saturates. In all tests, colorimetric output is the same across the range of 7 to 11 μM zinc. This enables the test to differentiate raw zinc concentrations between 0 and 4 μM. (B) Selected time course readings of test and standard reactions run with direct protein addition. A large array of standard reactions with 8 μM zinc and a range of regulator concentrations was run in parallel with test reactions that had set regulator concentration and a range of zinc concentrations. For each concentration of zinc tested, a standard reaction showed nearly identical colorimetric output to a test reaction. (C) Relationship between zinc concentration in the test reaction and the ZntR concentration in the standard reaction that most closely matches the test reaction for tests run with direct protein addition. Correlations are consistent across

experiments run on different days and in different batches of cell extract. We determined the optimal set of regulator concentrations to correspond to each zinc concentration by choosing the regulator concentration closest to the average regulator concentration across three runs. (D) Quantification of zinc concentrations in reactions with direct protein addition for all four test runs, at 70 minutes. Symbols falling inside the horizontal bars that correspond with the binned prediction ranges for each y-axis level indicate accurate predictions. (E) Quantification error metrics for tests run with direct protein addition. In all runs, the QEM of the correct predictions is far below the threshold, and the QEM of the incorrect predictions is above the threshold between 70 and 90 minutes.

4.3.5 Addition of small molecules enables equipment-free quantitation in serum

Ideally, for an equipment-free test, users could easily match the color of the test reaction to the color of standard reference reactions, similarly to how one reads a litmus test. The diverse array of colors that correspond with different levels of CPRG cleavage into CPR (Figure 25B) readily enables an easy interpretation of zinc levels. However, when the test is run in serum, the distinct colored intermediates (orange and red) are eliminated, and all intermediate reactions states are varying, difficult-to-interpret degrees of yellow and purple (Figure 36A). While this has minimal effect when quantifying test output via absorbance, lack of distinct intermediates makes quantitation by eye much more challenging.

To probe what could cause this color change, we looked at the absorption spectra of reactions that contained different ratios of CPR and CPRG, with or without 25% serum (Figure 36B). All reactions showed only two distinct peaks: one at 410 nm that is larger early in the reaction and another around 580 nm that grows as the reaction proceeds. In the presence of serum, the first peak is smaller, and, more prominently, the second peak shifts approximately 10 nm which greatly affects the perceived color.

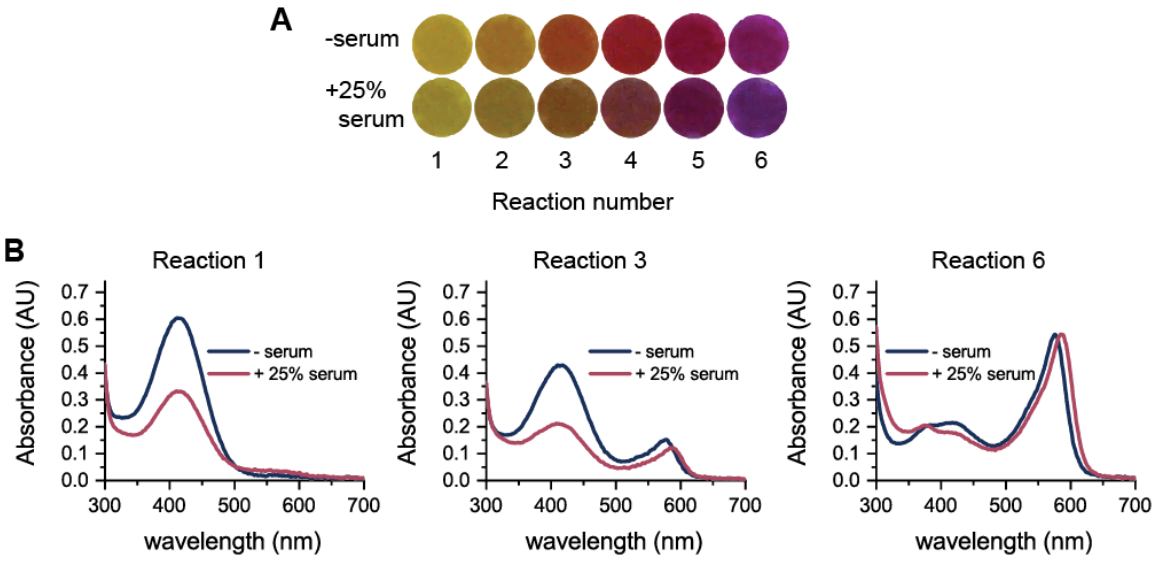

Figure 36: Serum alters the color of reactions, making test interpretation more difficult.
(A) Reactions run in serum appear different from reactions run in the absence of serum. Reactions with complete conversion of CPRG to CPR appear more purple in a 25% serum matrix. More importantly, in 25% serum the colored orange and red reaction intermediates initially observed are no longer visible. (B) Absorption spectra for incomplete reactions of CPRG cleavage to CPR in water and serum. Spectra correspond with the numbered reactions in (A). In both water and serum, only two peaks are visible. The peak at 400 nm decreases as the reaction proceeds, and the peak near 580 nm grows. There is a shift in the 580 nm peak of about 10 nm when reactions are run in serum.

Since dyes with similar structures to CPR are known to interact with serum albumin and to change color in the presence of albumin[116,117], we hypothesized that the color change observed could be caused by albumin interaction with CPR. We tested the effect of human serum albumin (HSA) on the spectrum of chlorophenol red and observed a nearly identical spectrum shift (Figure 37A) to that seen in serum. We used *E. coli* protein extract at the same overall protein concentration as serum to test whether this effect could be due to nonspecific protein interaction. This protein mixture caused a slight shift in the visible spectrum, but less than 30 percent of the shift that HSA caused, further supporting that

CPR's interaction with albumin, rather than with protein in general, is the primary cause of the color change.

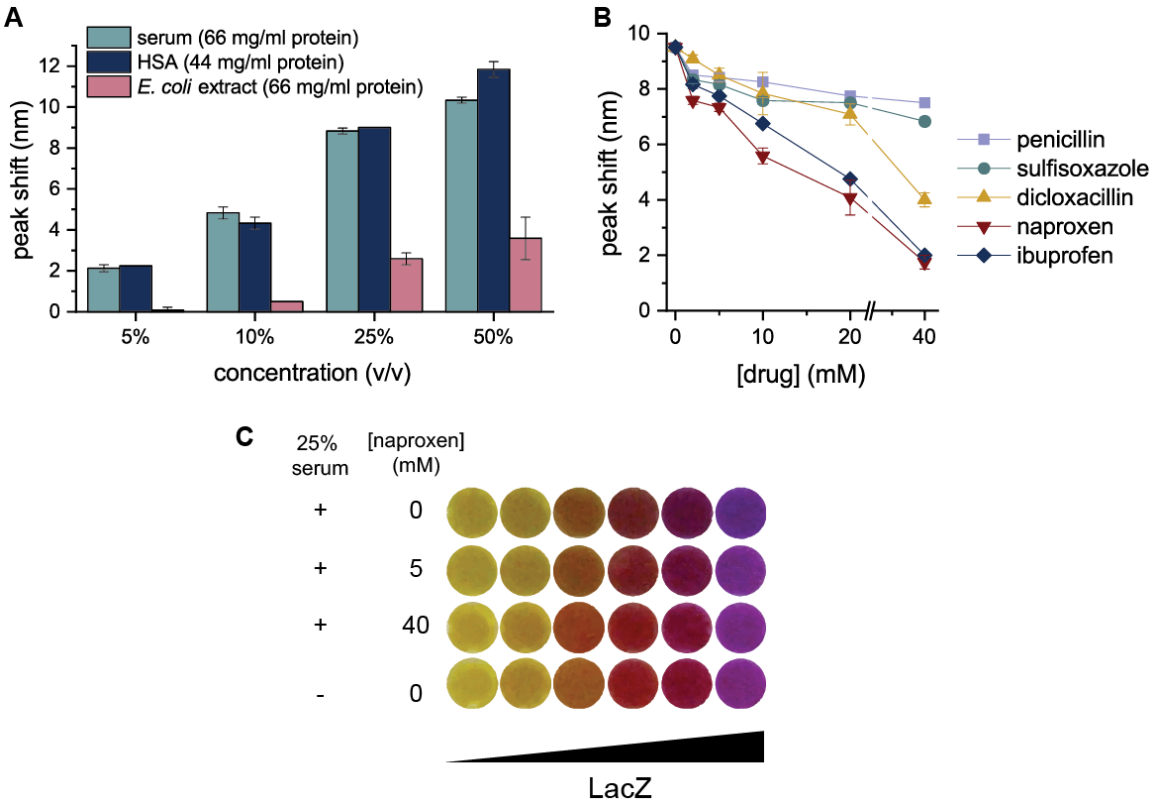

Figure 37: Addition of small molecules that interact with serum albumin reverses the spectral shift and restores distinct colored intermediates
(A) Human serum albumin (HSA) uniquely replicates the spectrum shift caused by serum. Data shown is the average spectrum shift from three biological replicates, and error bars indicate standard deviations. (B) Addition of small molecules that bind albumin reverses the spectrum shift. (C) Addition of naproxen restores distinct color intermediates. Naproxen added at 5 mM made completed reactions appear less purple but did not fully restore the orange and red colored intermediates. Naproxen added at 40 mM made the reaction colors visually indistinguishable from reactions run without serum.

Albumin binds a wide variety of compounds[118], and we explored whether we could reverse the color change by adding a molecule to displace CPR from albumin. Albumin has two primary binding pockets (referred to as Site I and Site II), and since molecules with

structures similar to CPR are known to bind to Site I, we first tested the effect of adding other known Site I binders: penicillin, dicloxacillin, and sulfisoxazole. All three slightly shifted the spectrum at high concentrations, and dicloxacillin had the strongest effect. We also explored the effect of adding Site II binders: naproxen and ibuprofen. Both of these dramatically shifted the spectrum, nearly restoring reaction color to its appearance without added serum (Figure 37B, Figure 37C)

We next tested whether CFE reactions were compatible with addition of these compounds at concentrations that would prevent spectral shifts. When reactions without serum were run in naproxen, ibuprofen, and dicloxacillin (the three most effective color-reversers), all small molecules (perhaps unexpectedly) decreased or eliminated expression when added at 5 mM (Figure 38), though reactions in serum better tolerated higher concentrations of added drug. However, even in reactions with serum, all drugs still decreased expression when added at a concentration of 5 mM, less than what is required to reverse the color change, and at concentrations of 10 mM, all drugs completely inhibited reaction progression (Figure 38). While these limitations preclude running reactions in the presence of the small molecules, these molecules can be added at the time of sample reading to ensure proper visible color, and if added in combination with LacZ inhibitors, they could even quench the CFE reaction as well, enabling long-term test storage and potential later test analysis.

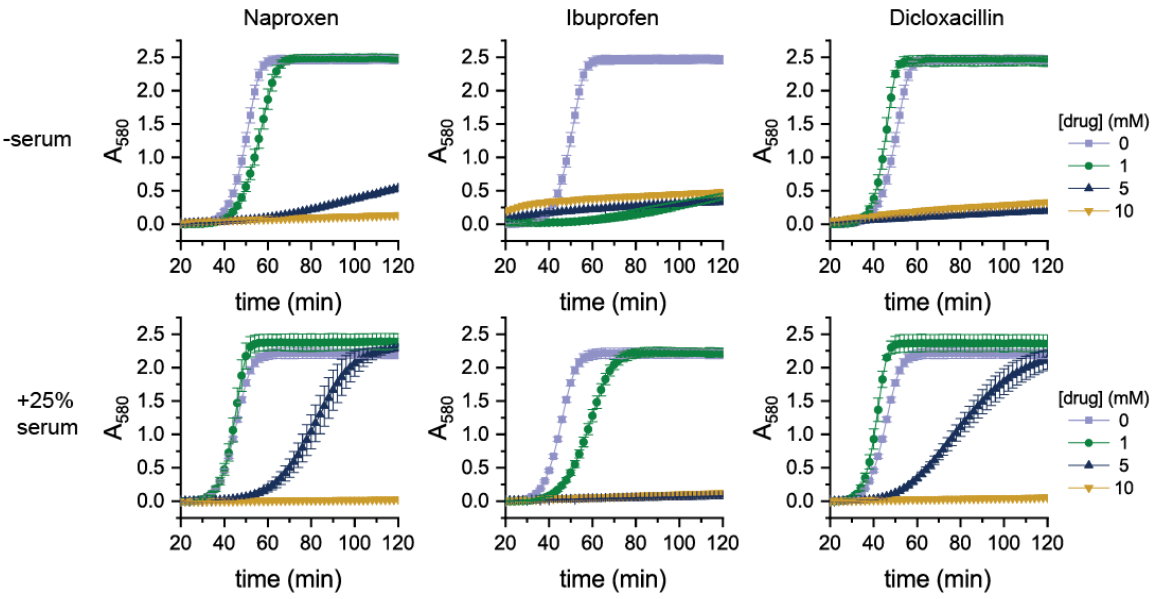

Figure 38: Effect of small molecules on output from CFE reactions.
The small molecules that had the greatest spectrum shift were added to CFE reactions with or without 25% serum. In water, all molecules decreased or eliminated expression when added at 5 mM. Notably, when 5 and 10 mM ibuprofen was added, reactions became cloudy, which likely caused the higher observed absorbance readings at early time points. In 25% serum, reactions ran more successfully with intermediate concentrations of added small molecules, but reactions still could not run in 10 mM of any added compound.

4.3.6 Tests reliably quantify zinc in the matrix of single-donor human serum

One of the main advantages of this test design is its ability to account for and overcome the matrix effects associated with serum samples compared to reactions not in a serum matrix. However, the design must also be robust to the matrix effects associated with variation in serum constituents across individual patient samples. To determine whether our diagnostic meets this criterion, we tested its ability to predict zinc levels in human serum taken from individual donors.

Blood samples were collected from four different donors, and serum was isolated from whole blood through centrifugation. Because the samples obtained had healthy levels

of serum zinc, we needed to first remove zinc from the sample to allow for tuning and selection of ZntR concentrations for standards. As in our initial serum testing, we depleted zinc from each sample, measured the zinc concentration of the treated serum (Figure 39A), and then supplemented zinc to create serum with a range of zinc concentrations.

To establish a complete proof-of-principle test, correct ZntR concentrations for test reactions in 25% serum matrix were then identified for our prediction method, as described above. Because of the better overall test performance and greater consistency when ZntR was expressed simultaneously in reactions, we only explored using this reaction scheme, and we used a reporter plasmid concentration such that the test would be interpretable between 50 and 60 minutes. We first identified that a set of standard reactions behaved identically across a raw concentration range of 8 to 16 μM added zinc (which corresponds to a serum zinc range of 32 to 64 μM zinc for reactions run in a 1:4 sample dilution) (Figure 39B). Then, to determine the optimal set of regulators to predict each zinc concentration, a set of test and standard reactions were run in pooled serum taken from the first three donors. From these test runs, we determined the optimal set of regulators to predict zinc concentration in the matrix of 25% human serum (Figure 39C). Though the relationship between regulator levels in prediction reactions and zinc concentrations in test reactions varied across test runs at high zinc concentrations, the optimal set of standards still successfully discriminated between zinc levels in pooled samples (Figure 39D).

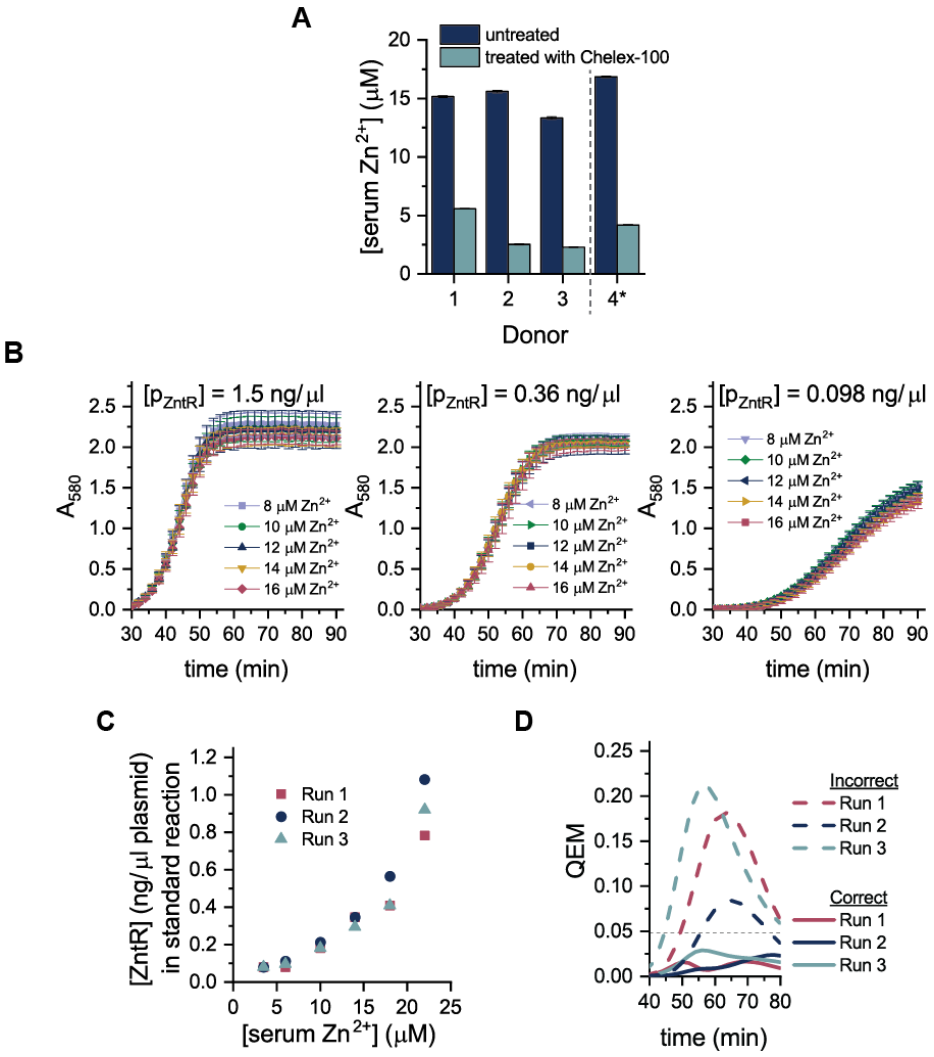

Figure 39: Development of CFE assay to assess serum zinc concentrations.
(A) Zinc concentrations in individual donor serum before and after treatment with Chelex-100 resin. Serum from donors 1-3 was used for test calibration and evaluation, and serum from donor 4 was used only in test validation, indicated by the asterisk. (B) Colorimetric response is identical across a range of zinc concentrations. Reactions with different regulator concentrations were run in a range of zinc concentrations. In all tests run in 25% serum, colorimetric output was the same across the raw range of 8 to 16 μM zinc, which corresponds with 32 to 64 μM zinc in the serum sample. (C) Scatter plot of zinc concentrations and the corresponding regulator concentrations that yield similar output in 25% human serum. Runs 1-3 represent experiments performed separately and in different batches of cell extract. Zinc values reported are the equivalent of those in the pure serum samples, translated from the raw values measured by the reactions. (D) QEM of Runs 1-3, using the optimum standards predicted from the correlation shown in (B).

We next evaluated the ability of the overall test to quantify serum zinc levels in samples from individual donors, using concentration bins with a width of 4 µM. The test accurately predicted zinc concentration for all samples, including serum from Donor 4, which notably was not used during the assay calibration described above. We added different amounts of zinc to the different zinc-depleted donor samples to probe how well the test quantified zinc concentrations on the outer edges of the bins. The test accurately classified all zinc concentrations between 0 and 20 µM (Figure 40A). Though the test inaccurately classified some higher zinc concentrations, the range of accurate predictions covers all physiologically relevant serum zinc concentrations. We further evaluated test accuracy and sensitivity as previously described. For each donor, the QEM of the correct prediction was far below the set threshold, and the QEM of the incorrect prediction was above the threshold (Figure 40B). The test was also robust to temperature variations and lyophilization (Figure 40C).

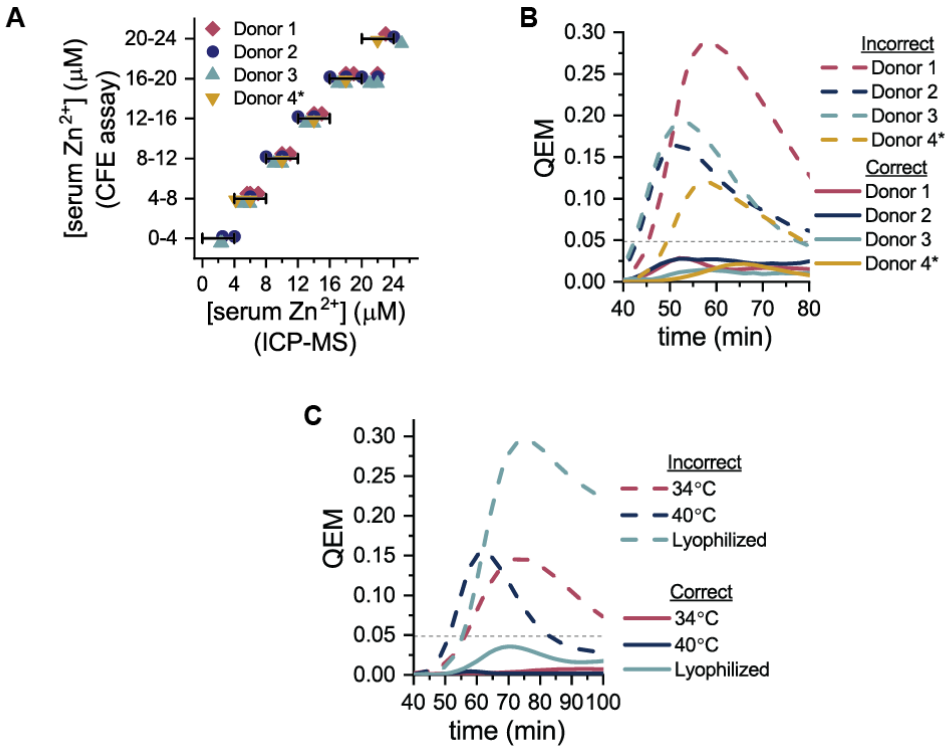

Figure 40: Accurate quantification of zinc in human serum.
(A) Quantification of serum zinc concentrations for all four donors tested, evaluated at 56 minutes. (B) Error quantification of all individual donor samples. (C) Error quantification in non-ideal reaction conditions with serum from Donor 4.

Finally, we demonstrated the equipment-free potential of our test. A set of test and standard reactions was run in serum from Donor 4 with different concentrations of added zinc (for test reactions) and a saturated zinc concentration (for standard reference reactions). After 50 minutes, either 40 mM naproxen or an equivalent volume of water were added to reactions. Test reactions clearly correspond with the appropriate binned standard reactions (Figure 41), and tests with added naproxen are more easily interpreted because of the distinct color intermediates.

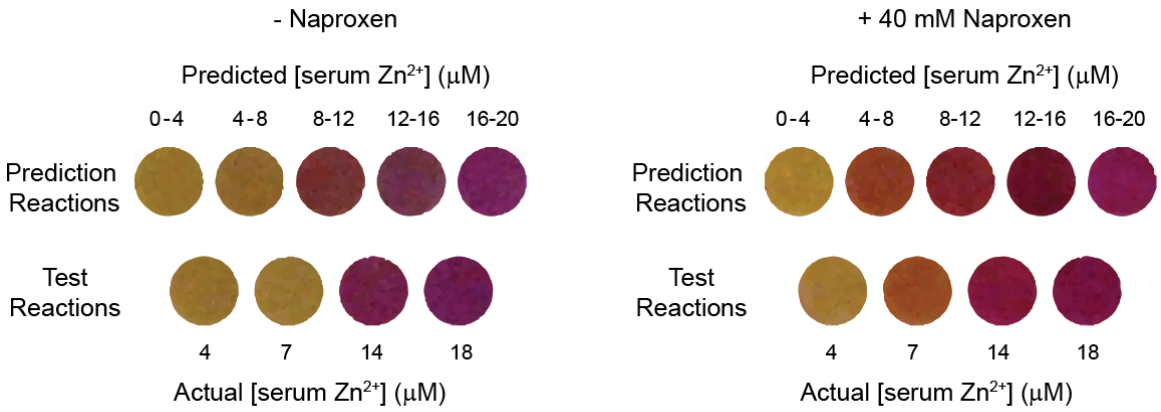

Figure 41: Equipment free test interpretation in 25% serum.
Tests were run for 50 minutes, and then visualized either with or without 40 mM naproxen addition. With added naproxen, the color of test reactions matches the color of the appropriate standard reference reaction.

4.3.7 Approach to semi-quantitation is generalizable to toehold sensors

To demonstrate the generalizability of our quantification approach, we applied the same framework to quantification of DNA with an established toehold switch, a sensing modality used in recently developed infectious disease diagnostics. Using previously characterized switch and trigger sequences[15], we expressed a toehold switch in CFE reactions, and added the corresponding trigger RNA (Figure 42A). We designed the system such that test reactions have a set amount of toehold switch (the response regulator) and variable amounts of toehold trigger (the analyte), and standard reference reactions have saturated levels of toehold trigger and variable amounts of the toehold switch. For each trigger concentration tested, a standard reaction shows a nearly identical colorimetric output (Figure 42B), and the relationship between trigger concentration in the test reactions and switch concentration in standard reactions is consistent across experiments (Figure

42C). From these data, we determined the optimal set of switch concentrations that match each trigger concentration.

When we evaluated each experiment with the optimal set of standards, the test accurately quantified trigger concentration for all trigger concentrations tested (Figure 42D). QEM quantification (Figure 42E) shows nearly ideal test behavior across time points, and the colors of the test reactions accurately match the color of the correct corresponding standard reactions (Figure 42F).

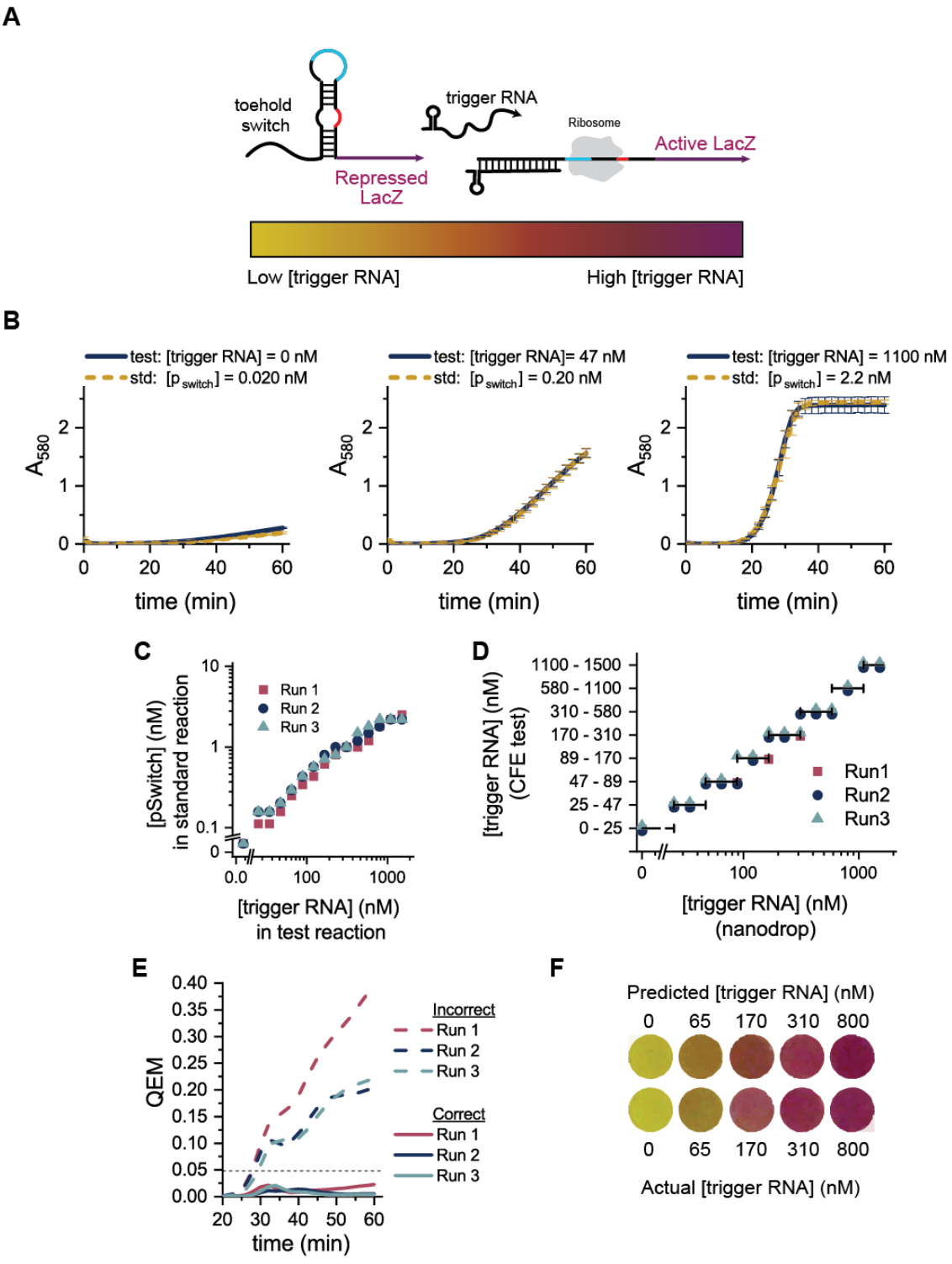

Figure 42: Quantification approach is generalizable to toehold switches.
(A) Schematic of toehold switch used to control LacZ production. Trigger RNA unfolds the toehold switch and enables LacZ translation. Increasing amounts of trigger RNA correspond with increased LacZ translation. (B) Selected time-course

readings of test and standard reactions for a toehold sensor. A large array of standard reactions with saturated trigger RNA concentrations and a range of switch concentrations was run in parallel with test reactions that had set switch concentration and a range of trigger concentrations. For each concentration of trigger tested, a standard reaction showed nearly identical colorimetric output. (C) Relationship between trigger concentration in the test reaction and the corresponding toehold switch concentration in the calibration reaction that most closely matches the test reaction. (D) Test quantification of trigger concentrations, evaluated at 40 minutes. Purified RNA was added to each sample at different, known concentrations. Symbols falling inside the horizontal bars that correspond with the binned prediction ranges for each y-axis level indicate that the CFE test accurately quantified DNA in the sample. (E) Quantification error for toehold sensing. (F) Visualization of test and standard reactions, evaluated at 40 minutes. The color of test reactions matches the color of the appropriate standard reference reaction.

4.4 Discussion

In this work, we develop a cell-free diagnostic platform capable of measuring a small analyte in a complex matrix. The output from our portable system can be monitored in a semi-quantitative manner with the naked eye. Importantly, rather than using common inducers (e.g., IPTG) for proof-of-principle development, we instead focused on a clinically-relevant target and developed an assay with imminent translational potential. We demonstrate that our approach can reliably quantify zinc in human serum at clinically relevant levels, and that it can be broadly applied to quantification of other molecules in complex matrices. By adding the same sample to both standard and test reactions, we account for all of the matrix effects introduced by serum samples and individual variation across samples. Our approach significantly expands the scope of CFE diagnostic tools to assessment of medical conditions that need more than just binary identification of presence or absence of a biomarker, and thus in turn significantly expands the potential impact of CFE diagnostics in biomedicine and global health.

To date, CFE diagnostics have been limited to infectious diseases and other conditions with nucleic acid biomarkers. In these cases, it is merely the presence or absence of the marker that matters for diagnosis, and so the important analytical figure of merit is sensitivity. However, many more medical conditions have biomarkers where binary identification of presence or absence is insufficient for diagnosis. In these cases, a usable diagnostic requires some degree of quantification, and relevant analytical considerations include accuracy, detection range of the measurement, resolution of the quantification, and robustness of the quantification to variations in the sample matrix.

In this work we specifically address the impacts of the sample matrix on accuracy and robustness of quantification with an approach that is effective even in resource-poor testing environments. In an analytical laboratory, reference samples are run in addition to the test samples, allowing the calibration of measured values to defined reference standards. However, even sophisticated analytical instruments (e.g., mass spectrometers) are prone to matrix effects, where their measurements change depending on the type of sample or sometimes even matrix variations across samples of the same type. These matrix effects can be greatly exaggerated by the simplified assay chemistries used in point-of-care diagnostics, making the creation of a calibration curve in the field infeasible. Use of pure chemical reference standards is thus not appropriate. Use of reference standards in the same matrix (e.g., blood) also presents a number of problems, from inter-individual variability in sample matrices that can impact assay readouts to lack of availability of appropriate reference material for each calibration value (e.g., availability of sufficient blood samples naturally depleted in a given biomarker for distribution to all test users).

Our approach addresses these issues by using the patient sample itself as the sample matrix for the parallel calibration standards. However, this raises another issue: the patient sample itself contains the biomarker to be measured, so how can calibration samples have fixed levels of the analyte when a variable amount of the analyte is to be added to those samples? We solve this problem in a generalizable way by saturating the samples with the biomarker analyte, and then using varying levels of a key reaction component (i.e., the biomarker-responsive transcriptional regulator) to recapitulate assay output for different levels of analyte. This insight is what ultimately allows for calibration standards to be run in the exact same matrix as the sample, increasing accuracy and robustness regardless of whether the test environment is resource-poor or not.

A major benefit of the approach presented here is the ability to interpret test output without any equipment. While simple instruments have been developed to interpret and process CFE colorimetric output[15,16], cell-free tests could be more broadly used if interpretation did not require any equipment, since equipment costs as low as even a few hundred dollars can still be an impediment to adoption for public health organizations across the world. The broad color spectrum that corresponds with different levels of LacZ cleavage of CPRG enables such equipment-free interpretation.

Previous CFE diagnostics used CPR/CPRG as a readout to enable visibly interpretable results for binary positive/negative discrimination of test results. For diagnoses requiring some degree of biomarker quantification, a two-color approach is not easily generalizable in an equipment-free fashion. We showed the nearly-binary readout (yellow to purple, with difficult-to-distinguish intermediate hues) is caused by serum albumin (which is consistent with previous work using albumin-coated paper). Serum

albumin affects the absorbance spectrum of CPR in a way that mutes the intermediate range of possible colors, precluding the use of these visibly distinguishable intermediate colors when testing human serum. We overcame this issue by adding a molecule to completed assays that displaces CPR from albumin, restoring the full spectrum of colors and enabling truly equipment-free interpretation of test results even in high serum concentrations.

While our approach to semi-quantitation in CFE assays has significant value in its generalizability, the specific zinc assay we developed has significant inherent value. Zinc deficiency causes over 100,000 annual childhood deaths, yet financial and logistical constraints associated with current zinc assays (which require an analytical laboratory) preclude diagnosis and treatment. The test described here is readily translatable to public health and clinical diagnostic applications.

Of foremost importance, our test detects relevant concentrations of serum zinc. Physiological serum zinc concentrations range from 2 μM to 20 μM[24] and clinically relevant thresholds for deficiency fall between 8.5 and 11.5 μM[21]. The developed test (in 25% serum) reliably distinguishes 4 μM increments between 0 and 20 μM serum zinc. (Figure 40). (Finer resolution is arguably possible based on our results to date, but 4 μM resolution is clear.) This enables distinction between sufficient, borderline, and low serum zinc levels. When run in a higher percentage of serum, CFE reactions respond to a concentration range of 2 to 22 μM zinc (Figure 30D), meaning that lyophilized assay reactions could be directly rehydrated with 100% serum and still provide reasonable quantification with perhaps even finer resolution. Here, we developed the proof-of-principle regulator concentrations for calibration in a 25% serum matrix for experimental simplicity and throughput (as lyophilization can be a bottleneck), but the regulator

concentrations for a 100% serum matrix could be developed in an identical fashion using lyophilized samples.

In addition, the developed test meets the requirements for field-friendly testing[18], in large part because it requires minimal equipment and processing steps. Since the clinical marker for zinc deficiency is serum or plasma zinc, a burden for any zinc test is the removal of red blood cells from patient samples. However, this can be easily accomplished using field-friendly blood separation methods that use no electricity[109] and that could potentially further streamline the processing and testing pipeline[119].

Beyond serum separation, the remainder of the required processing steps would be minimal. We have shown that our CFE sensor works even in 100% serum, meaning that minimal measurement or pipetting should be necessary. Even using 25% serum would require only a single 1:4 dilution for rehydration of lyophilized reactions, with no other processing. Finally, we note that all of these reactions are done at microliter scales, meaning that easily acquired finger-stick blood samples will provide sufficient sample (rather than necessitating venous blood draws that require a trained phlebotomist and have reduced patient acceptance).

Though we chose to measure zinc (based on its global public health relevance) for our proof-of-principle demonstration of equipment-free quantitation, the quantitation method used here can be easily applied to other CFE diagnostic sensors. Any sensor based on transcription factors that sense a biomarker analyte and propagate this signal based on transcription could be directly substituted into the current design by determining the correlation between transcription factor concentrations and target analyte concentrations.

Further, we showed that this approach can be easily generalized even to CFE diagnostics not mediated by transcription factors, including previously-described nucleic acid detection devices. Within about one week in the laboratory, we were able to calibrate a toehold switch sensor and demonstrate that it could reliably quantify input DNA.

In our test development and evaluation, we assumed that the human eye could differentiate between ten percent differences of the available color spectrum, and we set assessment thresholds accordingly. Though opinions may vary about just how different two colors must be in order to be distinguishable, the heuristic we use here is nonetheless useful as a guideline, and it can be refined as necessary to more specifically determine test resolution and performance under different assumptions. Alternatively, if previously-developed, relatively low-cost instruments for absorbance readings[15] are feasible for field deployment, our parallelized calibration approach can provide even greater resolution and higher confidence in measured values than the strictly visual approach assumed here.

The development of cell free expression systems for diagnostics was a watershed moment in synthetic biology that can now be brought to bear on sensing molecules beyond nucleic acids. By enabling semi-quantitative analysis of biomarker levels even in low-resource environments, we have expanded the potential of CFE diagnostics by broadening the scope of conditions they can assess beyond nucleic acids and infectious diseases. The combination of simplicity and semi-quantitative resolution of our approach suggests that it may be useful not only in resource-poor environments, but even as a low-cost clinical screen to determine if more precise (and expensive) assays are necessary. The zinc assay reported here and assays developed via translations of the diagnostic platform described here could thus have a truly broad and global reach.

CHAPTER 5. CONCLUSIONS AND FUTURE DIRECTIONS

I have presented the development of two different biosensing approaches that enable semiquantitative, equipment-free assessment of biomarkers in complex biological samples. I used these biosensors to assess zinc concentrations in human serum, moving closer to a field-deployable diagnostic for zinc deficiency. In this chapter, I will discuss the novelty and contribution of my thesis research, the remaining steps required to begin in-field zinc assessment, and how the biosensing platforms I developed can be extended to create new classes of diagnostics and therapeutics.

5.1 Novelty of thesis research

While biosensors have been developed for a wide variety of compounds, very few have been turned into deployable diagnostic tools, largely because of the challenges of in-field test assessment, sensor response range, and the matrix effects inherent to clinical samples. In both my whole-cell and cell-free development work, I developed novel approaches to overcome these problems, and these should be readily translatable to the creation of new types of sensors.

In developing a whole-cell zinc sensor, I showed how synthetic biology tools can be used to harness metabolite production, rather than protein production, to facilitate the creation of responsive metabolic factories. While previous research has built complex bacterial systems, nearly all synthetic biology work uses simple reporter proteins in building complex circuits, and nearly all metabolic engineering work uses simple circuits to control metabolite production. Integrating advanced circuitry with production of

complex chemicals poses unique challenges, and the tools I developed to tightly control metabolite production upon differential signal recognition can help to build new types of complex, responsive systems.

In recent years, cell-free systems have garnered great attention for their use as low-cost, field-deployable diagnostic tools, but they have been almost exclusively used for assessment of infectious diseases, and they have all required extensive upstream sample processing. A huge array of diseases and conditions require precise quantification — rather than just presence/absence assessment — of relevant biomarkers, and cell-free systems had been poorly equipped to do this. The quantification method I developed can expand the scope of cell-free diagnostics to entire new classes of diseases and conditions, and the matrix-specific quantification strategies I developed can minimize the sample processing required so that minimally-trained users can perform tests in minimally-equipped settings. These tests could help to expand healthcare to low-resource areas and even enable at-home health monitoring.

5.2 Development of a field-deployable biosensor for zinc deficiency

I initially aimed to develop a fast-responding biosensor to serve as the basis of a diagnostic for zinc deficiency, and in both my whole-cell and cell-free sensor development efforts, I have met this goal. Both respond to physiologically relevant zinc concentrations, can be interpreted without equipment, and require short incubation times. While both systems could potentially serve as the basis of a point-of-care diagnostic, the form factor of the cell-free assay makes it much more amenable to in-field micronutrient assessment.

The cell-free test I developed for serum zinc is imminently translatable: it requires just a finger prick of blood, can be lyophilized, and produces results within one hour. However, bridging the gap from lab success to in-field use requires a few additional steps. First, we need to calibrate the zinc diagnostic with real clinical serum samples. All serum samples analyzed to date have been collected from healthy donors, and we created artificially deficient serum samples by depleting zinc with Chelex-100, an ion-binding resin. Beyond removing zinc ions, the depletion process introduces slight, but still detectable, matrix effects that alter the output of CFE reactions. To make a test that accurately quantifies zinc in the matrix of untreated serum samples, we must calibrate the test with collected, unprocessed serum that has a range of zinc concentrations. I have spoken with a researcher at the Center for Disease Control (CDC) about obtaining aliquots of serum samples collected in previous nutrition assessments. Using these samples, we could create a calibration curve that we could use to quantify zinc in unprocessed serum samples.

Moving towards in-field testing would also require more extensive validation of our test manufacturing and storage processes. While we have demonstrated that lyophilized tests can be rehydrated in a serum sample and still accurately quantify zinc, we need to demonstrate that tests can be stored for extended periods of time, and in diverse temperature and pressures that reflect the conditions throughout the storage and shipment process. This assessment should be straightforward to complete, but poor performance of tests following long-term storage could require optimization of lyophilization and test packaging.

To make the testing process more streamlined, the CFE reactions could be incorporated into a paper microfluidic device that can separate serum from red blood cells. Such a device would eliminate the need for a separate processing step and thus simplify the testing process: Upon addition of a finger prick of blood, the device would separate serum from red blood cells, and the serum would rehydrate lyophilized CFE reactions. Advances in paper manufacturing could enable the entire testing process to occur in a self-contained device[20,120], insulated from the environment to control for evaporation. Through collaborations with groups at Georgia Tech that specialize in paper manufacturing, we are working to integrate our cell-free zinc assay into such a device.

Though a streamlined testing device would make the test even more field-friendly, integration of serum separation and biomarker assessment is not a critical requirement for field deployability. An inexpensive, portable, paper-based centrifuge[109] could alternatively be used to separate serum from blood. This serum could be used to rehydrate reactions lyophilized in tubes, and by simply closing the tubes, the reactions would be protected from evaporation and environmental contaminants.

Once tests are calibrated with real clinical samples and the storage process is optimized and validated, we can begin sending tests for pilot testing. Early in graduate school, I participated in NSF's I-Corps program to explore the commercialization potential of point-of-care micronutrient assays, specifically to learn whether there is a need for low-cost micronutrient tests and what requirements such tests must meet. I spoke with people at all levels of the nutritional surveillance pipeline: the leaders of organizations like UNICEF and the World Health Organization, program managers leading micronutrient assessment and intervention programs in Ethiopia, and academic researchers who evaluate

the effectiveness of different nutritional intervention strategies. Beyond hearing an overwhelming consensus that there is a great need for point-of-care assessment tools, I also made contacts with many people who expressed interest in testing a final, functional device. We could directly work with these people to begin pilot testing; or alternatively, we could work with PATH, an organization associated with the Bill and Melinda Gates Foundation that helps to facilitate collaborations between engineers, aid agencies, and companies so that technologies with global health applications can be fully validated, assessed, and produced at scale. PATH has previously expressed interest in incorporating our final zinc assay into their micronutrient assessment platform, which would be a potentially easier and more straightforward way to get our test into the hands of the people who need it.

5.3 Expansion of cell-free quantification platform to new biomarkers

Beyond creating a nearly field-deployable assay for zinc deficiency, I have created a generalizable quantification platform that can be expanded to assess a diversity of clinically relevant biomarkers. We have already demonstrated that our matrix-specific calibration approach can quantify different types of biomarkers (ions and nucleic acids) with different sensing methods (transcription factors and riboregulators). The platform can be easily used to quantify other types of biomarkers that have sensor and transducer elements that function in CFE reactions.

The primary challenge for using our system to quantify other clinically relevant biomarkers are limitations in naturally occurring sensors that specifically bind the target biomarker at relevant concentrations. Biomarkers that interact with bacterial transcription

factors should be immediately detectable in our cell-free platform, but the range of detection may fall outside the relevant concentration range. For example, I have used a cobalamin-responsive transcription factor to quantify B_{12} (another micronutrient of global health importance) in cell free reactions, but the sensor responds to concentrations far higher than those required for clinical B_{12} assessment. Protein engineering strategies could be used to increase sensitivity, but to do so efficiently would require extensive effort and high-throughput screening. While nature has evolved sensors for diverse types of compounds, finding sensors that detect clinically relevant biomarker concentrations will likely be a continued challenge.

The use of modular sensors, such as aptamers or antibody fragments, is a promising alternative to bioprospecting. Aptamers and antibody fragments can be readily evolved to specifically bind a target molecule with a user-defined affinity[121,122], which would enable the production of sensor systems for essentially arbitrary small molecules and proteins. To make diagnostics that use these interchangeable and evolvable sensor components, the primary challenge is making a reliable and modular signal transduction system so that target binding leads to a detectable change in transcription or translation. Small molecule-binding aptamers can be incorporated into riboswitches or ribozymes[123-125], which are RNA structures that differentially regulate either translation or transcription upon target binding. Though incorporation of new aptamers into these systems is notoriously difficult, thermodynamic prediction models have helped facilitate rational aptamer incorporation into RNA regulators[78]. Antibody fragments can be fused to transcription factors to enable differential gene expression upon target binding[126,127], but this regulation scheme has not yet been explored in the context of a cell-free reaction. Though creating aptamer and

antibody-based tests will require significant development, the resulting CFE assays could dramatically expand the scope of health surveillance programs, clinical diagnoses, and even at-home health assessment.

The company Theranos aimed to transform healthcare by making easy-to-use, small volume tests that could replace standard lab assay. Though the company failed to deliver functional products, the excitement and investment that Theranos generated illustrates the great public interest in changing the diagnostic paradigm with point-of-care tests[128]. Cell-free diagnostics have the potential to serve as the basis for this sort of diagnostic revolution. While these tests could be interpreted visually, they could also be incorporated into a minimal-equipment testing framework for automated, more precise quantification. A user could add a cartridge of lyophilized test and standard reactions for any desired biomarker to a low-cost absorbance reader, and use serum from just a finger prick of blood to rehydrate and activate the tests. The reader would then report a more precise, matrix-normalized biomarker concentration. These tests — whether interpreted visually or with equipment — would enable at-home health monitoring or could be used be used as rapid initial screens in clinics before ordering more expensive laboratory panels.

5.4 Microbial factories for targeted chemical production

Since the cell-free zinc sensor I developed is much more field-friendly than the developed whole-cell sensor, I find it unlikely that the whole cell zinc sensor will ever turn into a clinical assay. However, the methods that I developed to control microbial metabolite production (in the context of a zinc biosensor) are directly translatable to other systems that require precise chemical production upon sensing a specific target. Our approaches can be

directly applied to the development of pigment-based biosensors for new compounds or to the creation of "smart" bacterial therapies that produce a chemical upon sensing a target compound.

Whole cell biosensors could overcome some of the current limitations of cell-free diagnostics, specifically the lack of available sensors that are sensitive enough to detect clinically relevant concentrations of target biomarkers. Bacterial cells have exceptional environmental scavenging systems, which allow them to sense and respond to very small changes in their extracellular environments. Cell-free sensors cannot harness these scavenging systems and can only use the intracellular sensor proteins, which may respond to analyte concentrations orders of magnitude higher than extracellular concentrations. Thus, a whole-cell sensor would be more useful for sensitive detection of compounds that are actively transported into cells. The circuits I constructed for a pigment-based zinc test could be directly applied to detection of a new compound by simply replacing the zinc-responsive promoter P_{zntA} with a promoter that responds to a different biomarker. The same tuning approaches we used — modulation of regulator levels — can be used to tune the response ranges of the new sensor, enabling fast creation of tunable, pigment-based sensors for sensitive detection of different types of compounds. In ongoing, currently unpublished work, I am porting B_{12}-responsive elements into these circuits to create a colorimetric whole-cell B_{12} sensor.

The approaches we used to make a pigment-based sensor could also be used to make tunable sensors that produce different types of metabolites. These cells could serve as "theranostics" that produce a therapeutic payload upon target recognition. Responsive bacterial therapies have already been developed for treatment of cancer[10,11], metabolic

disorders[12,13], and inflammation[14], but nearly all produce individual proteins upon target recognition. Cells that produce complex chemicals (made via metabolic pathways) upon target recognition could dramatically expand the types of therapeutics that could be delivered. For example, bacteria could be engineered to produce a chemotherapeutic agent only upon recognition of a specific cancer biomarker. Bacterial cells have already been engineered to produce precursors for the chemotherapuetic Taxol[82], and they can also recognize metabolic states specific to the cancer microenvironment (such as elevated aspartate levels[129]). A potential bacterial therapeutic could combine these two capabilities so that cells produce Taxol only upon recognition of some threshold level of aspartate and — importantly — be inactive upon sensing baseline aspartate present in healthy organs. While metabolic engineering advances are certainly required to make this possible, the strategies this thesis developed for tunable, precise metabolite production could help enable the creation of this sort of therapy. Similar approaches could be applied to the creation of bacterial theranostics that modulate the gut microbiome. As we learn more about the microbiome's role in disease, there will likely be an increased demand for responsive microbial therapies to regulate the microbiome. Whole cells, rather than cell-free systems, are the ideal platform for drug delivery to the microbiome, because cells are self-contained, are optimized for survival in the host, and can colonize the host to serve as a continued delivery source[130].

While the strategies I developed to control metabolism could be broadly applied to creation of these theranostics, the specific approaches would vary based on the application. In creation of our whole-cell sensor, we used the repressor LacI as the master controller of the pigment production system, which fully repressed metabolic output during cell growth

to enable faster response upon induction and higher cell viability. For our application, adding LacI's chemical inducer (IPTG) at the time of testing was a viable strategy. However, for drug delivery within the body, this type of control would be difficult to implement. Alternative strategies could use transcription factors that respond to hypoxia (a characteristic of tumors)[12] or to xylan (an ingestible inducer)[131] to control when the sensing system is active. Beyond enabling faster responses, these control methods would serve as additional checks on drug production to prevent leaky, unwanted drug production in other parts of the body.

5.5 Closing remarks

In this thesis, I have described my efforts to engineer bacterial-based biosensors for use as diagnostic tools in low-resource settings. I developed ways to decouple bacterial growth from production of a target metabolite, which enables cell sensors to produce visible pigment within just a few hours of sample addition. I then incorporated zinc-responsive elements into this fast-responding sensor scaffold, and tuned the sensor's response range to enable fast assessment of physiologically relevant zinc concentrations in serum samples. By simply replacing either the zinc-responsive elements or pigment pathways, a user could create and tune sensors cells that selectively make metabolic compounds upon detection of a specific signal, enabling the creation of other types of diagnostics and responsive chemical production systems.

By porting the zinc-responding sensing machinery into a cell-free platform, I created a test for zinc that meets all of the WHO's ASSURED criteria and all of the requirements for in-field micronutrient assessment. Following minimal additional

calibration and validation, the test will be ready to send to researchers or aid agencies for initial pilot testing. This test can meet the need for an easy-to use, equipment-free assay that can help provide the information necessary for efficient and effective treatment of zinc deficiency.

In creating a cell-free zinc test, I developed a matrix-specific standardization approach that can drastically broaden the reach of cell-free diagnostics. Cell-free diagnostics, which had previously been restricted to simply presence/absence detection, can now assess different types of biomarkers in an equipment-free semiquantitative fashion, enabling the creation of low-cost, point-of-care diagnostics for a wide variety of diseases and conditions. While I showed that our test effectively quantifies zinc and nucleic acids, expansion to other markers will require development of sensors that bind to the target biomarker at the desired concentration. Developing cell-free sensors has become a major focus of our group, and ongoing and future research projects aim to develop a versatile sensing approach to enable detection of diverse types of biomarkers.

Through conversations with policy makers and aid workers, I learned of the huge impact that point-of-care tests could have on implementation and assessment of large-scale public health programs. This thesis has presented the development of a diagnostic tool to meet the need for in-field zinc assessment, and has laid the groundwork for the creation of diverse diagnostic assays that have the potential to broaden the scope of public health surveys and enable new types of clinical assessments in resource-limited settings.

REFERENCES

1 Balleza, E. *et al.* Regulation by transcription factors in bacteria: beyond description. *FEMS microbiology reviews* **33**, 133-151, doi:10.1111/j.1574-6976.2008.00145.x (2009).

2 Zschiedrich, C. P., Keidel, V. & Szurmant, H. Molecular Mechanisms of Two-Component Signal Transduction. *Journal of molecular biology* **428**, 3752-3775, doi:10.1016/j.jmb.2016.08.003 (2016).

3 Mellin, J. R. & Cossart, P. Unexpected versatility in bacterial riboswitches. *Trends in genetics : TIG* **31**, 150-156, doi:10.1016/j.tig.2015.01.005 (2015).

4 Dougherty, M. J. & Arnold, F. H. Directed evolution: new parts and optimized function. *Curr Opin Biotechnol* **20**, 486-491, doi:10.1016/j.copbio.2009.08.005 (2009).

5 Stocker, J. *et al.* Development of a set of simple bacterial biosensors for quantitative and rapid measurements of arsenite and arsenate in potable water. *Environmental science & technology* **37**, 4743-4750 (2003).

6 Ivask, A., Virta, M. & Kahru, A. Construction and use of specific luminescent recombinant bacterial sensors for the assessment of bioavailable fraction of cadmium, zinc, mercury and chromium in the soil. *Soil Biology & Biochemistry* **34**, 1439-1447, doi:10.1016/s0038-0717(02)00088-3 (2002).

7 Holowko, M. B., Wang, H., Jayaraman, P. & Poh, C. L. Biosensing Vibrio cholerae with Genetically Engineered Escherichia coli. *ACS Synth Biol* **5**, 1275-1283, doi:10.1021/acssynbio.6b00079 (2016).

8 Daeffler, K. N. *et al.* Engineering bacterial thiosulfate and tetrathionate sensors for detecting gut inflammation. *Molecular systems biology* **13**, 923, doi:10.15252/msb.20167416 (2017).

9 Riglar, D. T. *et al.* Engineered bacteria can function in the mammalian gut long-term as live diagnostics of inflammation. *Nat Biotechnol* **35**, 653-658, doi:10.1038/nbt.3879 (2017).

10 Forbes, N. S. Engineering the perfect (bacterial) cancer therapy. *Nature Reviews Cancer* **10**, 784-793, doi:10.1038/nrc2934 (2010).

11 Din, M. O. *et al.* Synchronized cycles of bacterial lysis for in vivo delivery. *Nature* **536**, 81-85, doi:10.1038/nature18930 (2016).

12 Isabella, V. M. *et al.* Development of a synthetic live bacterial therapeutic for the human metabolic disease phenylketonuria. *Nat Biotechnol* **36**, 857-864, doi:10.1038/nbt.4222 (2018).

13 Kurtz, C. B. *et al.* An engineered E. coli Nissle improves hyperammonemia and survival in mice and shows dose-dependent exposure in healthy humans. *Science translational medicine* **11**, doi:10.1126/scitranslmed.aau7975 (2019).

14 Hamady, Z. Z. *et al.* Treatment of colitis with a commensal gut bacterium engineered to secrete human TGF-beta1 under the control of dietary xylan 1. *Inflammatory bowel diseases* **17**, 1925-1935, doi:10.1002/ibd.21565 (2011).

15 Pardee, K. *et al.* Paper-based synthetic gene networks. *Cell* **159**, 940-954, doi:10.1016/j.cell.2014.10.004 (2014).

16 Pardee, K. *et al.* Rapid, Low-Cost Detection of Zika Virus Using Programmable Biomolecular Components. *Cell* **165**, 1255-1266, doi:10.1016/j.cell.2016.04.059 (2016).

17 Black, R. E. *et al.* Maternal and child undernutrition and overweight in low-income and middle-income countries. *Lancet* **382**, 427-451, doi:10.1016/s0140-6736(13)60937-x (2013).

18 Garrett, D. A., Sangha, J. K., Kothari, M. T. & Boyle, D. Field-friendly techniques for assessment of biomarkers of nutrition for development. *Am J Clin Nutr* **94**, 685S-690S, doi:10.3945/ajcn.110.005751 (2011).

19 Brindle, E. *et al.* A multiplex immunoassay method for simultaneous quantification of iron, vitamin A and inflammation status markers. *PLoS One* **9**, e115164, doi:10.1371/journal.pone.0115164 (2014).

20 Brindle, E. *et al.* Simultaneous assessment of iodine, iron, vitamin A, malarial antigenemia, and inflammation status biomarkers via a multiplex immunoassay method on a population of pregnant women from Niger. *PLoS One* **12**, e0185868, doi:10.1371/journal.pone.0185868 (2017).

21 King, J. C. *et al.* Biomarkers of Nutrition for Development (BOND)-Zinc Review. *The Journal of nutrition*, doi:10.3945/jn.115.220079 (2016).

22 Wessells, K. R. & Brown, K. H. Estimating the global prevalence of zinc deficiency: results based on zinc availability in national food supplies and the prevalence of stunting. *PLoS One* **7**, e50568, doi:10.1371/journal.pone.0050568 (2012).

23 Black, R. E. *et al.* Maternal and child undernutrition 1 - Maternal and child undernutrition: global and regional exposures and health consequences. *Lancet* **371**, 243-260, doi:10.1016/s0140-6736(07)61690-0 (2008).

24 Hess, S. Y., Peerson, J. M., King, J. C. & Brown, K. H. Use of serum zinc concentration as an indicator of population zinc status. *Food and nutrition bulletin* **28**, S403-429, doi:10.1177/15648265070283s303 (2007).

25 Watstein, D. M., McNerney, M. P. & Styczynski, M. P. Precise metabolic engineering of carotenoid biosynthesis in Escherichia coli towards a low-cost biosensor. *Metabolic engineering* **31**, 171-180, doi:10.1016/j.ymben.2015.06.007 (2015).

26 Watstein, D. M. & Styczynski, M. P. Development of a Pigment-Based Whole-Cell Zinc Biosensor for Human Serum. *ACS Synth Biol* **7**, 267-275, doi:10.1021/acssynbio.7b00292 (2018).

27 Balibar, C. J. & Walsh, C. T. In vitro biosynthesis of violacein from L-tryptophan by the enzymes VioA-E from Chromobacterium violaceum. *Biochemistry* **45**, 15444-15457, doi:10.1021/bi061998z (2006).

28 Duran, N. *et al.* Violacein: properties and biological activities. *Biotechnology and applied biochemistry* **48**, 127-133, doi:10.1042/ba20070115 (2007).

29 Fang, M. *et al.* Intermediate-sensor assisted push-pull strategy and its application in heterologous deoxyviolacein production in Escherichia coli. *Metabolic engineering* **33**, 41-51, doi:10.1016/j.ymben.2015.10.006 (2016).

30 Fang, M.-Y. *et al.* High crude violacein production from glucose by Escherichia coli engineered with interactive control of tryptophan pathway and violacein biosynthetic pathway. *Microbial Cell Factories* **14**, doi:10.1186/s12934-015-0192-x (2015).

31 Lee, M. E., Aswani, A., Han, A. S., Tomlin, C. J. & Dueber, J. E. Expression-level optimization of a multi-enzyme pathway in the absence of a high-throughput assay. *Nucleic Acids Research* **41**, 10668-10678, doi:10.1093/nar/gkt809 (2013).

32 Rodrigues, A. L., Becker, J., de Souza Lima, A. O., Porto, L. M. & Wittmann, C. Systems metabolic engineering of Escherichia coli for gram scale production of the antitumor drug deoxyviolacein from glycerol. *Biotechnol Bioeng* **111**, 2280-2289, doi:10.1002/bit.25297 (2014).

33 Rodrigues, A. L. *et al.* Systems metabolic engineering of Escherichia coli for production of the antitumor drugs violacein and deoxyviolacein. *Metabolic engineering* **20**, 29-41, doi:10.1016/j.ymben.2013.08.004 (2013).

34 Zalatan, J. G. *et al.* Engineering Complex Synthetic Transcriptional Programs with CRISPR RNA Scaffolds. *Cell* **160**, 339-350, doi:10.1016/j.cell.2014.11.052 (2015).

35 Alper, H., Fischer, C., Nevoigt, E. & Stephanopoulos, G. Tuning genetic control through promoter engineering. *Proceedings of the National Academy of Sciences*

of the United States of America **102**, 12678-12683, doi:10.1073/pnas.0504604102 (2005).

36 Alper, H., Jin, Y. S., Moxley, J. F. & Stephanopoulos, G. Identifying gene targets for the metabolic engineering of lycopene biosynthesis in Escherichia coli. *Metabolic engineering* **7**, 155-164, doi:10.1016/j.ymben.2004.12.003 (2005).

37 Alper, H., Miyaoku, K. & Stephanopoulos, G. Construction of lycopene-overproducing E-coli strains by combining systematic and combinatorial gene knockout targets. *Nature Biotechnology* **23**, 612-616, doi:10.1038/nbt1083 (2005).

38 Farmer, W. R. & Liao, J. C. Improving lycopene production in Escherichia coli by engineering metabolic control. *Nature Biotechnology* **18**, 533-537 (2000).

39 Jin, Y. S. & Stephanopoulos, G. Multi-dimensional gene target search for improving lycopene biosynthesis in Escherichia coli. *Metabolic engineering* **9**, 337-347, doi:10.1016/j.ymben.2007.03.003 (2007).

40 Yoon, S.-H. *et al.* Enhanced lycopene production in Escherichia coli engineered to synthesize isopentenyl diphosphate and dimethylallyl diphosphate from mevalonate. *Biotechnology and Bioengineering* **94**, 1025-1032, doi:10.1002/bit.20912 (2006).

41 Anthony, J. R. *et al.* Optimization of the mevalonate-based isoprenoid biosynthetic pathway in Escherichia coli for production of the anti-malarial drug precursor amorpha-4,11-diene. *Metabolic engineering* **11**, 13-19, doi:10.1016/j.ymben.2008.07.007 (2009).

42 Martin, V. J., Pitera, D. J., Withers, S. T., Newman, J. D. & Keasling, J. D. Engineering a mevalonate pathway in Escherichia coli for production of terpenoids. *Nat Biotechnol* **21**, 796-802, doi:10.1038/nbt833 (2003).

43 Ro, D. K. *et al.* Production of the antimalarial drug precursor artemisinic acid in engineered yeast. *Nature* **440**, 940-943, doi:10.1038/nature04640 (2006).

44 Wu, G. *et al.* Metabolic Burden: Cornerstones in Synthetic Biology and Metabolic Engineering Applications. *Trends in biotechnology* **34**, 652-664, doi:10.1016/j.tibtech.2016.02.010 (2016).

45 Xu, P., Li, L., Zhang, F., Stephanopoulos, G. & Koffas, M. Improving fatty acids production by engineering dynamic pathway regulation and metabolic control. *Proceedings of the National Academy of Sciences of the United States of America* **111**, 11299-11304, doi:10.1073/pnas.1406401111 (2014).

46 Zhang, F., Carothers, J. M. & Keasling, J. D. Design of a dynamic sensor-regulator system for production of chemicals and fuels derived from fatty acids. *Nature Biotechnology* **30**, 354-U166, doi:10.1038/nbt.2149 (2012).

47 McNerney, M. P., Watstein, D. M. & Styczynski, M. P. Precision metabolic engineering: The design of responsive, selective, and controllable metabolic systems. *Metabolic engineering* **31**, 123-131, doi:10.1016/j.ymben.2015.06.011 (2015).

48 Brockman, I. M. & Prather, K. L. Dynamic metabolic engineering: New strategies for developing responsive cell factories. *Biotechnology journal* **10**, 1360-1369, doi:10.1002/biot.201400422 (2015).

49 Venayak, N., Anesiadis, N., Cluett, W. R. & Mahadevan, R. Engineering metabolism through dynamic control. *Current Opinion in Biotechnology* **34**, 142-152, doi:10.1016/j.copbio.2014.12.022 (2015).

50 Solomon, K. V., Sanders, T. M. & Prather, K. L. J. A dynamic metabolite valve for the control of central carbon metabolism. *Metabolic engineering* **14**, 661-671, doi:10.1016/j.ymben.2012.08.006 (2012).

51 Soma, Y., Tsuruno, K., Wada, M., Yokota, A. & Hanai, T. Metabolic flux redirection from a central metabolic pathway toward a synthetic pathway using a metabolic toggle switch. *Metabolic engineering* **23**, 175-184, doi:10.1016/j.ymben.2014.02.008 (2014).

52 Ohashi, H., Kanamori, T., Shimizu, Y. & Ueda, T. A highly controllable reconstituted cell-free system--a breakthrough in protein synthesis research. *Current pharmaceutical biotechnology* **11**, 267-271 (2010).

53 Shimizu, Y. *et al.* Cell-free translation reconstituted with purified components. *Nat Biotechnol* **19**, 751-755, doi:10.1038/90802 (2001).

54 Shimizu, Y., Kanamori, T. & Ueda, T. Protein synthesis by pure translation systems. *Methods* **36**, 299-304, doi:10.1016/j.ymeth.2005.04.006 (2005).

55 Hodgman, C. E. & Jewett, M. C. Cell-free synthetic biology: thinking outside the cell. *Metabolic engineering* **14**, 261-269, doi:10.1016/j.ymben.2011.09.002 (2012).

56 Carlson, E. D., Gan, R., Hodgman, C. E. & Jewett, M. C. Cell-free protein synthesis: applications come of age. *Biotechnology advances* **30**, 1185-1194, doi:10.1016/j.biotechadv.2011.09.016 (2012).

57 Harbers, M. Wheat germ systems for cell-free protein expression. *FEBS letters* **588**, 2762-2773, doi:10.1016/j.febslet.2014.05.061 (2014).

58 Des Soye, B. J., Davidson, S. R., Weinstock, M. T., Gibson, D. G. & Jewett, M. C. Establishing a High-Yielding Cell-Free Protein Synthesis Platform Derived from Vibrio natriegens. *ACS Synth Biol* **7**, 2245-2255, doi:10.1021/acssynbio.8b00252 (2018).

59 Li, J., Wang, H., Kwon, Y. C. & Jewett, M. C. Establishing a high yielding streptomyces-based cell-free protein synthesis system. *Biotechnol Bioeng* **114**, 1343-1353, doi:10.1002/bit.26253 (2017).

60 Wiegand, D. J., Lee, H. H., Ostrov, N. & Church, G. M. Establishing a Cell-Free Vibrio natriegens Expression System. *ACS Synth Biol* **7**, 2475-2479, doi:10.1021/acssynbio.8b00222 (2018).

61 Zubay, G. In vitro synthesis of protein in microbial systems. *Annual review of genetics* **7**, 267-287, doi:10.1146/annurev.ge.07.120173.001411 (1973).

62 Sun, Z. Z. *et al.* Protocols for implementing an Escherichia coli based TX-TL cell-free expression system for synthetic biology. *Journal of visualized experiments : JoVE*, e50762, doi:10.3791/50762 (2013).

63 Kwon, Y. C. & Jewett, M. C. High-throughput preparation methods of crude extract for robust cell-free protein synthesis. *Scientific reports* **5**, 8663, doi:10.1038/srep08663 (2015).

64 Silverman, A. D., Kelley-Loughnane, N., Lucks, J. B. & Jewett, M. C. Deconstructing Cell-Free Extract Preparation for in Vitro Activation of Transcriptional Genetic Circuitry. *ACS Synth Biol* **8**, 403-414, doi:10.1021/acssynbio.8b00430 (2019).

65 Jewett, M. C. & Swartz, J. R. Mimicking the Escherichia coli cytoplasmic environment activates long-lived and efficient cell-free protein synthesis. *Biotechnol Bioeng* **86**, 19-26, doi:10.1002/bit.20026 (2004).

66 Takahashi, M. K. *et al.* Characterizing and prototyping genetic networks with cell-free transcription-translation reactions. *Methods* **86**, 60-72, doi:10.1016/j.ymeth.2015.05.020 (2015).

67 Shin, J. & Noireaux, V. An E. coli cell-free expression toolbox: application to synthetic gene circuits and artificial cells. *ACS Synth Biol* **1**, 29-41, doi:10.1021/sb200016s (2012).

68 Garamella, J., Marshall, R., Rustad, M. & Noireaux, V. The All E. coli TX-TL Toolbox 2.0: A Platform for Cell-Free Synthetic Biology. *ACS Synth Biol* **5**, 344-355, doi:10.1021/acssynbio.5b00296 (2016).

69 Sitaraman, K. *et al.* A novel cell-free protein synthesis system. *Journal of biotechnology* **110**, 257-263, doi:10.1016/j.jbiotec.2004.02.014 (2004).

70 Sun, Z. Z., Yeung, E., Hayes, C. A., Noireaux, V. & Murray, R. M. Linear DNA for rapid prototyping of synthetic biological circuits in an Escherichia coli based TX-TL cell-free system. *ACS Synth Biol* **3**, 387-397, doi:10.1021/sb400131a (2014).

71 Dudley, Q. M., Karim, A. S. & Jewett, M. C. Cell-free metabolic engineering: biomanufacturing beyond the cell. *Biotechnology journal* **10**, 69-82, doi:10.1002/biot.201400330 (2015).

72 Karim, A. S. & Jewett, M. C. A cell-free framework for rapid biosynthetic pathway prototyping and enzyme discovery. *Metabolic engineering* **36**, 116-126, doi:10.1016/j.ymben.2016.03.002 (2016).

73 Abudayyeh, O. O. *et al.* RNA targeting with CRISPR-Cas13. *Nature* **550**, 280-284, doi:10.1038/nature24049 (2017).

74 Gootenberg, J. S. *et al.* Multiplexed and portable nucleic acid detection platform with Cas13, Cas12a, and Csm6. *Science* **360**, 439-444, doi:10.1126/science.aaq0179 (2018).

75 Gootenberg, J. S. *et al.* Nucleic acid detection with CRISPR-Cas13a/C2c2. *Science* **356**, 438-442, doi:10.1126/science.aam9321 (2017).

76 Didovyk, A., Tonooka, T., Tsimring, L. & Hasty, J. Rapid and Scalable Preparation of Bacterial Lysates for Cell-Free Gene Expression. *ACS Synth Biol* **6**, 2198-2208, doi:10.1021/acssynbio.7b00253 (2017).

77 Wen, K. Y. *et al.* A Cell-Free Biosensor for Detecting Quorum Sensing Molecules in P. aeruginosa-Infected Respiratory Samples. *ACS Synth Biol* **6**, 2293-2301, doi:10.1021/acssynbio.7b00219 (2017).

78 Espah Borujeni, A., Mishler, D. M., Wang, J., Huso, W. & Salis, H. M. Automated physics-based design of synthetic riboswitches from diverse RNA aptamers. *Nucleic Acids Res* **44**, 1-13, doi:10.1093/nar/gkv1289 (2016).

79 McNerney, M. P. & Styczynski, M. P. Precise control of lycopene production to enable a fast-responding, minimal-equipment biosensor. *Metabolic engineering* **43**, 46-53, doi:10.1016/j.ymben.2017.07.004 (2017).

80 Zhao, J. *et al.* Engineering central metabolic modules of Escherichia coli for improving beta-carotene production. *Metabolic engineering* **17**, 42-50, doi:10.1016/j.ymben.2013.02.002 (2013).

81 Alper, H. & Stephanopoulos, G. Uncovering the gene knockout landscape for improved lycopene production in E. coli. *Applied microbiology and biotechnology* **78**, 801-810, doi:10.1007/s00253-008-1373-x (2008).

82 Ajikumar, P. K. *et al.* Isoprenoid Pathway Optimization for Taxol Precursor Overproduction in Escherichia coli. *Science* **330**, 70-74, doi:10.1126/science.1191652 (2010).

83 Alonso-Gutierrez, J. *et al.* Metabolic engineering of Escherichia coli for limonene and perillyl alcohol production. *Metabolic engineering* **19**, 33-41, doi:10.1016/j.ymben.2013.05.004 (2013).

84 Pitera, D. J., Paddon, C. J., Newman, J. D. & Keasling, J. D. Balancing a heterologous mevalonate pathway for improved isoprenoid production in Escherichia coli. *Metabolic engineering* **9**, 193-207, doi:10.1016/j.ymben.2006.11.002 (2007).

85 Dahl, R. H. *et al.* Engineering dynamic pathway regulation using stress-response promoters. *Nature Biotechnology* **31**, 1039-+ (2013).

86 Terpe, K. Overview of bacterial expression systems for heterologous protein production: from molecular and biochemical fundamentals to commercial systems. *Applied microbiology and biotechnology* **72**, 211-222, doi:10.1007/s00253-006-0465-8 (2006).

87 Guzman, L. M., Belin, D., Carson, M. J. & Beckwith, J. Tight regulation, modulation, and high-level expression by vectors containing the arabinose PBAD promoter. *Journal of bacteriology* **177**, 4121-4130 (1995).

88 Gibson, D. G. *et al.* Enzymatic assembly of DNA molecules up to several hundred kilobases. *Nat Methods* **6**, 343-345, doi:10.1038/nmeth.1318 (2009).

89 Shetty, R., Lizarazo, M., Rettberg, R. & Knight, T. F. Assembly of BioBrick standard biological parts using three antibiotic assembly. *Methods in enzymology* **498**, 311-326, doi:10.1016/b978-0-12-385120-8.00013-9 (2011).

90 Salis, H. M., Mirsky, E. A. & Voigt, C. A. Automated design of synthetic ribosome binding sites to control protein expression. *Nature Biotechnology* **27**, 946-U112, doi:10.1038/nbt.1568 (2009).

91 Xu, F., Yuan, Q. P. & Dong, H. R. Determination of lycopene and beta-carotene by high-performance liquid chromatography using sudan I as internal standard. *Journal of chromatography. B, Analytical technologies in the biomedical and life sciences* **838**, 44-49, doi:10.1016/j.jchromb.2006.04.004 (2006).

92 Lv, X. *et al.* Combinatorial pathway optimization in Escherichia coli by directed co-evolution of rate-limiting enzymes and modular pathway engineering. *Biotechnol Bioeng* **113**, 2661-2669, doi:10.1002/bit.26034 (2016).

93 Brockman, I. M. & Prather, K. L. J. Dynamic knockdown of E-coli central metabolism for redirecting fluxes of primary metabolites. *Metabolic engineering* **28**, 104-113, doi:10.1016/j.ymben.2014.12.005 (2015).

94 Hosseinidoust, Z. *et al.* Bioengineered and biohybrid bacteria-based systems for drug delivery. *Advanced drug delivery reviews* **106**, 27-44, doi:10.1016/j.addr.2016.09.007 (2016).

95 Choi, E. J. & Ling, G. S. F. Battlefield medicine: paradigm shift for pharmaceuticals manufacturing. *PDA journal of pharmaceutical science and technology / PDA* **68**, 312-312, doi:10.5731/pdajpst.2014.01002 (2014).

96 Perez-Pinera, P. *et al.* Synthetic biology and microbioreactor platforms for programmable production of biologics at the point-of-care. *Nat Commun* **7**, 12211, doi:10.1038/ncomms12211 (2016).

97 Dueber, J. E., Mirsky, E. A. & Lim, W. A. Engineering synthetic signaling proteins with ultrasensitive input/output control. *Nat Biotechnol* **25**, 660-662, doi:10.1038/nbt1308 (2007).

98 Ang, J., Harris, E., Hussey, B. J., Kil, R. & McMillen, D. R. Tuning response curves for synthetic biology. *ACS Synth Biol* **2**, 547-567, doi:10.1021/sb4000564 (2013).

99 Renda, B. A., Hammerling, M. J. & Barrick, J. E. Engineering reduced evolutionary potential for synthetic biology. *Molecular bioSystems* **10**, 1668-1678, doi:10.1039/c3mb70606k (2014).

100 Datsenko, K. A. & Wanner, B. L. One-step inactivation of chromosomal genes in Escherichia coli K-12 using PCR products. *Proc Natl Acad Sci U S A* **97**, 6640-6645, doi:10.1073/pnas.120163297 (2000).

101 Wilson, D. S. & Keefe, A. D. Random mutagenesis by PCR. *Current protocols in molecular biology* **Chapter 8**, Unit8.3, doi:10.1002/0471142727.mb0803s51 (2001).

102 Gupta, A., Reizman, I. M., Reisch, C. R. & Prather, K. L. Dynamic regulation of metabolic flux in engineered bacteria using a pathway-independent quorum-sensing circuit. *Nat Biotechnol* **35**, 273-279, doi:10.1038/nbt.3796 (2017).

103 Brodel, A. K., Jaramillo, A. & Isalan, M. Engineering orthogonal dual transcription factors for multi-input synthetic promoters. *Nat Commun* **7**, 13858, doi:10.1038/ncomms13858 (2016).

104 Xu, P. *et al.* Design and Kinetic Analysis of a Hybrid Promoter-Regulator System for Malonyl-CoA Sensing in Escherichia coli. *ACS Chemical Biology* **9**, 451-458, doi:10.1021/cb400623m (2014).

105 Gilston, B. A. *et al.* Structural and mechanistic basis of zinc regulation across the E. coli Zur regulon. *PLoS biology* **12**, e1001987, doi:10.1371/journal.pbio.1001987 (2014).

106 Shin, J. H. & Helmann, J. D. Molecular logic of the Zur-regulated zinc deprivation response in Bacillus subtilis. *Nat Commun* **7**, 12612, doi:10.1038/ncomms12612 (2016).

107 Schrodinger, L. The PyMOL Molecular Graphics System, Version~1.8. (2015).

108 McGinness, K. E., Baker, T. A. & Sauer, R. T. Engineering controllable protein degradation. *Molecular Cell* **22**, 701-707, doi:10.1016/j.molcel.2006.04.027 (2006).

109 Bhamla, M. S. *et al.* Hand-powered ultralow-cost paper centrifuge. *Nature Biomedical Engineering* **1**, 0009, doi:10.1038/s41551-016-0009 (2017).

110 Pardee, K. *et al.* Portable, On-Demand Biomolecular Manufacturing. *Cell* **167**, 248-259.e212, doi:10.1016/j.cell.2016.09.013 (2016).

111 Takahashi, M. K. *et al.* A low-cost paper-based synthetic biology platform for analyzing gut microbiota and host biomarkers. *Nat Commun* **9**, 3347, doi:10.1038/s41467-018-05864-4 (2018).

112 Vasan, R. S. Biomarkers of cardiovascular disease: molecular basis and practical considerations. *Circulation* **113**, 2335-2362, doi:10.1161/circulationaha.104.482570 (2006).

113 Goossens, N., Nakagawa, S., Sun, X. & Hoshida, Y. Cancer biomarker discovery and validation. *Translational cancer research* **4**, 256-269, doi:10.3978/j.issn.2218-676X.2015.06.04 (2015).

114 Combs, G. F., Jr. *et al.* Biomarkers in nutrition: new frontiers in research and application. *Annals of the New York Academy of Sciences* **1278**, 1-10, doi:10.1111/nyas.12069 (2013).

115 Sun, Z. Z. *et al.* Protocols for Implementing an Escherichia coli Based TX-TL Cell-Free Epxression System for Synthetic Biology. *J. Vis. Exp. (79), e50762* (2013).

116 Rodkey, F. L. Direct spectrophotometric determination of albumin in human serum. *Clinical chemistry* **11**, 478-487 (1965).

117 Sochacka, J. Application of phenol red as a marker ligand for bilirubin binding site at subdomain IIA on human serum albumin. *Journal of photochemistry and photobiology. B, Biology* **151**, 89-99, doi:10.1016/j.jphotobiol.2015.07.014 (2015).

118 Peters, T. in *All About Albumin* (ed Theodore Peters) 76-132 (Academic Press, 1995).

119 Songjaroen, T., Dungchai, W., Chailapakul, O., Henry, C. S. & Laiwattanapaisal, W. Blood separation on microfluidic paper-based analytical devices. *Lab on a chip* **12**, 3392-3398, doi:10.1039/c2lc21299d (2012).

120 Schilling, K. M., Lepore, A. L., Kurian, J. A. & Martinez, A. W. Fully enclosed microfluidic paper-based analytical devices. *Analytical chemistry* **84**, 1579-1585, doi:10.1021/ac202837s (2012).

121 McMahon, C. *et al.* Yeast surface display platform for rapid discovery of conformationally selective nanobodies. *Nature structural & molecular biology* **25**, 289-296, doi:10.1038/s41594-018-0028-6 (2018).

122 Ku, T. H. *et al.* Nucleic Acid Aptamers: An Emerging Tool for Biotechnology and Biomedical Sensing. *Sensors (Basel, Switzerland)* **15**, 16281-16313, doi:10.3390/s150716281 (2015).

123 Ketzer, P. *et al.* Artificial riboswitches for gene expression and replication control of DNA and RNA viruses. *Proc Natl Acad Sci U S A* **111**, E554-562, doi:10.1073/pnas.1318563111 (2014).

124 Mishler, D. M. & Gallivan, J. P. A family of synthetic riboswitches adopts a kinetic trapping mechanism. *Nucleic Acids Res* **42**, 6753-6761, doi:10.1093/nar/gku262 (2014).

125 Soukup, G. A. & Breaker, R. R. Design of allosteric hammerhead ribozymes activated by ligand-induced structure stabilization. *Structure (London, England : 1993)* **7**, 783-791 (1999).

126 Tang, J. C. *et al.* A nanobody-based system using fluorescent proteins as scaffolds for cell-specific gene manipulation. *Cell* **154**, 928-939, doi:10.1016/j.cell.2013.07.021 (2013).

127 Visintin, M., Tse, E., Axelson, H., Rabbitts, T. H. & Cattaneo, A. Selection of antibodies for intracellular function using a two-hybrid in vivo system. *Proc Natl Acad Sci U S A* **96**, 11723-11728 (1999).

128 Waltz, E. After Theranos. *Nat Biotechnol* **35**, 11-15, doi:10.1038/nbt.3761 (2017).

129 Kasinskas, R. W. & Forbes, N. S. Salmonella typhimurium lacking ribose chemoreceptors localize in tumor quiescence and induce apoptosis. *Cancer Res* **67**, 3201-3209, doi:10.1158/0008-5472.can-06-2618 (2007).

130 Mimee, M., Citorik, R. J. & Lu, T. K. Microbiome therapeutics - Advances and challenges. *Advanced drug delivery reviews* **105**, 44-54, doi:10.1016/j.addr.2016.04.032 (2016).

131 Farrar, M. D. *et al.* Engineering of the gut commensal bacterium Bacteroides ovatus to produce and secrete biologically active murine interleukin-2 in response to xylan. *Journal of applied microbiology* **98**, 1191-1197, doi:10.1111/j.1365-2672.2005.02565.x (2005).